

Mehdi Panahi

# Plantwide Control for Economically Optimal Operation of Chemical Plants

- Applications to GTL plants and CO<sub>2</sub> capturing processes

Thesis for the degree of philosophiae doctor

Trondheim, December 2011

Norwegian University of  
Science and Technology  
Faculty of Natural Science and Technology  
Department of Chemical Engineering



**NTNU – Trondheim**  
Norwegian University of  
Science and Technology

**NTNU**

Norwegian University of Science and Technology

Doctoral thesis  
for the degree of philosophiae doctor

The Faculty of Natural Sciences and Technology  
Department of Chemical Engineering

© 2011 Mehdi Panahi.

ISBN 978-82-471-3095-7 (printed version)  
ISBN 978-82-471-3096-4 (electronic version)  
ISSN 1503-8181

Doctoral theses at NTNU, 2011:265

Printed by NTNU-trykk

---

## Abstract

In this thesis, the systematic plantwide procedure of Skogestad (2004) is applied to two processes;

- 1- Post-combustion CO<sub>2</sub> capturing processes,
- 2- Natural gas to liquid hydrocarbons (GTL) plants,

in order to design economically efficient control structures, which keep the processes near-optimum when disturbances occur. Because of the large magnitude of energy consumption in both these processes, optimal operation is of great importance.

The self-optimizing concept, which is the heart of the plantwide procedure is used to select the right controlled variables in different operational regions, which when they are kept constant, indirectly give the operation close to optimum. The optimal is to reconfigure the self-optimizing control loops when the process is entered into a new active constraint region, but we try to arrive at a simple/single control structure, which does not need switching, where a reasonable loss in operating economic objective function is accepted.

The CO<sub>2</sub> capturing process studied here is an amine absorption/stripping system. The chosen objective function for this process is first to minimize the energy requirement while fixed CO<sub>2</sub> recovery of 90% is met. This leads to one unconstrained degree of freedom. Maximum gain rule is applied and a temperature close to the top of the stripper is found as the best controlled variable. Further, we introduce penalty on CO<sub>2</sub> amount released to the atmosphere, and this results in two unconstrained degrees of freedom. CO<sub>2</sub> recovery and a temperature close to the top of the stripper are found as the best individual controlled variables in low feedrate. In higher flue gas flowrates, stripper heat input saturates and the self-optimizing method is repeated to select the right controlled variable for the remaining degree of freedom. We validate the proposed control structures using dynamic simulations, where 5 different alternatives including decentralized control loops and multivariable controller are studied. We finally achieve a simple control structure, which handles a wide range of change in throughput and keeps the process close to optimum without the need for switching the control loops or updating the controlled variables setpoints by a costly real time optimizer.

The GTL process modeled in this thesis includes an auto-thermal reformer (ATR) for synthesis gas production and a slurry bubble column reactor (SBCR) for the Fischer-Tropsch (FT) reactions. The FT products distribution is determined using a well-known Anderson-Schultz-Flory (ASF) model, where carbon component in CO (consumption rate is found based on the proposed rate by Iglesia et al.) is distributed to a range of hydrocarbons. ASF is a function of chain growth probability and the chain growth is a function of H<sub>2</sub>/CO ratio. We study different scenarios for chain growth and we arrive at a suitable model for optimal operation studies. The optimal operation is considered in two modes of operation. In mode I, natural gas feedrate is assumed given and in mode II, natural gas feedrate is also a degree of freedom. After optimization, in both modes, there are three unconstrained degrees of freedom. The best individual self-optimizing controlled variables are found and since the worst-case loss value is rather notable, combination of measurements is done, which reduces the loss significantly. Mode II happens when oxygen flowrate capacity reaches the maximum and we show that operation in mode II in this case is in snowballing region where operation should be avoided. Operation at maximum oxygen flowrate capacity is where maximum practical profit can be achieved.



## Acknowledgements

First and most of all, I would like to gratefully thank my supervisor professor Sigurd Skogestad for his confidence and giving me the opportunity to do my PhD thesis under his supervision. I have really enjoyed learning and working with him in plantwide control area, where I gained a lot from his knowledge and his personal ethics. His simple way of thinking, but very deep insight to science, has opened a new window for me how to look at the scientific and engineering issues. He has been always available for discussion, proposing and stirring me in new and right directions. Without his invaluable inputs, this work had never been completed. I hope the science world can gain a lot from Sigurd for many years.

Special thanks to Dr. Dag Schanke, GTL specialist at Statoil research center in Trondheim for being available for discussion about different issues related to GTL process. His comments were significance for completing the GTL model.

I would like also to thank my colleagues in process systems engineering group at NTNU who all together provided a nice environment to work. Special thanks to Ramprasad Yelchuru for sharing our office and a lot of discussions in control.

I have also cooperated with other PhD students, Mehdi Karimi and Ahmad Rafiee in reactor technology/CO<sub>2</sub> capturing group here at NTNU that was a great team work.

Besides of all my professional colleagues, I have had a strong and continuous support from my family. Thanks to my parents in my hometown Tabas/Iran who have continuously supported and encouraged me from elementary school to end of my PhD. Special thanks to my lovely wife Nayyereh and our daughter Tara for their constant support and patience. Their support provided me an excellent situation to concentrate on my studies.



---

## Table of Contents

|  |               |
|--|---------------|
| <b>Chapter 1 Thesis overview .....</b>   | <b>1</b>      |
| 1.1 Motivation and contribution.....   | 1             |
| 1.2 Outline of the thesis.....   | 2             |
| 1.3 Publications .....   | 3             |
| <br><b>Chapter 2 Introduction.....</b>   | <br><b>5</b>  |
| 2.1 Systematic plantwide control procedure .....   | 5             |
| 2.1.1 Step 1: Definition of operational objective functions and constraints .....  | 7             |
| 2.1.2 Step 2: Identify degrees of freedom and optimize the process in nominal case and<br>in presence of disturbances .....    | 8             |
| 2.1.3 Step 3: Selection of the best controlled variables using self-optimizing method.....                                     | 8             |
| 2.1.4 Step 4: Select location of throughput manipulator (TPM) .....  | 12            |
| 2.1.5 Step 5: Select structure of regulatory control layer .....   | 12            |
| 2.1.6 Step 6. Select structure of supervisory control.....   | 13            |
| 2.1.7 Step 7. Select structure of (or need for) optimization layer (RTO).....  | 13            |
| 2.2 Case-studies.....  | 13            |
| 2.2.1 Post-combustion CO <sub>2</sub> capturing processes.....   | 13            |
| 2.2.2 Natural gas to liquid hydrocarbons (GTL) process .....   | 15            |
| <br><b>Chapter 3 Self-optimizing Control of a CO<sub>2</sub> Capturing Plant with 90% Recovery.....</b>                        | <br><b>19</b> |
| 3.1 Introduction .....   | 20            |
| 3.2 Self-optimizing control of a CO <sub>2</sub> capturing plant.....  | 21            |
| 3.2.1 Step 1: Define objective function and constraints.....   | 21            |
| 3.2.2 Step 2. Determine DOFs for optimization.....   | 21            |
| 3.2.3 Step 3. Identification of important disturbances .....   | 22            |
| 3.2.4 Step 4. Optimization (nominally and with disturbances), .....  | 22            |
| 3.2.5 Step 5. Identification of candidate controlled variables. ....   | 22            |
| 3.2.6 Step 6. Evaluation of loss .....   | 22            |
| 3.3 Dynamic simulation .....   | 24            |
| 3.4 Stability of the proposed control structure against large disturbances .....   | 26            |
| 3.4.1 Use of traditional PI controllers .....  | 26            |
| 3.4.2 Using of a multivariable controller in the proposed structure .....  | 27            |
| 3.5 Conclusions .....  | 28            |
| <br><b>Chapter 4 Optimal Operation of CO<sub>2</sub> Capturing Process, Part I: Selection of<br/>Controlled Variables.....</b> | <br><b>29</b> |
| 4.1 Introduction .....   | 30            |
| 4.2 Top down analysis: Self-optimizing control of CO <sub>2</sub> capturing process .....                                      | 32            |
| 4.2.1 Region I: Flowrate of flue gas is given .....  | 32            |
| 4.2.2 Region II: Large flowrates of flue gas (+30%) .....  | 36            |

---

|   |           |
|---|-----------|
| 4.2.3 Region III: Large flowrates of flue gas when process reaches minimum allowable CO <sub>2</sub> recovery ..... | 38        |
| 4.3 Discussion .....  | 39        |
| 4.4 Conclusions .....   | 40        |
| <b>Chapter 5 Optimal Operation of CO<sub>2</sub> Capturing Process, Part II: Design of Control Layers.....</b>      | <b>41</b> |
| 5.1 Introduction .....  | 41        |
| 5.2 Design of the control layers .....  | 44        |
| 5.3 Alternative control structures to handle larger throughputs .....   | 46        |
| 5.3.1 Alternative 2 (“reverse pairing”) .....   | 47        |
| 5.3.2 Operation in region II (Alternative 3) .....  | 50        |
| 5.3.3 Alternative 4 (regions I and II) .....  | 51        |
| 5.4 Performance of alternative control structures .....   | 51        |
| 5.4.1 Alternative 1 (region I) .....  | 52        |
| 5.4.2 Alternative 3 (region II) .....   | 53        |
| 5.4.3 Alternative 2 (regions I and II) .....  | 53        |
| 5.4.4 Alternative 4 (regions I and II) .....  | 56        |
| 5.4.5 Multivariable Controller (regions I and II) .....   | 56        |
| 5.5 Conclusions .....   | 58        |
| <b>Chapter 6 A Natural Gas to Liquids (GTL) Process Model for Optimal Operation.....</b>                            | <b>59</b> |
| 6.1 Introduction .....  | 59        |
| 6.2 Modeling and process description .....  | 60        |
| 6.2.1 The synthesis gas section .....   | 61        |
| 6.2.2 Fischer Tropsch section .....   | 62        |
| 6.3 Calculation of chain growth probability $\alpha$ .....  | 64        |
| 6.3.1 Using rates of Iglesia ( $\alpha_1$ ) .....   | 64        |
| 6.3.2 Using modified function of Yermakova and Anikeev ( $\alpha_2$ ) .....   | 65        |
| 6.3.3 Constant $\alpha$ ( $\alpha_3$ ) .....  | 65        |
| 6.4 Single-pass Fischer Tropsch reactor .....   | 65        |
| 6.5 Definition of optimal operation for overall process .....   | 67        |
| 6.5.1 Objective function .....  | 67        |
| 6.5.2 Operational Degrees of freedom (steady-state) .....   | 68        |
| 6.5.3 Operational constraints .....   | 68        |
| 6.6 Optimization results .....  | 69        |
| 6.7 Conclusions .....   | 71        |
| <b>Chapter 7 Selection of the Controlled Variables for a GTL Process.....</b>                                       | <b>75</b> |
| 7.1 Introduction .....  | 76        |
| 7.2 Process description .....   | 77        |

---

|   |            |
|---|------------|
| 7.3 Top-down analysis for operation of the GTL process.....                                       | 80         |
| 7.3.1 Mode I: natural gas flowrate is given.....  | 80         |
| 7.3.2 Model II: natural gas is a degree of freedom for optimization.....                          | 88         |
| 7.4 Conclusions.....  | 93         |
| <b>Chapter 8 Conclusions and future work.....</b>   | <b>95</b>  |
| 8.1 Concluding remarks .....  | 95         |
| 8.2 Directions for future work.....   | 97         |
| <b>Appendix A .....</b>   | <b>103</b> |
| <b>Appendix B (additional work) .....</b>   | <b>117</b> |
| <b>Appendix C (more information about CO<sub>2</sub> capture model used in this thesis) .....</b> | <b>125</b> |



# Chapter 1

## Thesis overview

In this chapter an outline of the thesis including motivation and scope of the thesis is presented. The contributions and explanations about the content of the chapters with a list of publications are given.

### 1.1 Motivation and contribution

Large magnitude of energy is usually necessary to operate the chemical plants. Continuously increasing energy prices encourages operating the chemical plants with the minimum energy requirements, while safety, environmental and products quality aspects are met. Disturbances during operation are unavoidable and one may need to implement costly advanced control systems to run the plant continuously in order to get maximum achievable profit.

Design a simple control system in a systematic manner by selecting of the right (individual/combinations) controlled variables (“self-optimizing controlled variables”), which can usually remove the need for costly advanced control systems, while the process operates near-optimum, has been a topic of the works in Skogestad group from the early 1990s.

The main contribution of this thesis is the application of the general plantwide procedure of Skogestad (Skogestad 2004) to two important processes; 1- Post-combustion CO<sub>2</sub> capturing process, 2- Natural gas to liquid hydrocarbons (GTL) process. This has been done by selection of the best self-optimizing controlled variables and validation of the proposed control structures using dynamic simulations.

For the CO<sub>2</sub> capture case, we studied different operational regions and at the end a simple control structure is synthesized, which keeps the plant near-optimum in the entire throughput

range (main disturbance) without the need for re-configuration of the control loops or updating the setpoints by an advanced control system/operator. We recommend the achieved structure for implementation in practice.

The GTL process has been modeled, which we believe as the first model in the public literature that describes properly all dependencies of the operating parameters. Further, this model is used for optimal operation studies. We studied two modes of operation. In mode I; for a fixed natural gas feedrate the variable income is maximized and in mode II; natural gas is also a degree of freedom in order to process maximum throughput. At the end, we propose a practical operating point with a simple control policy for achieving maximum profit.

## 1.2 Outline of the thesis

In chapter 2, the plantwide procedure of Skogestad is briefly described. In addition, post-combustion CO<sub>2</sub> capturing and natural gas to liquid (GTL) processes are introduced.

In chapter 3, self-optimizing method is applied to a CO<sub>2</sub> capturing plant for selection of the best controlled variables where CO<sub>2</sub> recovery is fixed at 90%. The objective function is to minimize required energy in the plant. In this case there is one unconstrained degree of freedom and maximum gain rule is applied to select the controlled variable that has the largest scaled gain from the input and the minimum optimal variation in presence of disturbances. Dynamic simulation is also done to validate the proposed structure. In addition, the performance of the structure in presence of large variation in load from the power plant is considered and since the proposed structure fails when reboiler duty of stripper reaches the maximum, a simple reconfiguration is proposed to make the control structure stable.

In chapter 4, the objective function in chapter 3 is modified to incorporate a penalty on CO<sub>2</sub> released to the air, which makes optimal to remove more amount of CO<sub>2</sub>. This results in having two unconstrained degrees of freedom in optimal nominal case (region I). When the load from power plant increases by approx. 20%, the reboiler duty saturates signifying the transition into region II where the number of unconstrained degree of freedom is reduced to one. The two operational regions are studied where at each self-optimizing method is applied to select the best individual measurements. Exact local method and maximum gain rule are used in regions I and II respectively to select the best controlled variables for each region.

In chapter 5, design of control layer consisting stabilizing CVs(CV2) and supervisory CVs(CV1) is done and the resulted structures are evaluated by dynamic simulations. The performance of four different alternatives of decentralized controllers and a multivariable controller is investigated. We conclude at the end a simple decentralized structure which works near-optimum in a wide range of disturbances (different operational regions) without the need for switching the self-optimizing CVs when transition between regions happen.

In chapter 6, a detailed GTL process model, which is appropriate for optimal operation studies, is developed. We look for such a model that Fischer-Tropsch (FT) products distribution is sensitive to change in reactor feed H<sub>2</sub>/CO. In addition, the effect of change in decision variables (feed ratios, recycles etc.) should appear through this ratio on products distribution and the economical objective function. Therefore three alternative expressions for chain growth probability  $\alpha$  are presented and discussed. The performance of these three alternatives is evaluated using the optimization of the process to maximize the variable income of the plant. Each alternative is optimized at two different price scenarios for heavy products (wax). Based

on the performance evaluation, the final model is selected and is used for self-optimizing analysis in chapter 7.

In chapter 7, self-optimizing method is applied to select the best controlled variables in two modes of operation. In mode I, natural gas feedrate is given where there are three unconstrained degrees of freedom (DOFs). We first select the best individual controlled variables, but the corresponding worst-case loss seems to be high therefore we go for selection of the best combination of the measurements to reduce the loss. In mode II, natural gas feedrate is also a degree of freedom for optimization. Profit increases almost linearly by increasing the natural gas flowrate until oxygen flowrate reaches the maximum capacity. Further increase in natural gas feedrate results in a small improvement in profit until the FT reactor volume becomes the bottleneck. Note that from the saturation point of oxygen plant capacity, the process operates in snowballing region where operation is not recommended, therefore the operating point where oxygen plant works at the maximum is suggested as the maximum practical throughput.

In the last chapter (chapter 8), conclusions of the thesis and some directions for the future work are given.

## 1.3 Publications

### Journal publications

1. **M. Panahi**, S. Skogestad, “Economically Efficient Operation of CO<sub>2</sub> Capturing Process; Part I: Self-optimizing Procedure for Selecting the Best Controlled Variables”, *Journal of Chemical Engineering and Processing: Process Intensification*, 50 (2011), 247-253 (chapter 4)
2. **M. Panahi**, S. Skogestad, “Economically Efficient Operation of CO<sub>2</sub> Capturing Process; Part II: Regulatory Control Layer”, submitted to *Journal of Chemical Engineering and Processing: Process Intensification* (chapter 5)
3. **M. Panahi**, A.Rafiee, S. Skogestad, M. Hillestad “A Comprehensive Natural Gas to Liquids (GTL) Process Model for Optimal Design and Operation”, submitted to *Industrial & Engineering Chemistry Research Journal* (chapter 6)
4. **M. Panahi**, S. Skogestad, “Selection of Controlled Variables for a Natural Gas to Liquids (GTL) Process Using Self-Optimizing Method” plan for submission to *Industrial & Engineering Chemistry Research Journal* (chapter 7)

### Book chapters

1. **M. Panahi**, M.Karimi, S. Skogestad, M. Hillestad, H. F. Svendsen “Self-Optimizing and Control Structure Design for a CO<sub>2</sub> Capturing Plant”, *Proceedings of 2<sup>nd</sup> Gas Processing Symposium*, Published in Aug. 2010 by Elsevier in book series “Advances in Gas Processing”, volume 2, pages 331-338, [doi:10.1016/S1876-0147\(10\)02035-5](https://doi.org/10.1016/S1876-0147(10)02035-5) (chapter 3)
2. **M. Panahi**, S. Skogestad, R. Yelchuru “Steady State Simulation for Optimal Design and Operation of a GTL process”, *Proceedings of 2<sup>nd</sup> Gas Processing Symposium*, Published in Aug.2010 by Elsevier in book series “Advances in Gas Processing”, volume 2, pages 275-284, [doi:10.1016/S1876-0147\(10\)02030-6](https://doi.org/10.1016/S1876-0147(10)02030-6) (appendix)

**Conference presentations**

1. **M. Panahi**, S. Skogestad, “Optimal Operation of a CO<sub>2</sub> Capturing Plant for a Wide Range of Disturbances” presented in AIChE’s 2011 annual meeting, 16-21 Oct. Minneapolis (chapters 4 and 5)
2. **M. Panahi**, S. Skogestad, “Controlled Variables Selection for a Gas-to-Liquids Process” presented in AIChE’s 2011 annual meeting, 16-21 Oct. Minneapolis (chapters 6 and 7)
3. **M. Panahi**, S. Skogestad, “Comparison of Decentralized Controller and MPC in Control Structure of a CO<sub>2</sub> Capturing Process”, presented in 16<sup>th</sup> Nordic Process Control Conference, Aug. 2010, Lund, Sweden (chapter 3)
4. **M. Panahi**, S. Skogestad, “Self-optimizing Control of a GTL process” presented in 1st Trondheim Gas Technology Conference, Oct. 2009, Trondheim, Norway (appendix)
5. V. Gera, N. Kaistha, **M. Panahi**, S. Skogestad, “Plantwide Control of a Cumene Manufacture Process”, Computer Aided Chemical Engineering, volume 29, 2011, pages 522-526, 21st European Symposium on Computer Aided Process Engineering (appendix)

# Chapter 2

## Introduction

Optimal operation of the chemical plants is to get the maximum achievable profit within the acceptable operating regions, while meeting environmental, safety and product requirements. Disturbances during operation are unavoidable and include change in feedstock flowrates, compositions etc. as well as change in the prices of raw materials and products. Efficient design of an offline control structure removes the necessity of the costly real time reoptimization when disturbances occur.

In this chapter, the proposed systematic procedure of Skogestad (Skogestad 2004) is reviewed with an emphasis on the latest developments of controlled variables selection (self-optimizing method) techniques. Controlled variable selection is the essential part of the procedure.

Finally, GTL (Gas to liquids) and post-combustion CO<sub>2</sub> capturing processes, which are the two processes that we have applied this procedure, are briefly described.

### 2.1 Systematic plantwide control procedure

Implementation of a control system is necessary to operate chemical plants economically optimal, safe and stable in the presence of disturbances which may frequently occur during operation. The implemented system for operating the plant generally includes different layers which operate at different time scales (Skogestad 2004).

- Scheduling (weeks),
- Site-wide optimization (days),
- Local optimization (hours),
- Supervisory (predictive, advanced) control (minutes),

- Regulatory control (seconds)

Supervisory and regulatory layers are “control” layers (with setpoint). Figure 2.1 illustrates the layers where they are linked by controlled variables. At each layer, the setpoint for controlled variables is given by the upper layer and implemented by the lower layer.

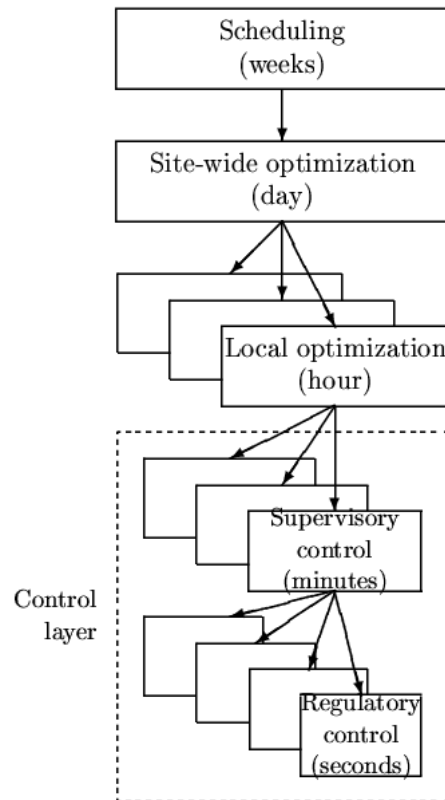


Figure 2.1 Typical control system hierarchy in a chemical plant (Skogestad 2004)

Skogestad’s general plantwide control procedure considers the lower three layers in Figure 2.1 where the objective is to remove the need for the upper of these three layers (the costly local optimization layer) by selection of the right controlled variables (self-optimizing CVs). The proposed stepwise design procedure is summarized in Table 2.1. The procedure is divided in two main parts:

### I. Top-down analysis

The Top-down analysis focuses on steady-state economics where an economical optimization problem is formulated. Optimization is performed both at nominal point and for important disturbances. Based on the optimization results, a self-optimizing analysis (explained in details later) is done for finding the active constraint regions and selecting the best controlled variables (CVs) in different operational regions. These CVs are named as primary CVs (CV1). Note that we are in a new operational region when a new active constraint comes into the picture when disturbances occur. For the top-down analysis, usually only a steady-state model of the process is required.

## II. Bottom-up analysis

The Bottom-up analysis focuses on dynamic control of the process. Dynamic model of the process is necessary to validate implementation of the proposed controlled variables from the top-down analysis. In this part, first stabilizing controlled variables (secondary CVs, CV2) are selected and paired with the proper manipulated variables (MVs) and then the structure of the supervisory control layer (pairing of the primary CVs with the remained manipulated variables) is determined.

Table 2.1 Plantwide control structure design procedure (Skogestad 2004; Skogestad 2011)

### I. Top-down part (focus on steady-state economics)

**Step 1.** Define operational objectives (optimal operation)

- (a) Identify a scalar cost function  $J$  (to be minimized)
- (b) Constraints

**Step 2.** Identify (a) steady-state degrees of freedom and (b) expected disturbances and (c) optimize the operation with respect to the degrees of freedom in the nominal case and for expected disturbances (offline analysis)

- Main objective: Find regions of active constraints

**Step 3.** (a) Identify candidate measurements and expected measurement error and (b) Select primary (economic) controlled variables CV1 with the objective of minimizing the economic loss

- One needs to find one CV1 for each steady-state degree of freedom
- In general, this step must be repeated for each constraint region
- To reduce the need for switching one may consider using the same CV1's in several regions. This is non-optimal and may even lead to infeasibility.

**Step 4.** Select location of throughput manipulator (TPM)

- Some plants, e.g., with parallel units, may have more than one TPM
- One may consider moving the TPM depending on the constraint region

### II. Bottom-up part (focus on dynamics)

**Step 5.** Select structure of the regulatory control layer (including inventory control)

- Select "stabilizing" controlled variables CV2
- Select inputs (valves) and "pairings" for controlling CV2
- Stabilize the process and avoid "drift"

If possible, use the same regulatory layer for all regions.

**Step 6.** Select structure of supervisory control which should:

- Control primary CV1's
- Supervise regulatory layer
- Perform switching between CV1's for different regions

**Step 7.** Select structure of (or need for) optimization layer (RTO) which should:

- Identify active constraints (identify regions)
- Update setpoints for CV1 (if necessary)

#### 2.1.1 Step 1: Definition of operational objective functions and constraints

In Skogestad's procedure, an optimization problem is formulated at first. An economical objective function is defined, which is usually maximizing the variable income (profit) of a plant and is defined using the terms which are related to operation typically as below:

Objective function ( $P$ ) = max. (Products sale - raw materials cost - utilities cost)

Equivalently, we may minimize the cost:

$$J = -P \quad (2.1)$$

Constraints are safety, environmental, product quality and capacity limitations of unit operations (minimum and maximum of flowrates, pressures, compositions, duties etc.), which need to be included in optimization framework.

### 2.1.2 Step 2: Identify degrees of freedom and optimize the process in nominal case and in presence of disturbances

In this step we determine the number of steady-state degrees of freedom ( $N_{ss}$ ). One approach is to first find the number of all MVs ( $N_m$ ) by process insight. This includes all the adjustable valves, electrical and mechanical variables, which need to be set during operation. To obtain the number of steady-state degrees of freedom we need to subtract from  $N_m$  the number of “variables” include MVs + variables that need to be controlled like levels, but where the setpoint has no steady-state effect (no effect on the objective function); for example liquid levels ( $N_{0y}$ ) and bypass streams ( $N_{0m}$ ) and then we have:

$$N_{ss} = N_m - (N_{0m} + N_{0y})$$

The implementation of active constraints removes  $N_{active}$  degrees of freedom. Therefore the number of unconstrained degrees of freedom that are left is:

$$N_{unconstrained} = N_{ss} - N_{active}$$

The self-optimizing method is applied in the next step to select the best controlled variables corresponding to the unconstrained degrees of freedom. Note that any independent set of variables can be chosen as unconstrained degrees of freedom during self-optimizing analysis. Table 2.2 gives the typical maximum number of steady-state degrees of freedom for some process units.

Table 2.2 Typical maximum number of steady-state degrees of freedom for some process unit (Skogestad 2002)

| Process unit  | DOF   |
|---|---|
| Each external feed stream                             | 1 (feedrate)  |
| Splitter  | n-1 split fractions (n is the number of exit streams) |
| Mixer   | 0   |
| Compressor, turbine and pump                          | 1 (work/speed)  |
| Adiabatic flash tank                                  | 0*  |
| Liquid phase reactor                                  | 1 (hold up)   |
| Gas phase reactor                                     | 0*  |
| Heat exchanger  | 1 (duty or net area)                                  |
| Columns (e.g. distillation) excluding heat exchangers | 0* + number of side streams                           |

\* add 1 degree of freedom for each extra pressure that is set (need an extra valve, compressor or pump), e.g. in flash tank, gas phase reactor or absorption column. Pressure is normally assumed to be given by the surrounding process and is then not a degree of freedom.

### 2.1.3 Step 3: Selection of the best controlled variables using self-optimizing method

The objective of this part is to find the controlled variables using the self-optimizing method. “Self-optimizing control is when we can achieve an acceptable loss with constant setpoint

values for the controlled variables without the need to reoptimize when disturbances occur” (Skogestad 2000). The idea of self-optimizing control is shown in Figure 2.2. It shows that if we control measurement  $z_1$ , loss in cost function  $J$  (deviation from the reoptimized cost function) is smaller compared to controlling measurement  $z_2$  when disturbance happens. Therefore  $z_1$  is a better measurement to be selected as self-optimizing CV. Skogestad (Skogestad 2000) has proposed the following systematic procedure for selection of the controlled variables.

Step 3.1. Definition of optimal operation (cost  $J$  and constraints),

Step 3.2. Determine degrees of freedom for optimization,

Step 3.3. Identification of important disturbances,

Step 3.4 . Optimization (nominally and with disturbances),

Step 3.5. Identification of candidate controlled variables,

Step 3.6. Evaluation of loss for alternative combinations of controlled variables (loss imposed by keeping constant setpoints when there are disturbances or implementation errors),

Step 3.7. Evaluation and selection (including controllability analysis).

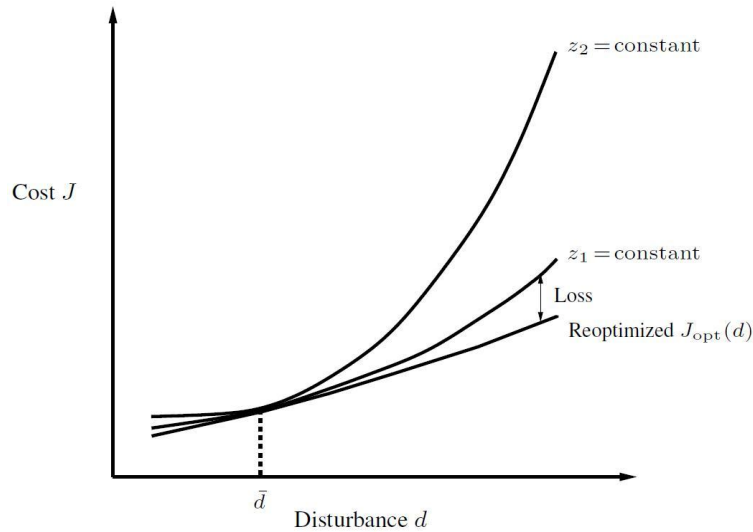


Figure 2.2 Loss  $L=J-J_{opt}(d)$ . Control of  $z_1$  compared to  $z_2$  results in smaller loss (difference with the reoptimized cost function) when disturbance occurs (Skogestad 2004)

### 2.1.3.1 Local methods

Rather than the cost  $J$ , we consider minimizing the closely related loss

$$L = J(u,d) - J_{opt}(d) \quad (2.2)$$

where  $u$  is the degrees of freedom and  $d$  is the disturbances. For each disturbance  $d$ , the cost  $J$  can be expressed in terms of a Taylor series around a moving optimum (Skogestad and Postlethwaite 1996).

$$J(u,d) = J_{opt}(d) + \underbrace{\left(\frac{\partial J}{\partial u}\right)_{opt}}_0 (u-u_{opt}(d)) + \frac{1}{2} (u-u_{opt}(d))^T \underbrace{\left(\frac{\partial^2 J}{\partial u^2}\right)_{opt}}_{J_{uu}} (u-u_{opt}(d)) + \dots \quad (2.3)$$

We eliminate the terms of order third and higher and assume the linear model between inputs (u) and controlled variables (c):

$$c = Gu + G_d d \quad (2.4)$$

where G and  $G_d$  are the steady-state gain matrix and disturbance model respectively. For a fixed d, we have  $c - c_{opt} = G(u - u_{opt})$ . If G is invertible we then get

$$u - u_{opt} = G^{-1}(c - c_{opt}) \quad (2.5)$$

Finally, the loss is expressed as a function of the controlled variables as below:

$$L = J - J_{opt} = \frac{1}{2}(c - c_{opt})^T G^{-T} J_{uu} G^{-1} (c - c_{opt}) \quad (2.6)$$

We look for a set of controlled variables with the minimum loss. Two methods for selection of the best controlled variables are explained: maximum gain rule and exact local methods.

#### 2.1.3.1.1 Maximum gain rule

The definition of maximum gain rule is as below (Skogestad and Postlethwaite 2005):

“Let G denote the steady-state gain matrix from inputs u (unconstrained degrees of freedom) to outputs z (candidate controlled variables). Scale the outputs using  $S_1$ :

$$S_1 = \text{diag} \left\{ \frac{1}{\text{span}(z_i)} \right\}, \quad \text{span}(z_i) = \max_{d,e} |z_i - z_{i,opt}| = \max_d e_{i,opt}(d) + \max_e |e_i| \quad (2.7)$$

where  $e_{i,opt}$  is optimization error and  $e_i$  is implementation error and assume that the worst-case combination of output deviations can occur in practice. Then to minimize the steady-state loss select controlled variables z that maximize  $\underline{\sigma}(S_1 G J_{uu}^{-1/2})$ .”

In this method the loss is formulated as below:

$$L_{\max} = \frac{1}{2} \frac{1}{\underline{\sigma}^2(S_1 G J_{uu}^{-1/2})} \quad (2.8)$$

For scalar case which usually happens in many cases the maximum expected loss is:

$$L_{\max} = \frac{|J_{uu}|}{2} \frac{1}{|S_1 G|^2} \quad (2.9)$$

In the scalar case  $J_{uu}$  does not matter for selecting the best controlled variable therefore the set with having the largest scaled gain ( $S_1 G$ ) will give the minimum loss.

Since the effect of disturbances and implementation error does not appear directly in calculating the loss, maximum gain rule cannot guarantee giving the best set with the minimum worst-case loss whereas exact local method explained in next section gives the best set. Maximum gain rule is useful for prescreening the sets of best controlled variables.

#### 2.1.3.1.2 Exact local method

Halvorsen et al. (2003) derived the following exact local method which gives the worst-case loss for each selected set of controlled variables. The set with the minimum worst-case loss is the best.

$$\text{worst-case Loss} = \frac{1}{2} \bar{\sigma}(M)^2 \quad (2.10)$$

$$M = J_{uu}^{1/2} (HG^y)^{-1} (H[FW_d \ W_n]) \quad (2.11)$$

$$F = G^y J_{uu}^{-1} J_{ud} - G_d^y \quad (2.12)$$

Here  $H$  is the selection matrix ( $c=Hy$ ),  $G^y$  is the gain of the selected measurements,  $J_{uu}$  is Hessian of the objective function with respect to unconstrained DOFs and  $J_{ud}$  is second derivative of objective function with respect to DOFs and disturbances. Alternatively, whereas the probability of occurring the worst-case disturbance is rare, one could replace the singular value  $\bar{\sigma}(M)$  by the Frobenius norm  $\|M\|_F$ , which represents the average loss (Kariwala et al. 2008), but this happens to give the same optimal  $H$  (Kariwala et al. 2008).  $F$  is the optimal sensitivity of the measurements with respect to disturbances. It can be found either by the expression 2.11, in which case one must also find gains,  $G_d^y$  from disturbances,  $d$  to measurements and  $J_{ud}$ , or numerically by reoptimization of the process in presence of different disturbances:

$$F = \frac{\Delta y^{\text{opt.}}}{\Delta d} \quad (2.13)$$

Based on our experience it is strongly recommended to find  $F$  numerically (from 2.13) by reoptimization of the process rather than calculating it from 2.11 which needs  $J_{uu}$  and is sensitive to errors as it needs several matrices that may not be consistent.  $F$  is the slope of the optimal sensitivity of the measurements respect to disturbances and should be linear in different magnitudes of disturbances.

Since there are usually a lot of candidate possible sets of measurements, Kariwala and Cao (2009) have developed a bidirectional branch and bound algorithm to find the optimal  $H$  using (2.10)-(2.12).

Skogestad (2000) explains the requirements for good controlled variables based on solutions of the local methods:

1. "Its optimal value is insensitive to disturbances." This implies to small  $F$  in exact local and small span ( $z_1$ ) in maximum gain rule. Note that this says that its optimal value and not its value because its value should be sensitive to disturbances so that it can be detected.
2. "It is easy to measure and control accurately." This implies that the implementation error is small (small  $W_n$  in exact local method and small  $e_i$  in maximum gain rule),
3. "Its value is sensitive to changes in the manipulated variables." This says that the gain from input to the controlled variable is large (so that  $G^{-1}$  is small)
4. "For cases with two or more controlled variables, the selected variables are not closely correlated." This is because gain matrix is not close to singular which results in a large  $G^{-1}$ .

By looking at the magnitude of worst-case/average loss, the necessity of combinations of measurements can be decided to get less loss compare to selection of individual self-optimizing measurements. We consider measurement combinations as  $CV=Hy$  where  $H$  is a "full matrix" in terms of the selected measurements, to get a smaller loss (Alstad et al. 2009). The optimal  $H$  is obtained by solving the following optimization problem.

$$\begin{aligned} \min_{\mathbf{H}} \|\mathbf{HY}\|_{\mathbf{F}}^2 \\ \text{s.t. } \mathbf{HG}^y = \mathbf{J}_{\text{uu}}^{1/2} \end{aligned} \quad (2.14)$$

where  $\mathbf{Y} = [\mathbf{FW}_d \ \mathbf{W}_n]$ . An analytical solution (Alstad et al. 2009) for 2.14 is:  $\mathbf{H}^T = (\mathbf{Y}\mathbf{Y}^T)^{-1} \mathbf{G}^y (\mathbf{G}^{yT} (\mathbf{Y}\mathbf{Y}^T)^{-1} \mathbf{G}^y)^{-1} \mathbf{J}_{\text{uu}}^{1/2}$ .

A partial branch and bound algorithm (Kariwala and Cao 2010) can be applied to find the best set of CVs with more measurements than number of unconstrained degrees of freedom.

#### 2.1.4 Step 4: Select location of throughput manipulator (TPM)

TPM definition (Aske and Skogestad 2009): “A TPM is a degree of freedom that affects the network flow and which is not directly or indirectly determined by the control of the individual units, including their inventory control.”

The production rate is usually set in the feed. This is mostly because the control system is usually decided at the design stage for a given feedrate, before building the plant. However during operation feed flowrate can also be considered as a degree of freedom. When the price of the products is high it will be economically optimum to produce as much as possible until reaching the “bottleneck” of the process. The rule is to set the production rate of the process at location of the bottleneck (Skogestad 2004) to optimize this mode of operation, where a lot of extra profit can be made. Note that location of the throughput manipulator is important since it determines the control structure of the remained inventory (level) control system and in addition it links the top-down and bottom-up parts of the procedure (Skogestad 2004; Aske and Skogestad 2009).

#### 2.1.5 Step 5: Select structure of regulatory control layer

The purpose of the regulatory layer is to “stabilize” the plant, preferably using a simple control structure with single-loop PID controllers (Skogestad 2004). “Stabilize” here means that the process does not “drift” away from acceptable operating conditions when there are disturbances. In addition, the regulatory layer should follow the setpoints given by the “supervisory layer”. Reassignments (logic) in the regulatory layer should be avoided. Preferably, the regulatory layer should be independent of the economic control objectives (regions of steady-state active constraints), which may change depending on disturbances, prices and market conditions (Skogestad 2004).

The main decisions are (Skogestad 2004):

- (a) Identify CV2s for the regulatory layer, these include “stabilizing” CVs, which are typically levels, pressures, reactor temperature and temperature profile in distillation column. In addition, active constraints (CV1) that require tight control (small back-off) may be assigned to the regulatory layer.
- (b) Identify pairings (MVs to be used to control CV2), taking into account:
  - Want “local consistency” for the inventory control (Aske and Skogestad 2009). This implies that the inventory control system is radiating around a given flow.
  - Avoid selecting as MVs in the regulatory layer, variables that may optimally saturate (steady-state), because this would require either
    - Reassignment of regulatory loop (complication penalty), or
    - Back-off for the MV variable (economic penalty)
  - Want tight control of important active constraints (to avoid back-off).

The general pairing rule is to “pair close” to achieve a small effective delay from input (MV) to outputs (CV2).

### 2.1.6 Step 6. Select structure of supervisory control

The aim is to control the primary (economic) controlled variables (CV1) using as manipulated variables (MVs) the setpoints to the regulatory layer or “unused” valves (from the original MVs). This layer is usually about a factor 10 or more slower than the regulatory layer. Since interactions are more important at longer time scales, multivariable control may be considered in this layer.

The control objectives for the supervisory control layer generally may change depending on the disturbances and active constraints. Therefore this CVs layer should perform switching during transition between the regions (Skogestad 2004; Skogestad 2011). Finally, this layer should supervise the lower stabilizing layer, for example to avoid MV saturation in stabilizing loops.

### 2.1.7 Step 7. Select structure of (or need for) optimization layer (RTO)

Real time optimization (RTO) layer is used to update the setpoints of the primary controlled variables when disturbances occur. The advantage of self-optimizing method is that it removes the necessity of RTO or at least it simplifies it by introducing the right controlled variables.

## 2.2 Case-studies

In this thesis, the general plantwide control procedure is applied to two important processes to select the best controlled variables (self-optimizing CVs). Different operational regions are considered. The simple control structures are designed and their performance is evaluated in presence of large disturbances. The processes, which are studied here, are:

1. Post-combustion CO<sub>2</sub> capturing processes
2. Converting of natural gas to liquid hydrocarbons (GTL)

### 2.2.1 Post-combustion CO<sub>2</sub> capturing processes

Greenhouse gases cause global warming and CO<sub>2</sub> is the major part of these emissions. Combustion of fossil fuels in power plants is one of the main sources of producing CO<sub>2</sub>. As the world energy demand increases, the need for fossil fuels is also increasing. 130% rise in CO<sub>2</sub> emissions is expected by 2050 and this magnitude could raise the global average temperatures by 6°C or probably even more (IEAReport 2008). Intergovernmental Panel on Climate Change (IPCC) has concluded that “Emissions must be reduced by 50% to 85% by 2050 if global warming is to be confined to between 2°C to 2.4°C” (IEAReport 2008). Therefore whereas fossil fuels are still the dominant sources of world energy supply, at least in next few decades, CO<sub>2</sub> capturing processes have an important role in succeeding the world climate plans.

Amine absorption/stripping processes are widely applied and studied as most mature technologies for CO<sub>2</sub> removal in downstream of the fossil fuel power plants. Figure 2.3 shows a CO<sub>2</sub> capturing process in downstream of a power plant.

These processes include two columns where in the first column (absorber), CO<sub>2</sub> is absorbed into lean amine solvent through fast reactions and the rich amine is sent to the second column (stripper) where the CO<sub>2</sub> content is stripped off. Stripping needs very high amount of energy that is supplied by the steam from power plant where its magnitude is around 15-30% of the net generated power in the power plant (Jassim and Rochelle 2005).

Since the required energy in the CO<sub>2</sub> plant is quite high and in addition the load from power plant may change a lot, economically optimal operation of this process is important to save

more energy. Therefore design a simple control structure which can handle a wide range of disturbances and operate the process close to optimum is a main part of this thesis.

Some other researchers have also been studying the operation of this process. Bedelbayev et al. (2008) have designed MPC to control the absorber only. Ziaii et al. (2009) have studied the dynamic modeling of the stripper only and considered two different configurations in order to operate the plant with the minimum energy requirement when the electricity price is high. Kvamsdal et al. (2009) have developed a dynamic model of the absorber only and considered the effect of load change from the power plant from 100% to 50%. Their model does not include stripper and recycle flow. Lawal et al. (2009) and Lawal et al. (2010) have developed an integrated CO<sub>2</sub> capture plant with a large scale power plant. They have considered the effect of change in CO<sub>2</sub> removal percentage and different amine (MEA) concentration on power plant efficiency and CO<sub>2</sub> capturing performance. In addition, the effect of reduction in power plant capacity has been investigated. However, magnitude of the disturbances is not so large.

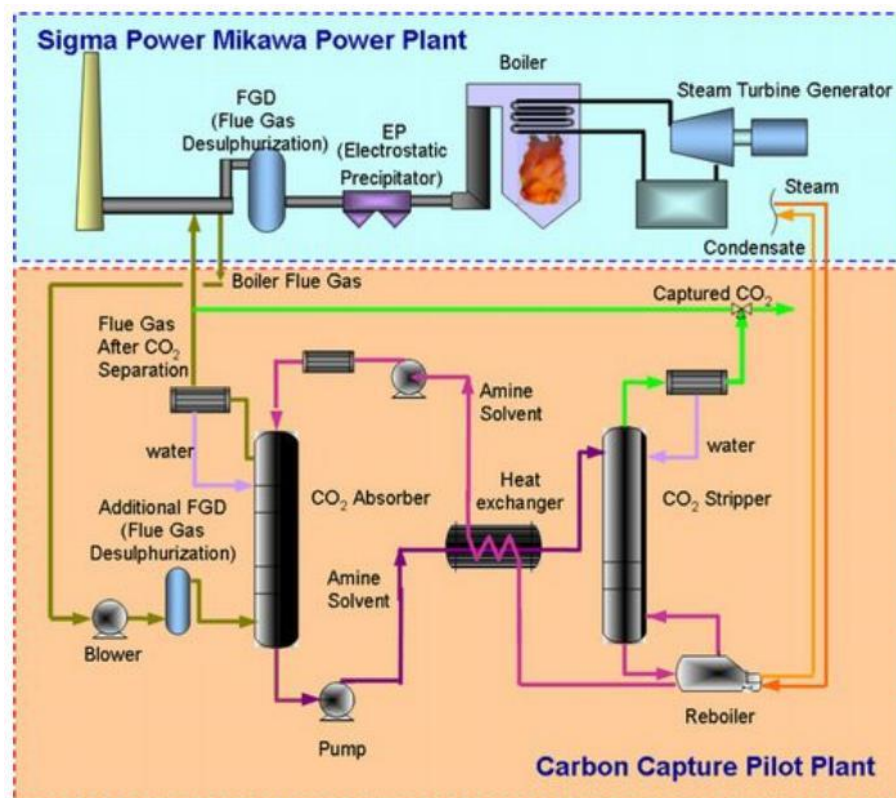


Figure 2.3 An amine absorption/stripping CO<sub>2</sub> capturing process (Toshiba 2008)

Lin et al. (2010) have also designed a plantwide control structure using dynamic simulation for CO<sub>2</sub> capture process. Their proposed structure is mostly based on intuitive understanding of the process and the range of the disturbances is not wide and only one operational region has been studied. Schach et al. (2010a) and Schach et al. (2010b) have investigated techno-economic analysis of CO<sub>2</sub> capturing plants with considering 4 different alternatives. They finally concluded that process with using intercooler in the absorber gives the minimum CO<sub>2</sub> avoided cost. Schach et al. (2011) have recently applied the self-optimizing method of Skogestad to find a control structure for their proposed CO<sub>2</sub> process configuration. Although a wide range of

change in load from power plant is studied, but only reduction in the load is included where there is no capacity constraint. Therefore only one operational region has been studied. In addition, validation of their proposed structure is needed. Jayarathna et al. (2011) have developed a simple dynamic model for the absorption column only and they try to model whole the process for the purpose of optimization and control.

To show the importance of optimal operation of this process, Figure 2.4, which has been plotted for two different CO<sub>2</sub> recovery % (90% in chapter 3 and 95.26% in chapters 4 and 5) illustrates that how required energy in the plant can be minimized by proper manipulating amine recycle flowrate in different CO<sub>2</sub> recovery percentages.

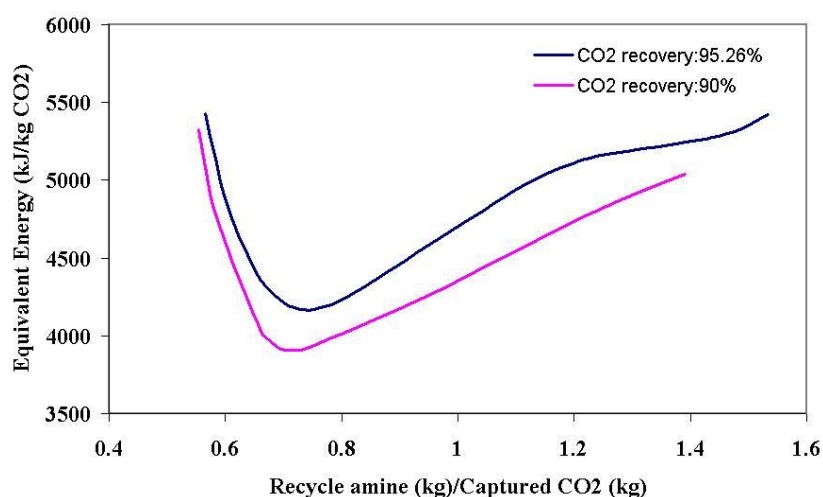


Figure 2.4 Dependency of equivalent energy in CO<sub>2</sub> capture plant verses recycle amine flowrate

Too small recycle requires extra energy in the stripper to make leaner amine, whereas a too large recycle also increases energy consumption. Especially one may expect a large energy penalty if the recycle is set too low.

In this thesis, plantwide control procedure is applied to select the best self-optimizing CVs in different active constraint (operational) regions corresponding the different magnitude of disturbances. Finally a simple control structure is synthesized in a systematic manner which works near-optimum in all operational regions. The proposed structure removes the need for switching logic (which is necessary in self-optimizing when transition regions) and the use of RTO for updating the setpoints.

### 2.2.2 Natural gas to liquid hydrocarbons (GTL) process

High prices of oil and stringent regulations on sulphur content of the fuels encourage the oil companies to look for new alternatives to produce cleaner fuels from other carbon sources. Among the new alternatives, converting the natural gas to hydrocarbon liquids (GTL) through Fischer-Tropsch reactions is one of the technologies which has been commercialized and is capable to produce clean fuels (almost sulphur free). Figure 2.5 shows the gas commercialization options and situation of GTL processes comparing to other possibilities of transportation, converting or usages. It shows that in the case of availability to supply at least 200 million scf/day natural gas and provided the distance to the markets is far away than 2500 km, GTL is more economical compared to other usages of natural gas.

Figure 2.6 illustrates a simple flowsheet of a GTL process. In GTL technology, methane in reaction with steam and oxygen first breaks to synthesis gas (syngas) which is a mixture of hydrogen and carbon monoxide. Syngas is then converted to a range of hydrocarbons through highly exothermic FT reactions. There are different routes for syngas production: auto-thermal reforming (ATR), steam reforming, combined reforming and gas heated reforming (Steynberg and Dry 2004). Fischer Tropsch reactions take place on either iron or Cobalt catalysts. If the desired product is gasoline, fixed bed reactor using iron catalyst in high FT temperatures (300-350°C) is the best and if the interest is in producing heavier hydrocarbons (diesel) then slurry reactor using Cobalt catalyst in low FT temperatures (200-240°C) is the best choice (Spath and Dayton 2003).

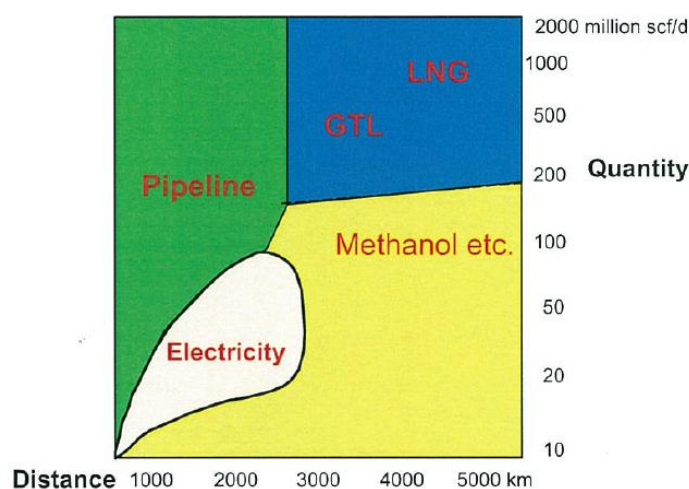


Figure 2.5 Gas commercialization options and situation of GTL processes (GTL-Workshop 2010)

FT products include a wide range of hydrocarbons mainly Olefins and Paraffins from methane ( $C_1$ ) to heavy waxes ( $C_{20+}$ ). The well-known Anderson-Schultz-Flory (ASF) model can describe the products distribution (see Figure 2.7). In ASF model weight fraction of the hydrocarbons is a function of chain growth probability ( $\alpha$ ). FT products are converted further in upgrading unit to the desired fuels. The currently largest operating GTL plant is the Oryx plant in Qatar with a production capacity of 34,000 bbl/day liquid fuels. This plant includes two parallel trains with two Cobalt based slurry bubble column FT reactors, each with the capacity of 17,000 bbl/day operating at low temperature FT conditions (LTFT). In this plant, syngas is produced using ATR technology.

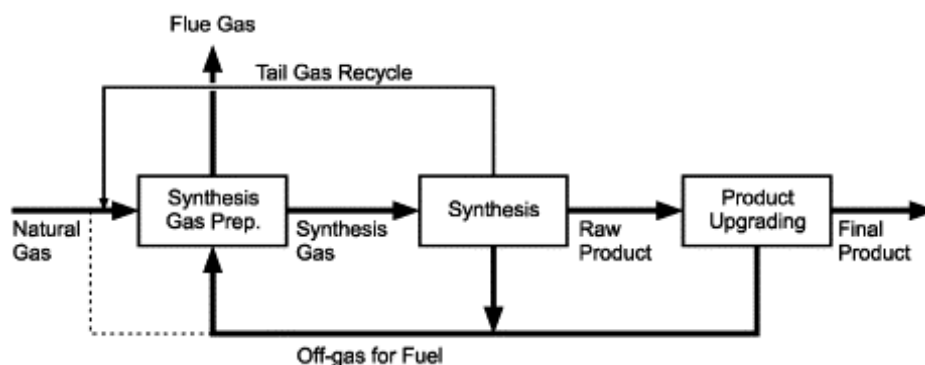


Figure 2.6 A simple flowsheet of a GTL process (Rostrup-Nielsen et al. 2000)

Shell is also commissioning a world scale GTL plant (Pearl GTL plant) in 2011 with the capacity of 260,000 bbl/day; 120,000 bbl/day upstream products and 140,000 bbl/day GTL products (Schijndel et al. 2011). This plant is also located close to Oryx GTL plant. Shell uses Cobalt based fixed bed reactors. Pearl GTL plant has 24 parallel fixed bed reactors each with the production capacity of 6,000 bbl/day (GTL-Workshop 2010).

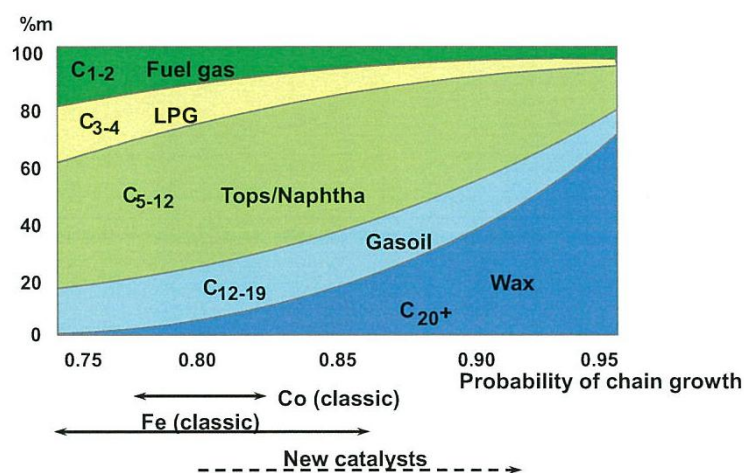


Figure 2.7 The relevance of Catalyst selectivity (GTL-Workshop 2010)

A few works are available in literature which study simulation and optimization of GTL process. In addition, in the available ones chain growth probability is assumed fixed which makes the FT products distribution independent of change in process variables like steam and oxygen to hydrocarbons ratio (syngas unit), recycles flowrate, Fired heater and ATR temperatures, etc. Kim et al. (2009) have simulated a GTL process in order to find optimum temperature conditions. In their work, because of difficulties in simulating the entire FT products by kinetics, CO conversion has been calculated in a spreadsheet and then using ASF with a fixed  $\alpha$ , FT products have been distributed in different stream. Bao et al. (2010) have also simulated a GTL process for the purpose of economic analysis where they use a fixed  $\alpha = 0.95$ . Schijndel et al. (2011) have started synthesizing a computational tool to support GTL process designs. Their focus is on design rather than operation. With our best knowledge about this process, the current work is the first that investigate the optimal operation of GTL process.

For optimal operation studies, we have tried to achieve a reasonable process model which can well describe the dependencies of all important parameters in whole process. A single train similar to Oryx GTL plant with the capacity of 17,000 bbl/day was simulated in UniSim process simulator. ATR is used for syngas production and Cobalt based slurry reactor is used for FT reactor. The obtained model was used to study two modes of operation. In mode I, natural gas feedrate is given and in mode II, natural gas is also a degree of freedom for optimization to achieve the maximum possible profit. Self-optimizing method of Skogestad was applied to select the best individual and combination of controlled variables for unconstrained degrees of freedom.

## Chapter 3

# Self-optimizing Control of a CO<sub>2</sub> Capturing Plant with 90% Recovery

This chapter is an extended version of the published paper “Self-Optimizing and Control Structure Design for a CO<sub>2</sub> Capturing Plant”, in book series “Advances in Gas Processing”, volume 2, pages 331-338

This chapter describes how the best controlled variables are selected using self-optimizing method and control structure is designed for a post-combustion CO<sub>2</sub> capturing process where a fixed recovery of 90% is the target.

Capturing and storing the greenhouse gas carbon dioxide (CO<sub>2</sub>) produced by power plants could play a major role in minimizing climate change. In this chapter a post-combustion CO<sub>2</sub> capture plant using MEA is designed, simulated, and optimized using the UniSim process simulator. The focus of this work is the subsequent optimal operation and control of the plant with the aim of staying close to the optimal operating conditions. The cost function to minimize is the energy demand of the plant. It is important to identify good controlled variables (CVs) and the first step is to find the active constraints, which should be controlled to operate the plant optimally. Next, for the remaining unconstrained variables, we look for self-optimizing variables which are controlled variables that indirectly give close-to-optimal operation when held at constant setpoints, in spite of changes in the disturbances. For the absorption/stripping process, a good self-optimizing variable was found to be a temperature close to the top (tray no.17) of the stripper. To validate the proposed structure, dynamic simulation was done and performance of the control structure was tested.

### 3.1 Introduction

Aqueous absorption/stripping with aqueous solvents such as MEA has been used effectively for removing acid gases (CO<sub>2</sub> and H<sub>2</sub>S) from natural gas, oil refineries, power plant flue gas and the production of ammonia and synthesis gas. Figure 3.1 shows a typical flow diagram of the process for a simple reboiled stripper. The system consists of two columns: the absorber, in which the CO<sub>2</sub> is absorbed into an amine solution via a fast chemical reaction, and the stripper, where the amine is regenerated and then sent back to the absorber for further absorption. Prior to CO<sub>2</sub> removal, particulates, sulfur dioxide, and NO<sub>x</sub> are removed from the flue gas. The flue gas from the power plant is typically cooled before the absorber from 150 to 55 °C (its adiabatic saturation temperature) or to 40 °C if cooling water is used.

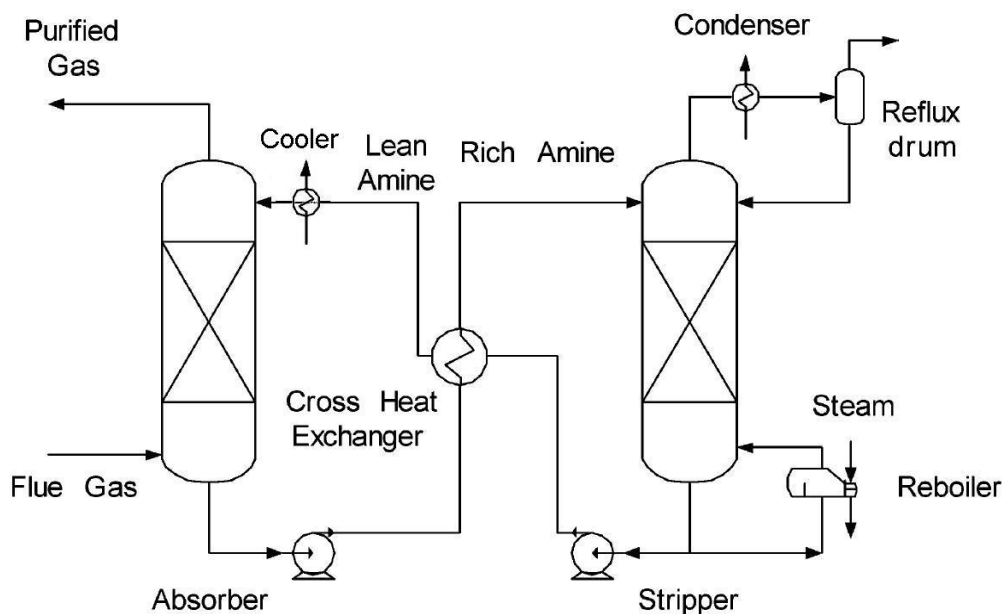


Figure 3.1 Typical absorber/stripper process for CO<sub>2</sub> capture (Jassim and Rochelle 2005)

One problem with using MEA as a solvent is the high cost of operation. This is simply due to the excessive energy requirement for solvent regeneration, which contributes about 70 per cent of the process utility cost. In fact, the energy consumption in the CO<sub>2</sub> capturing plant is estimated to be 15-30% of the net power production of a coal-fired power plant (Jassim and Rochelle 2005). A lot of work have been done to reduce energy consumption of CO<sub>2</sub> units, but little has been done on studying how this can be implemented in practice when the process is subjected to disturbances. This is the aim of the present study where we focus on selecting good controlled variables which can be kept at constant setpoints without the need to re-optimize when disturbances occur. To select the controlled variables we look for self-optimizing control, one may use the stepwise procedure of Skogestad (Skogestad 2004). The plant was modelled using the UniSim flowsheet simulator from Honeywell (UniSim 2008) using the amine package for the thermodynamic calculations.

## 3.2 Self-optimizing control of a CO<sub>2</sub> capturing plant

### 3.2.1 Step 1: Define objective function and constraints

In the CO<sub>2</sub> plant there are operational costs related to the two utilities: Steam (heat) for the reboiler of stripper and electricity (power) for driving the pumps. To avoid using prices we convert the heat to equivalent thermodynamic work (power). We assume that the temperature of steam in reboiler ( $T_H$ ) is 10°C higher than reboiler temperature and steam condenses at 40°C in the turbine ( $T_C$ ). The total equivalent work for the plant (the objective function) is then

$$W_{eq} = Q_r \left( 1 - \frac{T_C}{T_H} \right) \times \eta + W_{Pumps} \quad W_{eq} \left( \frac{\text{kJ}}{\text{kg CO}_2} \right) \quad (3.1)$$

Where  $T_H = T_C + 10$  [K] and  $T_C = 313$  K. The efficiency  $\eta$  of the imagined Carnot cycle (heat pump) that generates heat from power is assumed to be 75%.

The constraints are:

- 1- Environmental requirement: Capture 90% of CO<sub>2</sub>.
- 2- Temperature of lean solution to the absorber is 51°C (to get a good operation of the absorber).
- 3- Because of the MEA degradation problem, pressure should be less than 2 bar. Stripper top pressure is therefore kept at 1.8 bar.
- 4- The stripper condenser temperature should be as low as possible and is here assumed to be at 30°C.

### 3.2.2 Step 2. Determine DOFs for optimization

We have 9 valves (Figure 3.2) which give 9 dynamic degrees of freedom. However, there are 4 levels (2 in stripper, 1 in absorber, 1 surge tank) that need to be controlled and since these levels have no steady state effect, the number of degrees of freedom (DOFs) for steady-state optimization is 5.

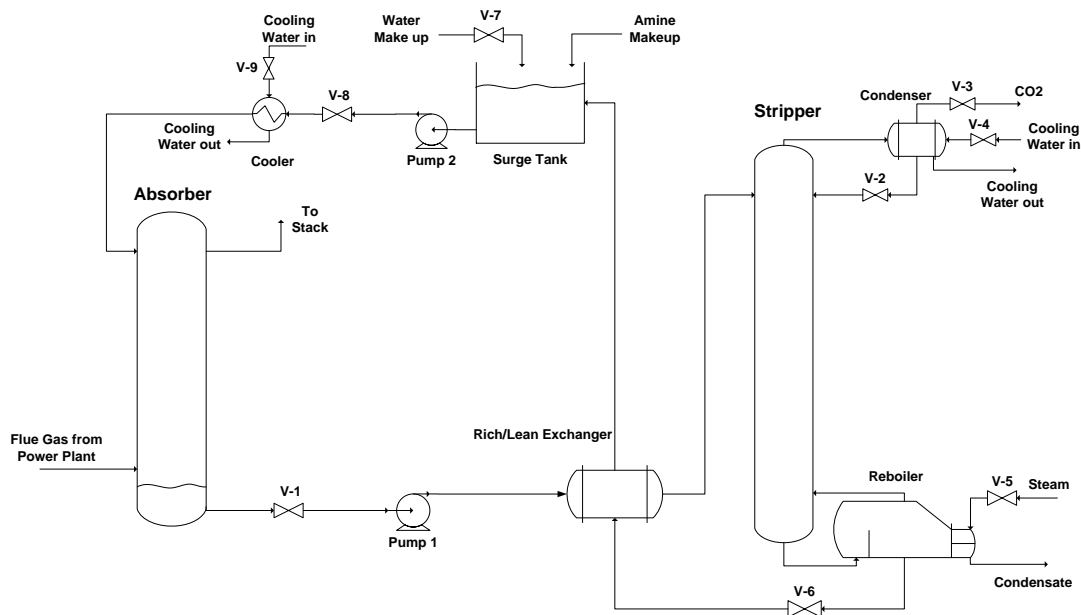


Figure 3.2 Process with 9 dynamic DOFs (valves)

### 3.2.3 Step 3. Identification of important disturbances

The main disturbances are the feed (flue gas) flow rate and its composition. In addition all active constraints should be considered as disturbances.

The objective function is defined as the energy per kg of removed CO<sub>2</sub> (which is a good objective for a given feedrate, but for cases where we would like to maximize the amount of treated gas), so small variations in the CO<sub>2</sub> recovery constraint have a small influence on the objective function. In practice, the inlet temperature of lean solution is around 51°C and even if it changes in the range 40-60°C has no effect on the energy consumption. The only equality constraint that may have significant effect on the objective function is change in pressure of the stripper.

Finally, we consider three main disturbances. (Table 3.1)

Table 3.1 Main disturbances

| Disturbance |                   | Nominal  | Change  |
|-------------|-------------------|--|---------|
| d1          | Gas flowrate      | 219.3 kmol/hr  | ±5%     |
| d2          | Gas composition   | CO <sub>2</sub> : 0.1176, N <sub>2</sub> : 0.7237, O <sub>2</sub> : 0.0502, H <sub>2</sub> O: 0.1085 | ±5%     |
| d3          | Stripper pressure | Top: 180 kPa, Bottom: 200 kPa  | +10 kPa |

### 3.2.4 Step 4. Optimization (nominally and with disturbances),

To control the 4 equality constraints we need 4 DOFs and we need 4 DOFs to control 4 levels then we have one degree of freedom left for optimization,  $N_{opt.free} = 9 - 4 - 4 = 1$ .

Objective function: min.  $W_{eq}$

Subject to: The four constraints in section 2.1 and:

$$5. \quad 0.005 \leq \text{CO}_2 \text{ fraction in bottom of stripper} \leq 0.05.$$

At the nominal operating (no disturbances) point we get:

$$\text{Optimal objective function: } W_{eq} = 640.5 \frac{\text{kJ}}{\text{kg CO}_2}$$

CO<sub>2</sub> composition in the bottom of stripper = 0.0227 (so the optimum is unconstrained).

### 3.2.5 Step 5. Identification of candidate controlled variables.

The remaining unconstrained DOF could for example be selected as the reboiler duty. However, rather than keeping it constant, it may be better to use it to control some other variables (CV), and we consider two alternatives:

1. Tray temperature at some stage in the stripper column.
2. CO<sub>2</sub> composition in the bottom of the stripper.

### 3.2.6 Step 6. Evaluation of loss

For evaluation and initial screening of the candidate controlled variables we use the maximum scaled gain rule (Skogestad and Postlethwaite 2005).

3.2.6.1 Procedure for scalar case (Jensen 2008):

1. Make a small perturbation in each disturbances  $d_i$  and re-optimize the operation to find the optimal disturbance sensitivity for each candidate CV,  $\frac{\partial \Delta y_{opt}}{\partial d_i}$ , where  $\Delta d_i$  denotes the expected

magnitude of disturbance  $i$ . From this we compute the overall optimal variation (here we choose the 2-norm):

(Skogestad and Postlethwaite 2005)

$$\Delta y_{\text{opt}} = \sqrt{\sum_i \left( \frac{\partial \Delta y_{\text{opt}}}{\partial d_i} \cdot \Delta d_i \right)^2} \quad (3.2)$$

2. Identify the expected implementation error  $n$  for each candidate controlled variable  $y$  (measurement).
3. Make a perturbation in the independent variables  $u$  (in our case  $u$  is reboiler duty) to find the unscaled gain ( $G$ ),

$$G = \frac{\Delta y}{\Delta u} \quad (3.3)$$

4. Scale the gain with the optimal span where  $n$  is implementation error to obtain for each candidate output variable  $y$ :

$$\text{Span } y = \Delta y_{\text{opt}} + n \quad (3.4)$$

The scaled gain is then:

$$|G'| = \frac{|G|}{\text{Span } y} \quad (3.5)$$

The worst-case loss  $L_{\text{wc}} = J(u,d) - J_{\text{opt}}(u,d)$  (the difference between the cost with a constant setpoint and re-optimized operation) is then for the scalar case:

$$L_{\text{wc}} = \frac{|J_{\text{uu}}|}{2} \frac{1}{|G'|^2} \quad (3.6)$$

Where  $J_{\text{uu}} = \frac{\partial^2 J}{\partial u^2}$  is the Hessian of the cost function  $J$ . In our case  $J = W_{\text{eq}}$ .

Note that  $J_{\text{uu}}$  does not matter for selecting CVs in the scalar case.

By using a Matlab script interfaced with UniSim, the scaled gains were found for different candidate CVs. The results are shown in Table 3.2.

Table 3.2 Scaled gain for different candidate CVs

| Candidate CV                | Scaled gain   | Candidate CV       | Scaled gain |
|-----------------------------|---------------|--------------------|-------------|
| CO <sub>2</sub> composition | 0.2463        | Temp. Gain Tray 10 | 0.1358      |
| Temp. Gain Tray 20          | 0.0203        | Temp. Gain Tray 9  | 0.151       |
| Temp. Gain Tray 19          | 0.056         | Temp. Gain Tray 8  | 0.108       |
| Temp. Gain Tray 18          | 0.1276        | Temp. Gain Tray 7  | 0.0788      |
| <b>Temp. Gain Tray 17</b>   | <b>0.2845</b> | Temp. Gain Tray 6  | 0.0614      |
| Temp. Gain Tray 16          | 0.2693        | Temp. Gain Tray 5  | 0.0499      |
| Temp. Gain Tray 15          | 0.2279        | Temp. Gain Tray 4  | 0.0409      |
| Temp. Gain Tray 14          | 0.1913        | Temp. Gain Tray 3  | 0.0334      |
| Temp. Gain Tray 13          | 0.1632        | Temp. Gain Tray 2  | 0.0264      |
| Temp. Gain Tray 12          | 0.1446        | Temp. Gain Tray 1  | 0.0200      |
| Temp. Gain Tray 11          | 0.1332        |                    |             |

From Table 3.2, the best candidate CV is found to be the temperature on tray no. 17. The CO<sub>2</sub> composition has also a good (high) scaled gain but it is still ranked 3<sup>rd</sup> after temperature of tray

no.16. To validate the proposed controlled variable, dynamic simulation were performed in the next step.

### 3.3 Dynamic simulation

To switch to the dynamic mode in the UniSim simulator, sizing of the equipments and pressure flow specification was done. There is some discrepancy between the steady- state and dynamic models which seems to be caused by a difference in the thermodynamic models used by UniSim for two modes. The main effect is that recycle amine flow between the columns is smaller, which results in a smaller objective function ( $W_{eq}$ ) in the dynamic case. For our purposes this does not matter very much and the relative order of the control structures remains the same.

All control loops were implemented and tuned individually using the SIMC method (Skogestad 2003). The final control structure with 9 feedback loops is shown in Figure 3.3 for the proposed case where the CV is stripper tray temperature no.17. The paring of the loops is quite obvious in this case and is based on minimizing the effective time delay from inputs to outputs. The reboiler duty is used as the MV to control tray temperature no. 17.

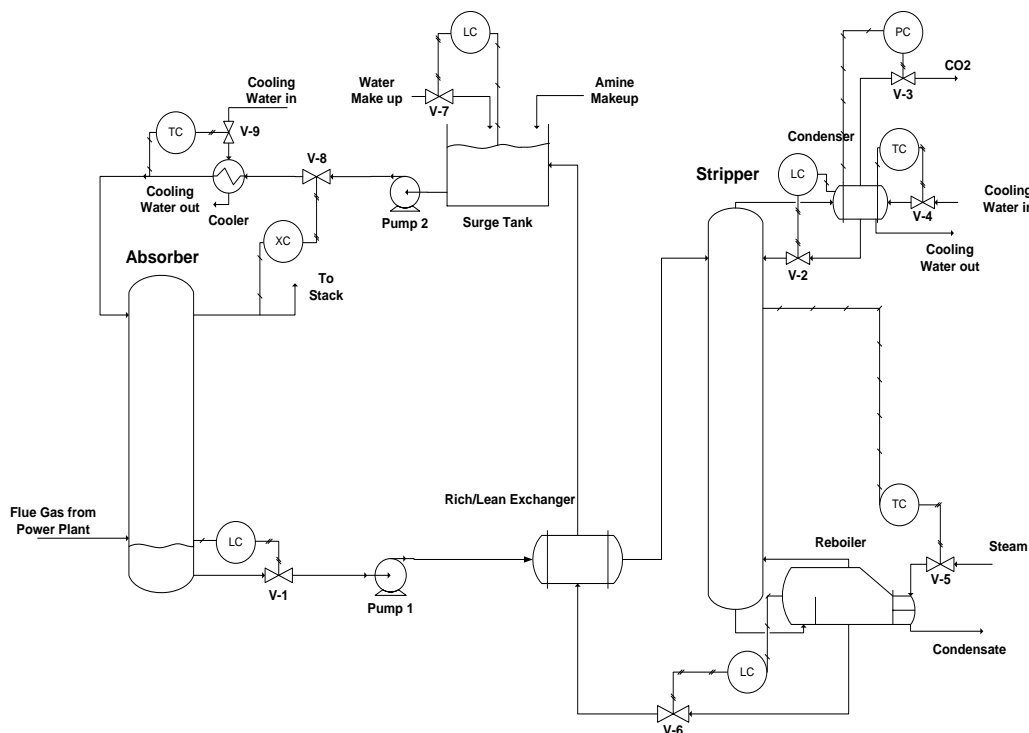


Figure 3.3 Process flowsheet with control loops

Figure 3.4a shows the performance of the proposed structure. This can be compared to the case where bottom temperature (tray no.1 is controlled (Figure 3.4b) which results in larger losses, especially at steady-state for the pressure disturbance (disturbance 6).

As expected the losses are also small if we control the CO<sub>2</sub> composition in the bottom of stripper (Figure 3.4c). However, temperature control is much easier, faster and cheaper than

composition. Therefore, control temperature of tray no.17 that we found by self-optimizing concept is the best controlled variable.

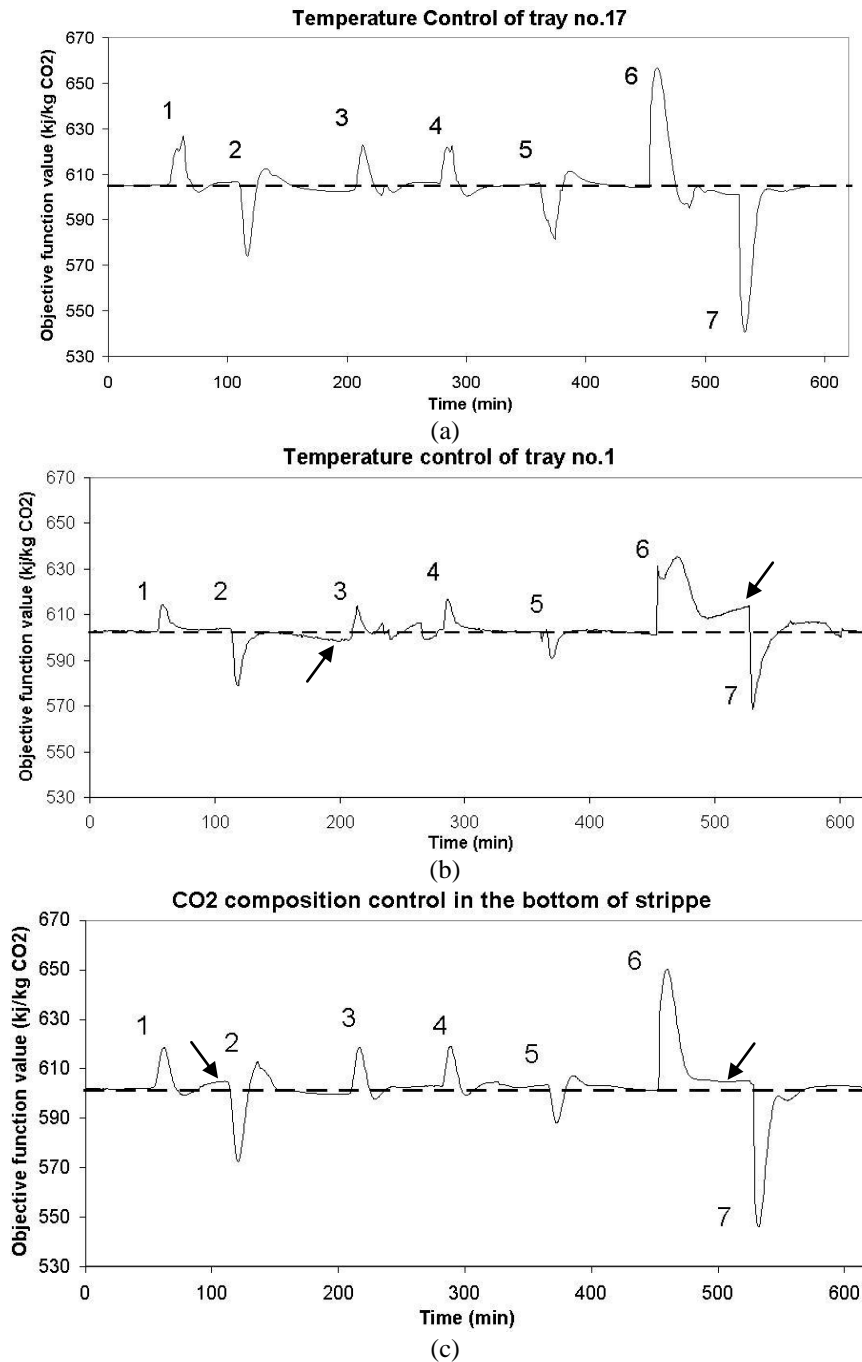


Figure 3.4 Objective function ( $W_{eq}$ ) in presence of disturbances 1) d1:+5% change from base case, 2) d1:-10%, 3) back to base case 4) d2:+5% change from base case 5) back to base case, 6) d3:+10 kPa, 7) back to base case. Arrows indicate cases with large steady-state losses.

Note that the loss that we imply in Figure 3.4 is not the same loss that is talked in self-optimizing procedure but it can be a good index to show the deviation of the objective function from the optimal nominal value.

### 3.4 Stability of the proposed control structure against large disturbances

In this section, stability of the proposed control structure in presence of large changes in flue gas flowrate is considered. We have assumed a minimum allowable of 80% CO<sub>2</sub> recovery for the process.

#### 3.4.1 Use of traditional PI controllers

Figure 3.5 shows the performance of the structure in Figure 3.3. Flue gas flowrate increases gradually with interval of +5% (Figure 3.5a). Behavior of the structure shows that before saturation of reboiler duty (Figure 3.5b), self-optimizing CV (Figure 3.5c) and CO<sub>2</sub> recovery (Figure 3.5d) are kept in their setpoints. With saturation of the reboiler duty which happens when flue gas increases by +25%, temperature control is not controlled in its setpoint while CO<sub>2</sub> recovery is still controlled at 90%. Further increase in flue gas flowrate (+30%) results in significant decline in temperature and accumulation of CO<sub>2</sub> in the process due to insufficient heat input in the stripper. This makes whole the structure unstable. Minimum allowable CO<sub>2</sub> recovery is also violated.

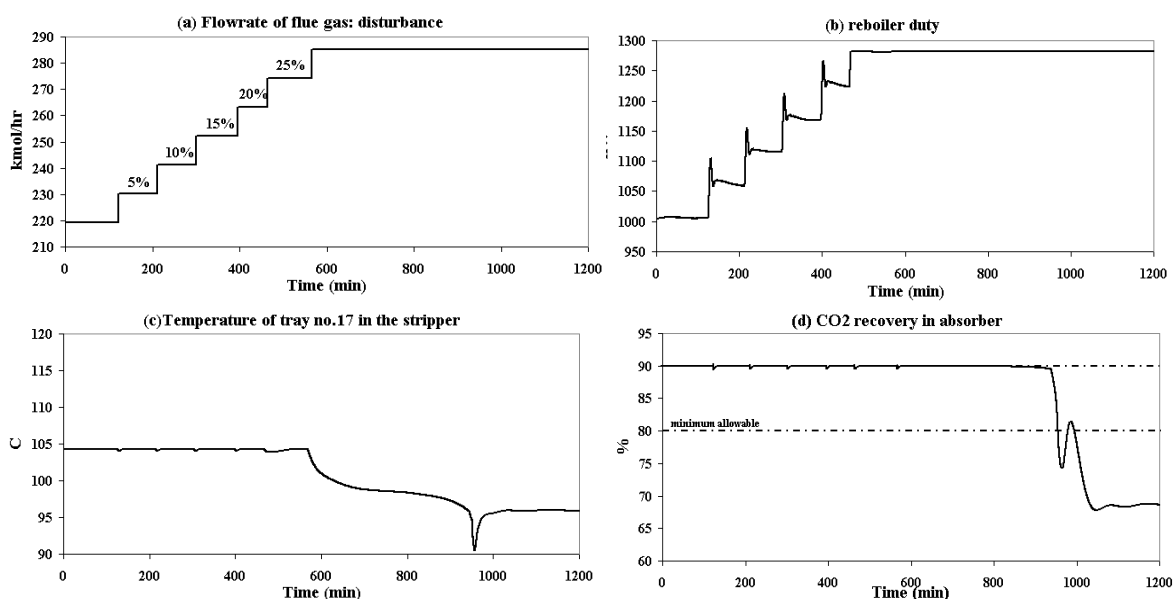


Figure 3.5 Performance of the proposed control structure in presence of large flue gas flowrates

To overcome this problem the idea is to give up CO<sub>2</sub> recovery control when reboiler duty saturates and control the temperature of tray no. 17 in the stripper using recycle amine flowrate. Note that in general, self-optimizing CVs are valid as long as a new active constraint has not come to the picture. With saturation of heat input in the stripper, the optimal is to repeat self-optimizing procedure and find the best new CV but here we control the same self-optimizing CV found before saturation also in the new operational region. We discuss these issues in details in chapters 4 and 5.

Figure 3.6 shows performance of the reconfigured control structure which can handle further increase in flue gas flowrate while reboiler duty has been saturated. When flowrate of flue gas increases by +41%, CO<sub>2</sub> recovery of 80% is met.

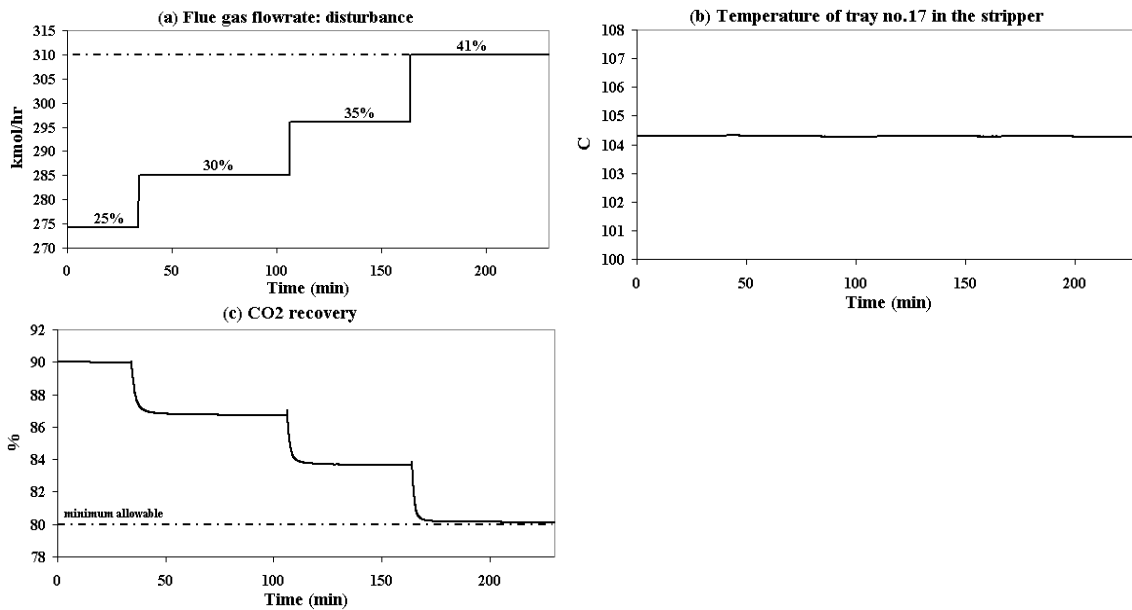


Figure 3.6 Performance of the reconfiguration of the control structure when reboiler duty saturates

### 3.4.2 Using of a multivariable controller in the proposed structure

As it was shown in the previous section, we used recycle amine flowrate to control CO<sub>2</sub> recovery and reboiler duty to control the self-optimizing CV. With saturation of the reboiler duty, recycle amine was used to control temperature of the stripper. This idea could overcome the instability of the initial proposed control structure in presence of higher flue gas flowrates. Due to having such strong interactions from one input to two different CVs, applying a multivariable controller can be useful. Therefore we used Robust Model Predictive Control Technology (UniSim 2008) to control some parts of the proposed control structure. To design and implement this controller we define 2 MVs (recycle amine flowrate and reboiler duty) + 1 disturbance (change in flue gas flowrate) as inputs and 2 CVs (CO<sub>2</sub> recovery and temperature of tray no. 17 in the stripper) as outputs. Identification of the model is done using Profit Design Studio (PDS 2007) and then the controller is built in the same software. We load the controller in UniSim Flowsheet and consider the performance against changes in flue gas flowrates.

Figure 3.7 shows the performance. As it has been shown, this controller is able to overcome the large disturbances even when reboiler duty has been saturated.

In chapters 4 and 5 we define a new objective function for operating of this process where we introduce tax on released CO<sub>2</sub> to the air. This results in having 2 unconstrained degrees of freedom that is more complicated to be solved. We follow in details the Skogestad's plantwide control procedure and discuss application of decentralized PI controllers and MPC in different operational regions.

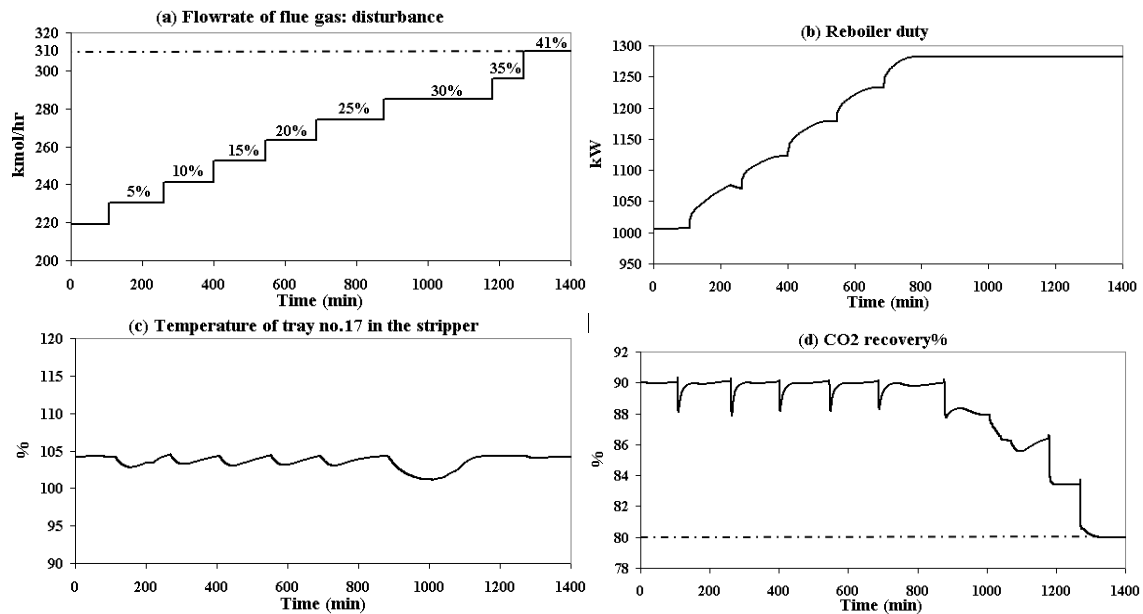


Figure 3.7 application of a multivariable controller (RMPCT) to control a part of the proposed control structure

### 3.5 Conclusions

A self-optimizing concept control structure was designed for a post-combustion CO<sub>2</sub> capturing plant where a fixed recovery of 90% was the target. The losses are small which means that it is not necessary to re-optimize the process when different disturbances occur. The plant has 9 dynamic degrees of freedom; 4 of them were used to control equality constraints and 4 of them were used for level control. We found the temperature close to the top (tray no. 17) of the stripper to be a good CV for the remaining unconstrained degree of freedom.

The proposed structure can handle the increase in flue gas flowrates up to +25% where saturation of reboiler duty happens. With saturation of reboiler duty, we reconfigured the control structure; CO<sub>2</sub> recovery is given up and the temperature of the stripper is controlled using recycle amine although the optimal is to find the new best self-optimizing CV that is a disadvantage of this method. In addition a multivariable controller was implemented that the results show almost the same performance as the reconfigured decentralized control structure.

In chapters 4 and 5, we discuss in details, selecting of the self-optimizing CVs in different operational regions with a modified objective function and we try to reach a single control structure that can handle all regions with a small loss comparing with the optimal structure at each region.

## Chapter 4

# Optimal Operation of CO<sub>2</sub> Capturing Process, Part I: Selection of Controlled Variables

This chapter is based on the published paper “Economically Efficient Operation of CO<sub>2</sub> Capturing Process; Part I: Self-optimizing Procedure for Selecting the Best Controlled Variables”, in *Journal of Chemical Engineering and Processing: Process Intensification*, 50 (2011), 247-253

In this chapter, we study optimal operation of a post-combustion CO<sub>2</sub> capturing process where optimality is defined in terms of a cost function that includes energy consumption and penalty for released CO<sub>2</sub> to the air. Three different operational regions are considered.

In region I, with a nominal flue gas flowrate, there are two optimally unconstrained degrees of freedom (DOFs) and the corresponding best self-optimizing controlled variables (CVs) are found to be the CO<sub>2</sub> recovery in the absorber and the temperature at tray no. 16 in the stripper. In the region II, with an increased flue gas flowrate, the heat input is saturated and there is one unconstrained DOF left. The best CV is temperature at tray no. 13 in the stripper. In region III, when the flue gas flowrate is further increased, the process reaches the minimum allowable CO<sub>2</sub> recovery of 80% and there is no unconstrained DOF. We have then reached the bottleneck and a controller is needed to adjust the feed flowrate to avoid violating this minimum.

The exact local method and the maximum gain rule are applied to find the best CVs in each region.

## 4.1 Introduction

Fossil fuel power plants are one of the major sources of world energy. However, the combustion of fossil fuels invariably produces the greenhouse gas CO<sub>2</sub> that causes global warming. Due to the effect of CO<sub>2</sub> emissions on global warming, different countries are starting to impose taxes or regulations on the amount of CO<sub>2</sub> released to the air.

We consider an absorption/stripping amine process to remove most of the CO<sub>2</sub> from the combustion flue gas stream. Figure 4.1 shows a typical CO<sub>2</sub> capturing process. In the first column (absorber), CO<sub>2</sub> in the flue gas is absorbed into a 30 wt% monoethanolamine (MEA) solution at atmospheric pressure.

The rich amine with about 5.3 mole% CO<sub>2</sub> is pumped to the second column (stripper) after preheating it by the recycled lean cooling amine solution which contains about 2.3 mole% CO<sub>2</sub>. In the stripper, CO<sub>2</sub> is stripped off at a pressure lower than 2 bar.

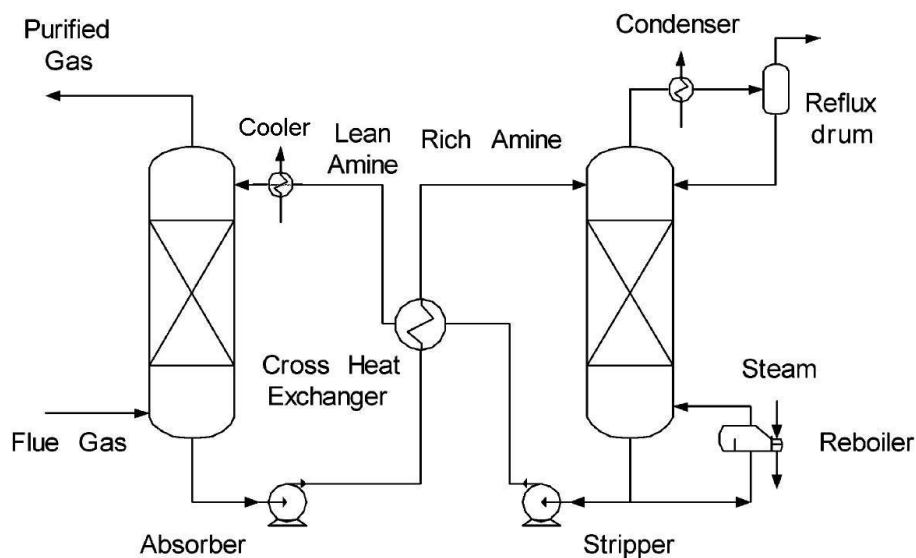


Figure 4.1 Flowsheet of typical absorption/stripping CO<sub>2</sub> process (Jassim and Rochelle 2005)

The energy consumption in the reboiler of the stripper is very large; typically around 15-30% of the net power generated of a coal-fired power plant (Jassim and Rochelle 2005). To operate the process optimally in presence of different disturbances, Skogestad (Skogestad 2004) has developed a systematic procedure based on self-optimizing control to find the best controlled variables (CVs). The idea is that the process is indirectly kept close to its optimum when the CVs are held constant at their optimal nominal setpoints.

The proposed plantwide control procedure consists of two main parts:

- I- A top-down analysis to optimize the process for various disturbances and identify primary self-optimizing controlled variables.
- II- A bottom-up analysis to identify secondary controlled variables and find the structure of the control system (pairing).

In the present work, the top-down analysis is performed for three different operational regions for the CO<sub>2</sub> capturing process. An operation region is here defined as a region with a given set

of active constraints. In general, we want to find good control policies for all active constraints regions.

Region I: The flowrate of the flue gas is at its nominal value and there are two unconstrained degrees of freedom.

Region II: The flowrate of the flue gas is increased so that the reboiler duty saturates and there is one unconstrained degree of freedom left.

Region III: The flowrate of the flue gas is increased further so that the minimum allowable CO<sub>2</sub> recovery is reached and the remaining unconstrained degree of freedom is saturated.

In chapter 3 (Panahi et al. 2010), we designed the control structure using this method when a fixed amount of CO<sub>2</sub> (90%) was removed from the flue gas stream and the objective was to minimize the energy usage. In this study, there is a tax on the CO<sub>2</sub> released to the air which makes it optimal to remove more of the CO<sub>2</sub> to get an optimal trade off between CO<sub>2</sub> removal and energy usage. The UniSim (UniSim 2008) process simulator with the Amine thermodynamic package is used for the simulations. The simulation is based on data from a pilot plant (J. N. Knudsen 2007) that recovers around 1ton/hr CO<sub>2</sub>, corresponds to that produced in a 1MW coal-fired power plant. The Nominal optimal data for the process are given in Figure 4.2. The feed flue gas at 48°C is assumed to be saturated with water.

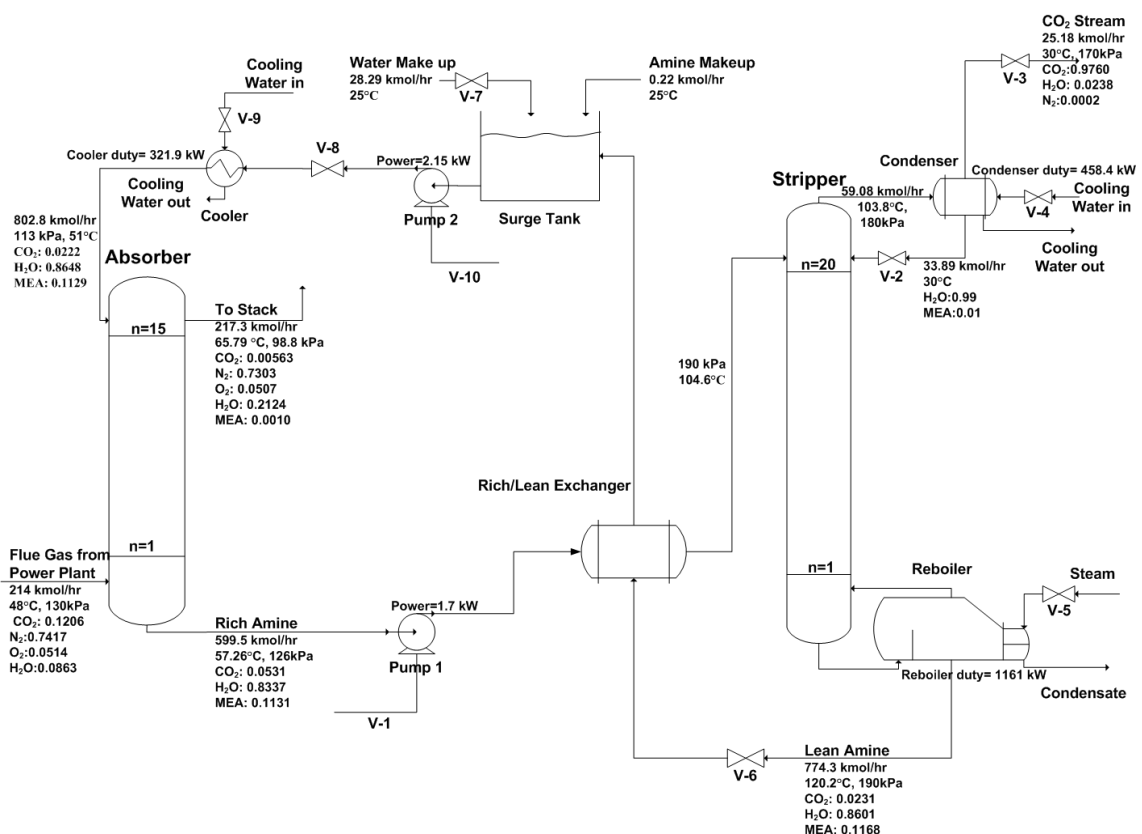


Figure 4.2 Process with 10 dynamic DOFs (valves)

## 4.2 Top down analysis: Self-optimizing control of CO<sub>2</sub> capturing process

### 4.2.1 Region I: Flowrate of flue gas is given

The steps of the top-down analysis are as follows.

#### 4.2.1.1 Step 1- Define objective function and constraints

In general, the cost function should be the negative profit of the process. However in cases where we consider only part of the plant like a utility or an auxiliary unit, other cost functions may be more relevant. We assume there is a penalty of 50 USD/ton on CO<sub>2</sub> released to the environment or equivalently a price of 50 USD/ton CO<sub>2</sub> captured which must be traded against the energy required for CO<sub>2</sub> removal in the stripper and work for the pumps. The reboiler energy is converted to power via a factor  $f$  which assumes that the energy used in the reboiler could have been used to produce power (Jassim and Rochelle 2005). The total required equivalent work of the reboiler and pumps is then:

$$W_{\text{Total}} = Q_{\text{reboiler}} f + W_{\text{Pumps}} \quad (4.1)$$

The pumps include pump 1 and pump 2 in Figure 4.2 plus the pumps for cooling water in the condenser and cooler which are not shown in the flowsheet. The power price is assumed to be 0.063 USD/kWh (Goldstein 2010) and the conversion factor is  $f = \left(1 - \frac{T_c}{T_H}\right) \times \eta$  where

$T_H = T_{\text{reboiler}} + 10$  [K] and  $T_c = 313$  K. The efficiency  $\eta$  is assumed to be 75%. We have not included the feed flue gas blower, but this does not change the conditions, since the blower power is very weakly dependent on the operation of the absorber/stripper system.

The objective is to get an optimal trade off between the cost of CO<sub>2</sub> released to the air and the energy usage in the process to strip off the removed CO<sub>2</sub>. Since we are considering an individual unit we divide the cost by the amount of flue gas to remove the effect of the feed rate. The cost to be minimized is then:

$$J \left[ \frac{\text{USD}}{\text{kg}_{\text{flue gas}}} \right] = \frac{W_{\text{Total}} (\text{kW}) \times 0.063 \frac{\text{USD}}{\text{kWh}} + \dot{m}_{\text{CO}_2 \text{ in purified flue gas}} \left( \frac{\text{kg}}{\text{h}} \right) \times 0.05 \frac{\text{USD}}{\text{kg}}}{\dot{m}_{\text{flue gas}} \left( \frac{\text{kg}}{\text{h}} \right)} \quad (4.2)$$

We consider the following inequality constraint:

1- For environmental reasons at least 80% of the CO<sub>2</sub> must be removed,

and the following four equality constraints:

- 2- The temperature of the lean solution to the absorber is kept at 51°C to get good operation in absorber; see also the discussion,
- 3- The stripper top pressure is kept at 1.8 bar to avoid MEA degradation. At higher pressures, the bottom temperature will be above 120°C which will increase significantly amine degradation (Davis and Rochelle 2009),
- 4- The stripper condenser temperature is kept at 30°C, which is assumed to be the lowest achievable temperature. A low temperature is desired because it reduces the compression work for the captured CO<sub>2</sub> in the downstream process.
- 5- The outlet pressure of pump 2 should be 4 bar to transfer the recycle lean amine to the top of the absorber.

In addition, all flowrates must be non-negative and we assume maximum capacities compared to nominal values for the reboiler duty (+20%), cooler (+50%) and pumps (+40%).

#### 4.2.1.2 Step 2. Identify DOFs for optimization (Panahi et al. 2010)

We have 8 valves and 2 pumps (Figure 2) which give 10 dynamic degrees of freedom. However, there are 4 levels (1 in absorber, 2 in stripper, 1 surge tank) that need to be controlled and since these levels have no steady state effect, the number of degrees of freedom (DOFs) for steady-state optimization is 6. Note that there is no bypass on the rich/lean heat exchanger because maximum heat exchange (zero bypass) is optimal. The small amine make up flowrate is not considered as a degree of freedom because it is assumed that it is adjusted to keep the amine concentration constant.

#### 4.2.1.3 Step 3. Identification of important disturbances (Panahi et al. 2010)

The main disturbances are the feed (flue gas) flow rate and its composition. In addition, the active constraints should generally be considered as disturbances. The stripper top pressure is included as a disturbance and this also takes into account changes in pressure drop due to load changes.

#### 4.2.1.4 Step 4. Optimization (nominally and with disturbances),

To control the 4 equality constraints we need 4 DOFs and we need 4 DOFs to control the 4 levels which have no steady-state effect. There are then two degrees of freedom left for optimization,

$$N_{\text{opt.free}} = 10 - 4 - 4 = 2$$

These may be viewed as the CO<sub>2</sub> recovery ( $u_1 \geq 80\%$ ) in the absorber and the CO<sub>2</sub> mole fraction at the bottom of stripper ( $u_2 \geq 0$ ), but note that this choice is not unique and any independent set variables can be selected as “base” DOFs.

By optimization, we find for the nominal operating point (no disturbances) that the two remaining DOFs are unconstrained:

CO<sub>2</sub> recovery,  $u_1 = 95.26\%$

CO<sub>2</sub> mole fraction at the bottom of stripper,  $u_2 = 0.0231$

Optimal objective function = 2.526 USD/ton flue gas

#### 4.2.1.5 Step 5. Identification of candidate controlled variables

To find the best set of two single measurements (CVs) for the two unconstrained DOFs, we consider 39 candidate measurements, including the two DOFs:

1. CO<sub>2</sub> recovery in the absorber,  $u_1$ , ( $y_1$ )
2. CO<sub>2</sub> mole fraction at the bottom of the stripper,  $u_2$ , ( $y_2$ )
3. Tray temperature of absorber column, 15 possible stages, ( $y_3$ - $y_{17}$ )
4. Tray temperature of stripper column, 20 possible stages, ( $y_{18}$ - $y_{37}$ )
5. Recycle lean amine flowrate ( $y_{38}$ )
6. Reboiler duty ( $y_{39}$ )

#### 4.2.1.6 Step 6. Selection of CVs

One of the main assumptions in the methods used below is that the cost function has quadratic behavior around optimal point and is twice differentiable. Figure 4.3 confirms this assumption in our case.

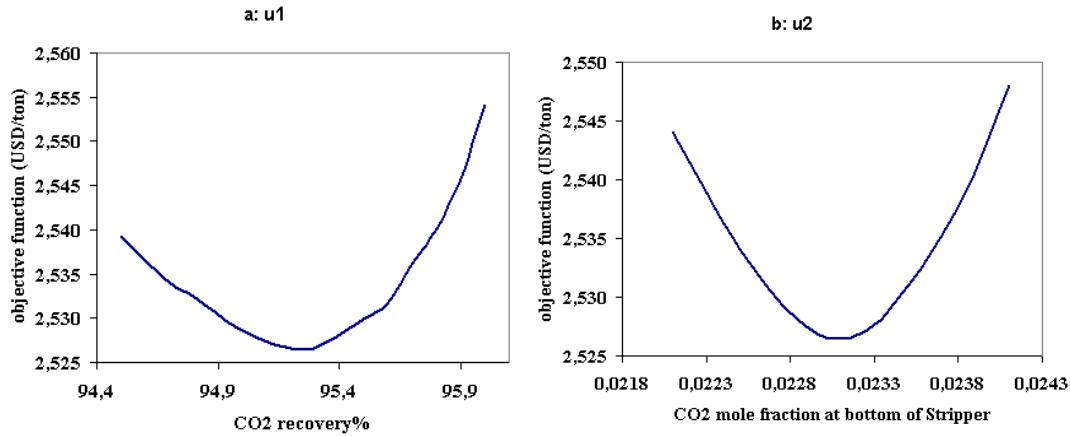


Figure 4.3 quadratic behavior of the objective function around optimal point in the region I  
a: CO<sub>2</sub> recovery, b:CO<sub>2</sub> composition at the bottom of the stripper

To find the best set of two CVs, we apply the exact local method which gives the worst case loss  $\bar{\sigma}(M)$  imposed by each candidate CV set (Halvorsen et al. 2003). The set with the minimum worst-case loss is the best.

$$\text{worst-case Loss} = \frac{1}{2} \bar{\sigma}(M)^2 \quad (4.3)$$

$$M = J_{uu}^{1/2} (HG^y)^{-1} (H[FW_d \ W_n]) \quad (4.4)$$

$$F = G^y J_{uu}^{-1} J_{ud} - G_d^y \quad (4.5)$$

Here  $H$  is the selection matrix ( $c=Hy$ ),  $G^y$  is the gain of the selected measurements,  $J_{uu}$  is Hessian of the objective function with respect to unconstrained DOFs and  $J_{ud}$  is second derivative of objective function with respect to DOFs and disturbances. Alternatively, one could replace the singular value  $\bar{\sigma}(M)$  by the Frobenius norm,  $\|M\|_F$  which represents the average loss (Kariwala et al. 2008), but this happens to give the same optimal  $H$  (Kariwala et al. 2008).

$F$  is the optimal sensitivity of the measurements with respect to disturbances. It can be found either by the expression (4.5), in which case one must also find gains,  $G_d^y$  from disturbances,  $d$  to measurements and  $J_{ud}$ , or numerically by reoptimization of the process in presence of different disturbances:

$$F = \frac{\Delta y^{\text{opt.}}}{\Delta d} \quad (4.6)$$

Based on our experience it is strongly recommended to find  $F$  numerically (from 4.6) by reoptimization of the process rather than calculating it from (4.5) which needs  $J_{uu}$  and is sensitive to errors as it needs several matrices that may not be consistent.  $F$  is the slope of the optimal sensitivity of the measurements respect to disturbances and should be linear in different magnitudes of disturbances. We chose a magnitude of 5% for disturbances ( $\Delta d$ ) and reoptimized the process to get the optimal sensitivity. In our case where we have 39 candidate measurements and 3 disturbances, the size of matrix  $F$  is  $39 \times 3$ . To see how the matrices are

found, the reader is referred to reference (de Araújo et al. 2007). Finally, the expected magnitude of individual disturbances ( $W_d$ ) and magnitude of the implementation error of CVs ( $W_n$ ) must be specified. Table 4.1 and Table 4.2 show these data for our case.

Table 4.1 Expected magnitude of individual disturbances

|       | $d_1$ : flowrate of flue gas | $d_2$ : composition of CO <sub>2</sub> in flue gas | $d_3$ : pressure of stripper |
|-------|------------------------------|--|------------------------------|
| $W_d$ | 20%                          | 10%  | 30 kPa                       |

Table 4.2 Magnitude of the implementation error for CVs

|       | CO <sub>2</sub> recovery | temperature | composition | flowrate | reboiler duty |
|-------|--------------------------|-------------|-------------|----------|---------------|
| $W_n$ | 0                        | 1°C         | 0.1%        | 10%      | 10%           |

Kariwala and Cao (2009) have developed a bidirectional branch and bound algorithm to find the optimal H using (4.3)-(4.5). We applied this algorithm, except that we found F from (4.6), and the results are shown in Table 4.3.

Table 4.3 The best candidate CV sets in region I

| Rank of sets | CVs   |  | worst case loss (USD/ton flue gas) |
|--------------|---|--|------------------------------------|
| 1            | $y_1$ :CO <sub>2</sub> recovery                   | $y_{33}$ :Temperature on tray no. 16 in the stripper | 0.0057                             |
| 2            | $y_1$ :CO <sub>2</sub> recovery                   | $y_{32}$ :Temperature on tray no. 15 in the stripper | 0.0064                             |
| 3            | $y_1$ :CO <sub>2</sub> recovery                   | $y_{34}$ :Temperature on tray no. 17 in the stripper | 0.0067                             |
| 4            | $y_1$ :CO <sub>2</sub> recovery                   | $y_{31}$ :Temperature on tray no. 14 in the stripper | 0.0092                             |
| 5            | $y_1$ :CO <sub>2</sub> recovery                   | $y_{35}$ :Temperature on tray no. 18 in the stripper | 0.0130                             |
| 6            | $y_1$ :CO <sub>2</sub> recovery                   | $y_{30}$ :Temperature on tray no. 13 in the stripper | 0.0174                             |
| 7            | $y_5$ : Temperature on tray no. 3 in the absorber | $y_{33}$ :Temperature on tray no. 16 in the stripper | 0.0198                             |
| 8            | $y_5$ : Temperature on tray no. 3 in the absorber | $y_{32}$ :Temperature on tray no. 15 in the stripper | 0.0202                             |
| 9            | $y_5$ : Temperature on tray no. 3 in the absorber | $y_{34}$ :Temperature on tray no. 17 in the stripper | 0.0206                             |
| 10           | $y_5$ : Temperature on tray no. 3 in the absorber | $y_{31}$ :Temperature on tray no. 14 in the stripper | 0.0218                             |

In the list of the best sets of CVs in Table 4.3, controlling the CO<sub>2</sub> recovery ( $y_1$ ) is common in all six best sets. The best 2<sup>nd</sup> measurement is the temperature control of tray no.16 ( $y_{33}$ ) in the stripper. From the ranking, other good second stripper measurements are the temperatures of neighboring trays. Figure 4.4 shows the proposed control structure in region I.

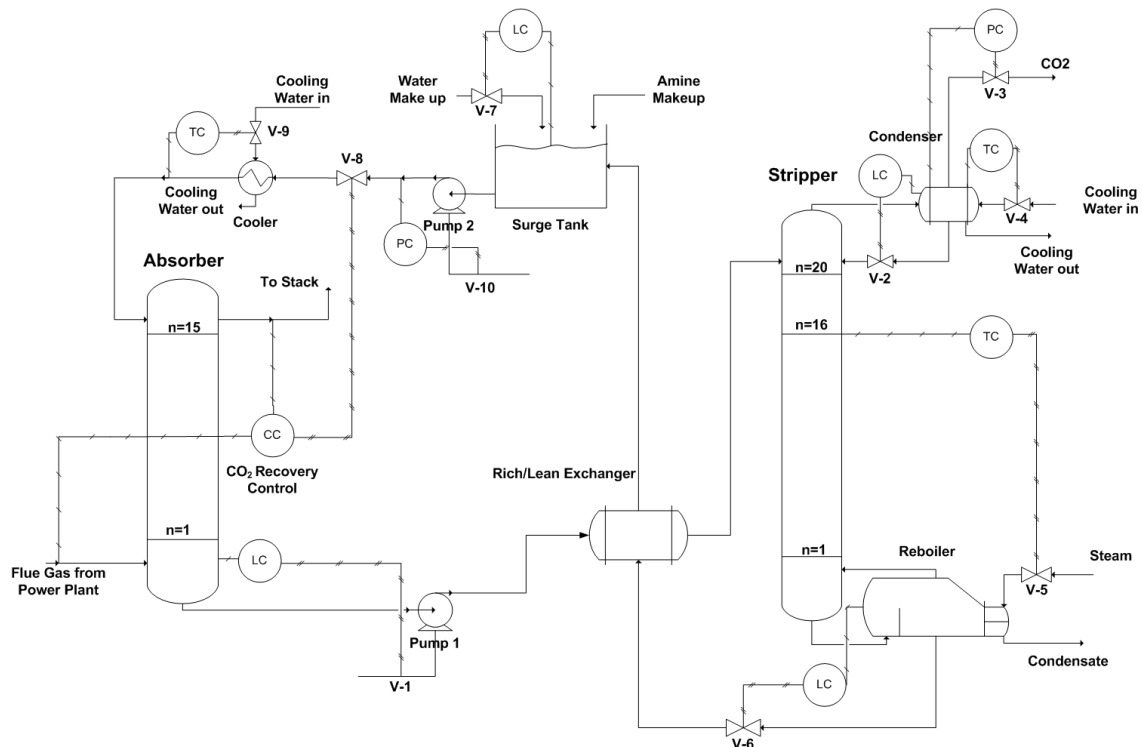


Figure 4.4 Proposed control structure with given flue gas flowrate (region I)

Also, note that the losses are very small; about 0.01USD per ton of flue gas treated. This means that there is little reason to consider measurement combinations as CVs.

#### 4.2.2 Region II: Large flowrates of flue gas (+30%)

The active constraints and thus the optimal control strategy will change as we increase the flue gas flowrate. To study this, we keep constant the best self-optimizing CVs found in region I and gradually increase flowrate of flue gas (Table 4.4). We find that the first constraint we encounter is the reboiler duty which saturates when the flue gas is increased by 19.35% and we are in region II. In general when the process reaches a new constraint region, we need to identify new self-optimizing CVs. In region II there is only one unconstrained degree of freedom which may be selected as the lean amine flowrate, so we need to find one CV.

We further increase the flowrate of the flue gas so that the total increase is +30% (278.2 kmol/h) and then reoptimize the process (Table 4.4). This point is selected as the optimal nominal point in this region. The same procedure as region I is repeated here. Note that one new active constraint (reboiler duty) has been added to the previous active constraints.

We could use the exact local method but we choose to use the closely related maximum gain rule (Skogestad and Postlethwaite 2005) to select the best CV which has the highest scaled gain. In the maximum gain rule the loss has inverse proportion to the square of the scaled gain:  $Loss \sim 1/(G_s)^2$ . It is worth noting that since there is only one DOF left, the maximum gain rule and exact local method give the same result.

Table 4.4 Increasing the flowrate of flue gas with the control policy in region I; saturation of reboiler duty occurs when feed flowrate is +19.35%

|                                       | Feedrate of flue gas (kmol/h) | Pump1 duty (kW) | Pump2 Duty (kW) | Self-optimizing CVs in region I               |   | Cooler duty (kW) | Reboiler duty (kW)       | Objective function (USD/ton) |
|---------------------------------------|-------------------------------|-----------------|-----------------|---|---|------------------|--------------------------|------------------------------|
|                                       |                               |                 |                 | CO <sub>2</sub> recovery (y <sub>1</sub> ), % | Temperature of tray no. 16 (y <sub>33</sub> ), °C |                  |                          |                              |
| Optimal nominal point                 | 214                           | 1.70            | 2.15            | 95.26   | 106.9   | 321.90           | 1161                     | 2.53                         |
| +5% feedrate                          | 224.7                         | 1.78            | 2.26            | 95.26   | 106.9   | 347.3            | 1222                     | 2.53                         |
| +10% feedrate                         | 235.4                         | 1.86            | 2.36            | 95.26   | 106.9   | 371.0            | 1279                     | 2.53                         |
| +15% feedrate                         | 246.1                         | 1.94            | 2.46            | 95.26   | 106.9   | 473.3            | 1339                     | 2.53                         |
| +19.35%, when reboiler duty saturates | 255.4                         | 2.00 (+12.36%)  | 2.55 (12.83%)   | 95.26   | 106.9   | 419.4 (+30.29%)  | <b>1393 (max)</b> (+20%) | 2.54                         |
| +30% feedrate (reoptimized)           | 278.2                         | 2.03            | 2.58            | 91.60   | 103.3   | 359.3            | <b>1393 (max)</b>        | 2.69                         |

To see how the scaled gains are calculated see (Panahi et al. 2010). There are 38 candidate measurements which is like before except for the reboiler duty which is saturated. Table 4.5 shows that temperature of tray no. 13 (y<sub>30</sub>) in the stripper has the largest scaled gain and is the best CV to be controlled using recycle lean amine flowrate. Figure 4.5 shows the resulting control structure in region II.

Tray no.13 (y<sub>30</sub>) is not the same as in region I (tray no.16, y<sub>33</sub>), which is a disadvantage because of the logic needed to reconfigure CVs as we switch between regions.

Table 4.5 The best candidate CVs with the largest scaled gain in region II

| rank | CV   | 100×scaled gain |
|------|--|-----------------|
| 1    | y <sub>30</sub> : Temperature on tray no. 13 in the stripper | 6.03            |
| 2    | y <sub>31</sub> : Temperature on tray no. 14 in the stripper | 5.77            |
| 3    | y <sub>29</sub> : Temperature on tray no. 12 in the stripper | 5.63            |
| 4    | y <sub>32</sub> : Temperature on tray no. 15 in the stripper | 4.95            |
| 5    | y <sub>28</sub> : Temperature on tray no. 11 in the stripper | 4.81            |
| 6    | y <sub>27</sub> : Temperature on tray no. 10 in the stripper | 3.89            |
| 7    | y <sub>33</sub> : Temperature on tray no. 16 in the stripper | 3.88            |
| 27   | y <sub>1</sub> : CO <sub>2</sub> recovery                    | 0.19            |

However from Table 4.5 we see that y<sub>33</sub> has the 7<sup>th</sup> largest scaled gain and is still a good CV in region II but it must have a new setpoint when we change regions. The change is from 106.9°C to 103.3°C which illustrates that is not the truly optimal controlled variable in both regions. This alternative structure will be discussed in next chapter.

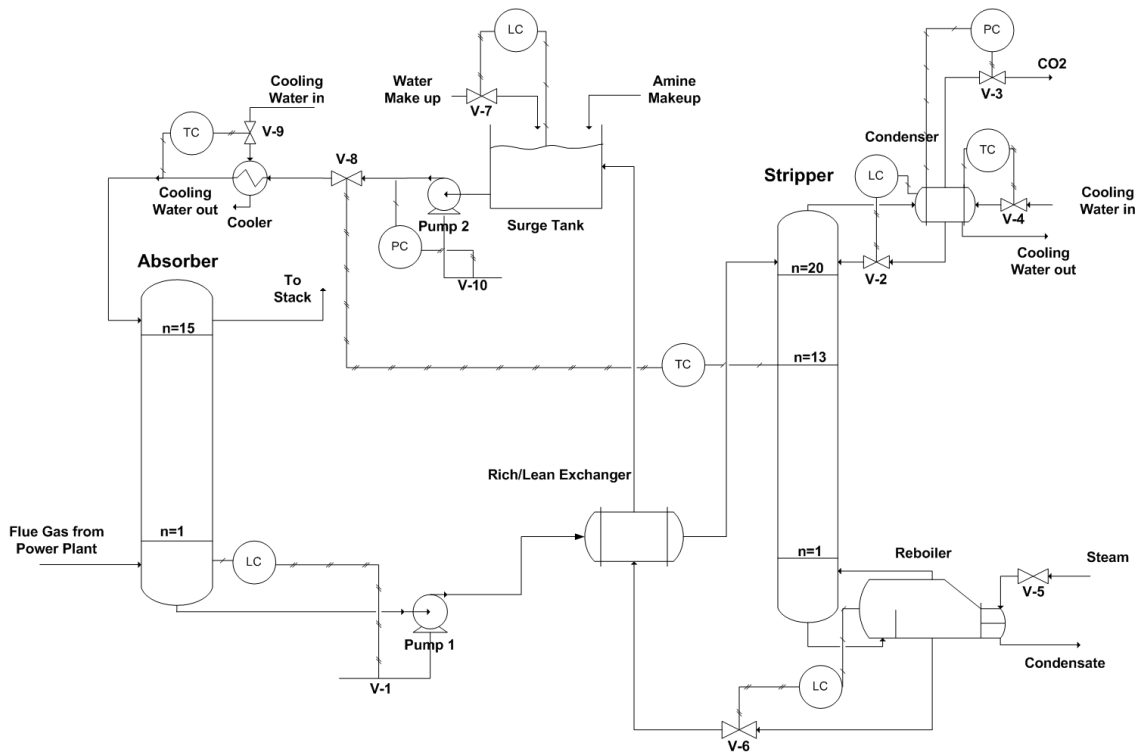


Figure 4.5 Proposed control structure in presence of large flowrates of flue gas when reboiler is saturated (region II)

#### 4.2.3 Region III: Large flowrates of flue gas when process reaches minimum allowable CO<sub>2</sub> recovery

We keep  $y_{30}$  (the best CV in region II) constant and further increase the flowrate of flue gas. When the flowrate of flue gas reaches 326.9 kmol/hr (+52.76%), the CO<sub>2</sub> recovery reaches its lower bound constraint of 80% and we have reached the bottleneck where no further increase is possible (Table 4.6).

Table 4.6 Increasing of the flowrate of flue gas with control policy in region II and reaching to the minimum allowable CO<sub>2</sub> recovery

|   | Feedrate of fluegas (kmol/hr) | Pumps duty (kW) | CO <sub>2</sub> recovery % | Self-optimizing CV in region II         | Cooler duty (kW) | Reboiler duty (kW) | Objective function (USD/ton) |
|---|-------------------------------|-----------------|----------------------------|---|------------------|--------------------|------------------------------|
|   |                               |                 |                            | Temperature of tray 13 ( $y_{30}$ ), °C |                  |                    |                              |
| Optimal nominal case in region II (+30% feedrate)                     | 278.2                         | 4.61            | 91.60                      | 109                                     | 359.3            | <b>1393 (max)</b>  | 2.69                         |
| +40% feedrate   | 299.6                         | 4.58            | 86.46                      | 109                                     | 315.5            | <b>1393</b>        | 3.01                         |
| +50% feedrate   | 321                           | 4.55            | 81.31                      | 109                                     | 290.3            | <b>1393</b>        | 3.36                         |
| +52.76% feedrate, reach to minimum allowable CO <sub>2</sub> recovery | 326.9                         | 4.54            | <b>80 (minimum)</b>        | 109                                     | 284.6            | <b>1393</b>        | 3.45                         |

A controller or manual control is needed to set the feedrate of flue gas such that the recovery stays above 80%.

To validate the proposed control structures in different regions, dynamic simulation of the process is done. These results are presented in the next chapter.

### 4.3 Discussion

The lean amine temperature to the absorber was assumed to be 51°C. In practical CO<sub>2</sub> capturing processes using 30% MEA, lean amine is usually fed to the absorber at around 40°C, which gives a good balance between the kinetics and thermodynamics for absorption reactions. The value of 40°C is reported frequently in the literature when 90% recovery is the target (Jassim and Rochelle 2005). However in our case we use a higher recovery because of a trade off between the cost of energy and the tax on the CO<sub>2</sub> released to the air, and this results in a higher optimal temperature, as shown in Figure 4.6.

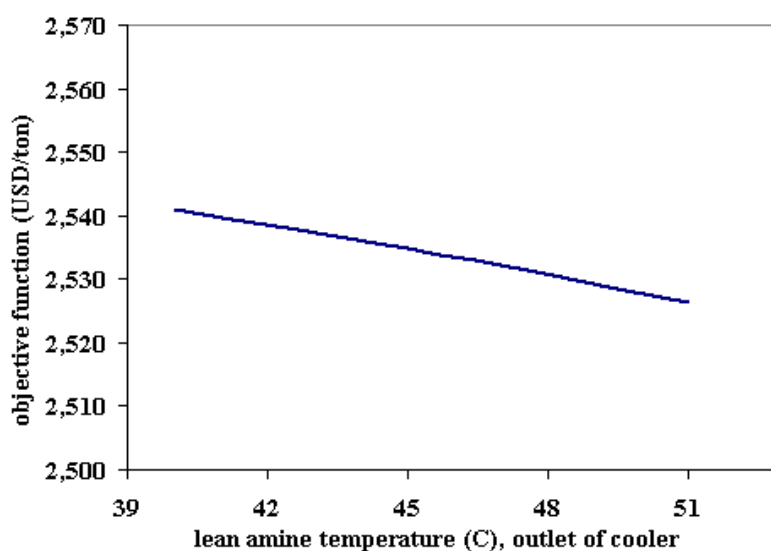


Figure 4.6 Objective function with change in lean amine temperature

We did not increase the temperature further above 51°C, because this would increase amine losses and because we did not want to be too far from the current practical temperatures.

In this chapter, we assumed that the *stripper reboiler duty* was the first capacity constraint to become active. Note here that a constraint on reboiler duty (vapor boilup) is almost equivalent to a constraint on gas capacity in the stripper (e.g., due to flooding). If instead the gas capacity of the *absorber* was the first capacity constraint to become active (e.g., due to flooding), then this would be a bottleneck and no more flue gas could be handled. Thus, in terms of control structure selection, there are no options except for reducing the feed flue gas flowrate. Here, we have considered the less obvious case which is saturation of reboiler duty where the feedrate can still be increased further. (Region II)

The price for power (electricity) and the CO<sub>2</sub> tax can vary widely and their ratio will determine the optimal amine recirculation and reboiler duty. However, we believe the structural issues regarding selecting good CVs will be less sensitive to this.

## 4.4 Conclusions

In this study a control structure is designed for a CO<sub>2</sub> capturing process with the aim to achieve optimal CO<sub>2</sub> removal. Self-optimizing method is used to select the best CVs in three different operational regions;

Region I: in low feedrates of flue gas and having two unconstrained degrees of freedom

CV1= $y_1$ =CO<sub>2</sub> recovery (95.26%)

CV2= $y_{33}$ = Temperature of tray no. 16 in stripper (106.9°C)

Region II: in intermediate feedrates of flue gas with saturation of heat input and having only one unconstrained degree of freedom

CV1= Max. reboiler duty ( $y_1$ = CO<sub>2</sub> recovery is given up)

CV2= $y_{30}$ = Temperature of tray no. 13 in stripper (109°C)

However, we argued that an alternative with an only slightly larger loss would be to select CV2= $y_{33}$  also in region II.

Region III: in large feedrates of flue gas when minimum allowable CO<sub>2</sub> recovery (80%) meets, a controller is needed to set the flowrate of flue gas such that the minimum is satisfied.

## Chapter 5

# Optimal Operation of CO<sub>2</sub> Capturing Process, Part II: Design of Control Layers

This chapter is based on the submitted paper “Economically Efficient Operation of CO<sub>2</sub> Capturing Process; Part II: Regulatory Control Layer” to Journal of Chemical Engineering and Processing: Process intensification

In chapter 4, control structures were proposed for different operational regions of a post-combustion CO<sub>2</sub> capturing process using the top-down steady-state economic part of the plantwide procedure. In the current chapter, the bottom-up part of the complete procedure is considered. For this purpose, dynamic simulation is used to validate the proposed control structures. Different control configurations using decentralized controllers and model predictive control (MPC) are considered. At the end, a simple control configuration is proposed which keeps the process close to the optimum in all operational regions without the need for switching the control loops.

### 5.1 Introduction

We study optimal operation of a post-combustion CO<sub>2</sub> capturing process, where the objective is to minimize the sum of the energy cost and the penalty cost for releasing CO<sub>2</sub> to the atmosphere. In chapter 4, a top-down analysis of the complete plantwide control procedure (Table 5.1) was performed to identify different operational regions of active constraints as a function of the throughput (flow rate of flue gas) and to select self-optimizing controlled variables (CVs) in

each region. In region I, the flue gas flow rate is given at its nominal value and there are two unconstrained degrees of freedom (DOFs), which may be considered as the CO<sub>2</sub> recovery in the absorber and the CO<sub>2</sub> mole fraction at the bottom of the stripper. The best associated CVs were found to be the CO<sub>2</sub> recovery in the absorber and the temperature on tray no.16 in the stripper (Panahi and Skogestad 2011) (see Figure 5.1).

Table 5.1 Plantwide control procedure (Skogestad 2004)

### I. Top-down part (focus on steady-state economics)

Step 1. Define operational objectives (economic cost  $J$  to be minimized) and constraints

Step 2. Identify degrees of freedom (MVs) and optimize the operation for important disturbances (offline analysis) to identify regions of active constraints

Step 3. Each region of active constraints: Select primary (economic) controlled variables CV1 (**Decision 1**):

- Active constrains
- “Self-optimizing” CVs for the remaining unconstrained degrees of freedom

Step 4. Select location of throughput manipulator (TPM) (**Decision 3**)

### II. Bottom-up part (focus on dynamics)

Step 5. Choose structure of regulatory control layer (including inventory control)

a. Select “stabilizing” controlled variables CV2 (**Decision 2**)

b. Select inputs (valves) and “pairings” for controlling CV2 (**Decision 4**)

Step 6. Select structure of supervisory control layer

Step 7. Select structure of (or need for) optimization layer (RTO)

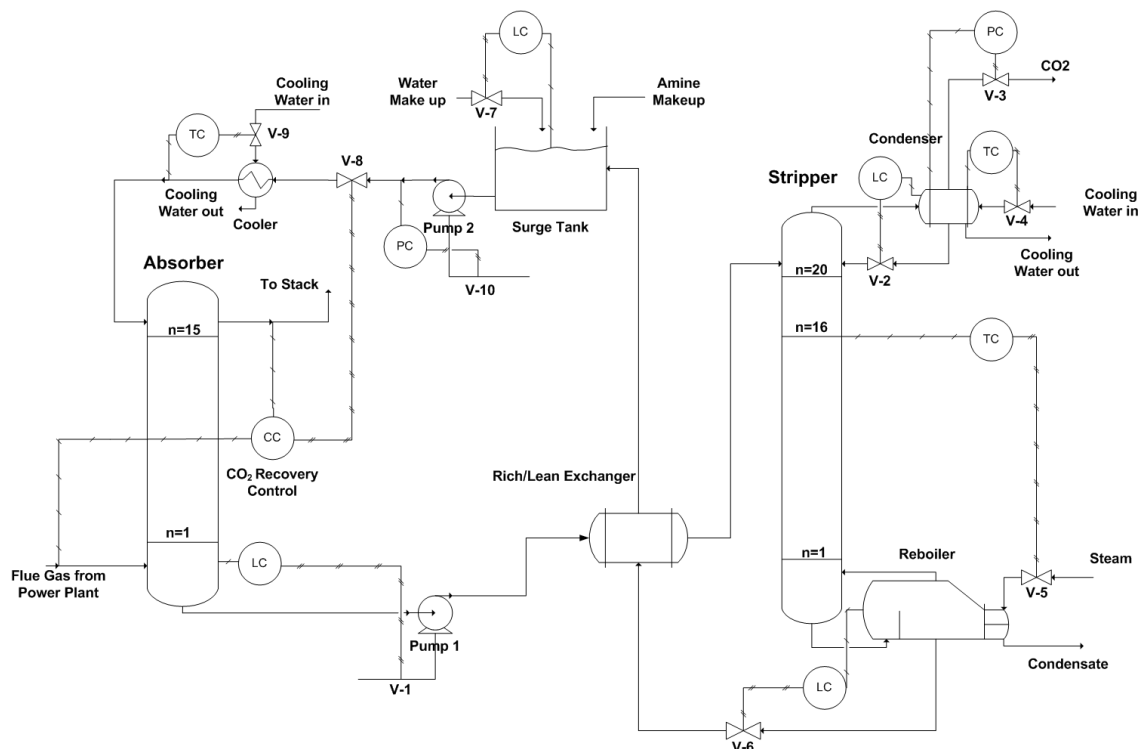


Figure 5.1 Alternative 1, proposed decentralized control structure for region I with given flue gas flowrate (Panahi and Skogestad 2011)

However, these CVs are not necessarily the best in all operating regions and for larger flowrates of the flue gas (region II), where the reboiler duty reaches its maximum, the temperature of tray 13 in the stripper was found to be the best unconstrained CV (Panahi and Skogestad 2011). For even larger flue gas flowrates, one reaches the minimum allowable CO<sub>2</sub> recovery of 80% and we have reached the bottleneck where a further throughput increase is infeasible (region III) (Panahi and Skogestad 2011).

In this work, we focus on the bottom-up part of the procedure in Table 5.1, where we want to identify a control structure (as simple as possible) that implements in practice the steady-state control objectives from part I over the entire feasible throughput range. A main issue is to handle transition from region I to region II where an unconstrained degree of freedom is lost due to a constraint becoming active. In general, some logical switching or reconfiguration of control loops would be necessary to manage the transition. Here, using prior knowledge of the constraint that becomes active, we synthesize a simple control structure that does not require any loop reconfiguration and thus provides near-optimal operation over the entire feasible throughput range. The details on how we arrived at the chosen pairings are the main issue for the present paper.

Towards the synthesis of such a simple structure, four different control configurations (including the one in Figure 5.1) using decentralized PI controllers, briefly summarized below, are considered.

Alternative 1: The two unconstrained self-optimizing CVs for region I are controlled using the most obvious pairings (Figure 5.1).

Alternative 2: The two self-optimizing CVs for region I are controlled using the reverse pairings compared to Alternative 1.

Alternative 3: The best self-optimizing CV for region II is controlled.

Alternative 4: Recommended modification of Alternative 2 which provides near optimal operation over the entire throughput range (regions I and II).

Also, the possibility of using multivariable control is considered.

To validate the proposed control structures, dynamic process simulation is performed in UniSim (UniSim 2008).

There are some other works that study the dynamic behavior of the CO<sub>2</sub> capturing processes ((Ziaii et al. 2009), (Lin et al. 2010), (Lawal et al. 2009) and (Kvamsdal et al. 2009)) but the current study is the first to consider different operational regions and synthesizes a simple control structure that works in the different regions.

In chapter 3, we designed a control structure for a CO<sub>2</sub> capturing process where the objective function was to minimize energy requirement with fixed CO<sub>2</sub> recovery (90%). In the current study, an economic penalty on the CO<sub>2</sub> released to the air is further imposed, which makes it optimal to remove higher amounts of CO<sub>2</sub> (~95%). However, at higher flue gas rates, when the capacity constraint for the stripper is reached, the CO<sub>2</sub> recovery will drop, and at the capacity bottleneck it will reach the minimum allowed recovery which is set to 80%. The details about the objective function, optimization and selection of the best self-optimizing controlled variables are given in chapter 4.

This chapter is organized as follows. In section 5.2, design of the control loops for primary (CV1) and secondary (CV2) controlled variables in regulatory and supervisory control layers is presented. In section 5.3, alternative control structures to handle larger throughputs are introduced and discussed. The dynamic performance of the alternative control structures is evaluated for large disturbances in section 5.4 and the best control structure for (near) optimal operation over the entire throughput range is recommended.

## 5.2 Design of the control layers

In general, the control system can be divided in two main layers (see Figure 5.2).

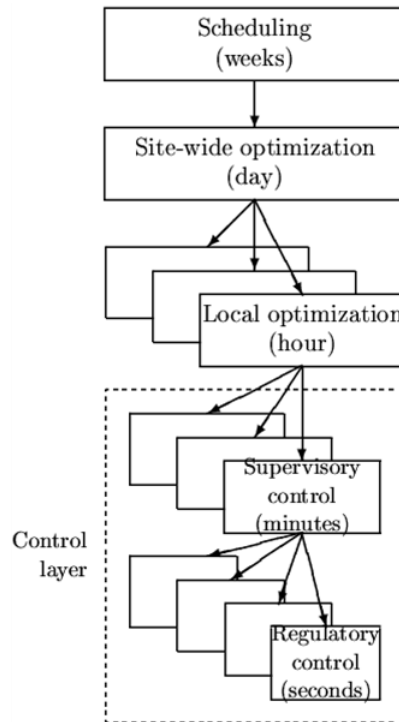


Figure 5.2 Typical control hierarchy in a chemical plant (Skogestad 2004)

**Regulatory layer:** Control of secondary (stabilizing) controlled variables (CV2). This layer usually involves the use of single loop PID controller.

**Supervisory (economic) control layer:** Control of the primary (economic) controlled variables (CV1) using as manipulated variables (MVs) the setpoints to the regulatory layer or “unused” valves (from the original MVs). This layer is usually about a factor 10 or more slower than the regulatory layer. Since interactions are more important at longer time scales, multivariable control may be considered in this layer.

Let us start with the control objectives for the supervisory control layer, which generally may change depending on the disturbances and active constraints. As a result of Step 3 in the procedure (Table 5.1), in region I (low feed rates) the primary (economic) controlled variables were identified as (Panahi and Skogestad 2011):

$$\begin{aligned} CV1_1 &= \text{CO}_2 \text{ recovery in the absorber,} \\ CV1_2 &= \text{Temperature at tray 16 in the stripper.} \end{aligned}$$

In region II with higher feedrates, the stripper reboiler duty is at maximum, so there is one less degree of freedom and the best CV was identified as (Panahi and Skogestad 2011):

$$CV1 = \text{Temperature at tray 13 in the stripper.}$$

Furthermore, before starting the bottom-up part of the procedure, which starts with the choice of the regulatory layer (Step 5), one generally needs to locate the throughput manipulator (Step 4). However, the CO<sub>2</sub> capture plant is a part of the overall power plant, and the throughput

manipulator is located further upstream in the power plant. This means that the feed (flue gas) to the CO<sub>2</sub> capture plant is given and will act as a disturbance, and the control system must be set up to handle this disturbance. However, the CO<sub>2</sub> capture contains a closed amine/water system and one must set the amine flow between the columns. The location of the amine recycle flow manipulator is an important decision.

The details of the regulatory layer design (Step 5) are given in Table 5.2. In addition to the comments given in Table 5.2, one would generally like to combine control tasks in order to simplify the control system. For example, one may select to control the same stripper tray temperature in both regions I and II although there may be a small economic penalty. Furthermore, stabilizing the stripper temperature profile is necessary to maintain the CO<sub>2</sub> inventory circulating around the amine recycle loop. The stripper temperature control loop may therefore be moved to the regulatory layer.

---

Table 5.2 Details on Step 5. Structure of regulatory (stabilizing) layer (Skogestad 2004)

---

- **The purpose of the regulatory layer is to “stabilize”** the plant, preferably using a simple control structure with single-loop PID controllers. “Stabilize” here means that the process does not “drift” away from acceptable operating conditions when there are disturbances. In addition, the regulatory layer should follow the setpoints given by the “supervisory layer”.
- **Reassignments (logic) in the regulatory layer should be avoided:** Preferably, the regulatory layer should be independent of the economic control objectives (regions of steady-state active constraints), which may change depending on disturbances, prices and market conditions.

The main decisions are:

- (a) Identify CV2s for the regulatory layer, these include “stabilizing” CVs, which are typically levels, pressures, reactor temperature and temperature profile in distillation column. In addition, active constraints (CV1) that require tight control (small back-off) may be assigned to the regulatory layer.
  - (b) Identify pairings (MVs to be used to control CV2), taking into account:
    - Want “local consistency” for the inventory control (Aske and Skogestad 2009). This implies that the inventory control system is radiating around a given flow.
    - Avoid selecting as MVs in the regulatory layer, variables that may optimally saturate (steady-state), because this would require either
      - Reassignment of regulatory loop (complication penalty), or
      - Back-off for the MV variable (economic penalty)
    - Want tight control of important active constraints (to avoid back-off).
    - The general pairing rule is to “pair close” to achieve a small effective delay from input (MV) to outputs (CV2).
- 

Let us go back to the decisions involved in designing the control layer (Table 5.2).

(a) The first issue is to identify the variables that need to be controlled to “stabilize” the operation. Here “stabilization” means that the process does not “drift” too far away from the designed operational point when there are disturbances. For our process, we identify the following seven “stabilizing” CVs which need to be controlled (CV2):

1. Absorber bottom level,
2. Stripper (distillation column) temperature,
3. Stripper bottom level,
4. Stripper top level,
5. Stripper pressure,
- 6,7. Recycle surge tank: inventories of water and amine.

Note that there is no need to control the absorber temperature for the purpose of stabilization its profile. However, the temperature inside the absorber needs to be kept at a given value for good operation. We select to do this by controlling the absorber liquid feed temperature at 51°C (Panahi and Skogestad 2011) in the regulatory layer.

The absorber pressure is not controlled (“floating”) because a fixed value would require a valve which would give an undesired loss. It is set indirectly by the ambient pressure. In addition, the inventories of water and amine in the recycle system must be controlled to make up for losses. However, these are small so even manual control may be possible.

**(b)** The next decision is to select the inputs “pairings” to control these variables (CV2).

Let us consider operation in region I (Figure 5.1). We start with the inventory control system, that is, control of levels and pressure. The feed flow is given so the inventory control system needs to be in the direction of flow (Skogestad 2004; Aske and Skogestad 2009). However, for this particular process this does not really fix any loops, except for the pressure control of stripper using the CO<sub>2</sub> outflow (V-3). Next, we consider the closed recycle system of amine and water where we, as mentioned, need to decide on where to set the recycle flowrate. We choose to set it using the recycle liquid flow to the absorber column (V-8). The choice of V-8 as the flow manipulator in the recycle loop is an important decision (we will reconsider it later), because the “radiation rule” (Table 5.2) implies that inventory control in the recycle loop “downstream” of this location must be in the direction of flow. Thus, the bottom levels in the absorber and stripper must be controlled by their outflows (V-1 and V-6 respectively).

The pump V-10 in the recycle controls the pump outlet pressure but this is mainly for simulation purposes and the pump could also be set to run on constant power. However, when the pump controls pressure, the pressure measurement must be after the pump (in the opposite direction of flow). Finally, the stripper has a partial condenser, and the condenser level is controlled by the reflux flow (V-2).

Next, with the inventory control system fixed, we consider the stabilizing temperature loop for the stripper. We choose to use the reboiler duty (steam V-5) as the MV which is the only remaining option. To combine regulatory and supervisory control, the temperature sensor is located at tray 16, which was identified as a self-optimizing variable in region I. Finally, the temperature of the absorber liquid feed is kept at 51°C using the cooler duty (V-9).

Let us finally consider the supervisory layer which operates at a slower time scale. The stripper condenser temperature, which should be low to reduce the required work for CO<sub>2</sub> compression in the downstream process, should clearly be controlled using the cooling water flow (V-4). The remaining “economic” variable to be controlled is the CO<sub>2</sub> recovery and as a MV we may use the recycle amine flowrate to the absorber column (V-8), which was not used in the regulatory layer. This will be a relatively slow loop. The final control structure for region I is shown in Figure 5.1.

### 5.3 Alternative control structures to handle larger throughputs

In region II, the stripper reboiler duty (steam) is at its maximum so the stabilizing temperature loop used for region I (Figure 5.1) will no longer work. This is to be expected, because we have not followed the recommendation in Table 5.2 that says “Avoid selecting as MVs in the regulatory layer, variables that may optimally saturate”. The problem is that there are no obvious alternative for controlling the column temperature. The reflux is often used for

distillation columns, but this is a stripper where the reflux of the key component ( $\text{CO}_2$ ) is very small and the reflux has no effect on column temperature. In addition, from the steady state optimization, it is optimal with maximum cooling to minimize the  $\text{CO}_2$  compressor work in the downstream process (Panahi and Skogestad 2011). Therefore, reflux must be used to control condenser level. Alternatively, the column federate could be used, but this is already used for controlling the absorber sump level.

### 5.3.1 Alternative 2 (“reverse pairing”)

To find alternative solutions, let us start with region I. We consider the problem of controlling the two self-optimizing CVs

$y_1$ :  $\text{CO}_2$  recovery

$y_2$ : temperature on tray no.16 in the stripper

using the two available MVs

$u_1$ : recycle amine flowrate (V-8)

$u_2$ : reboiler duty (V-5)

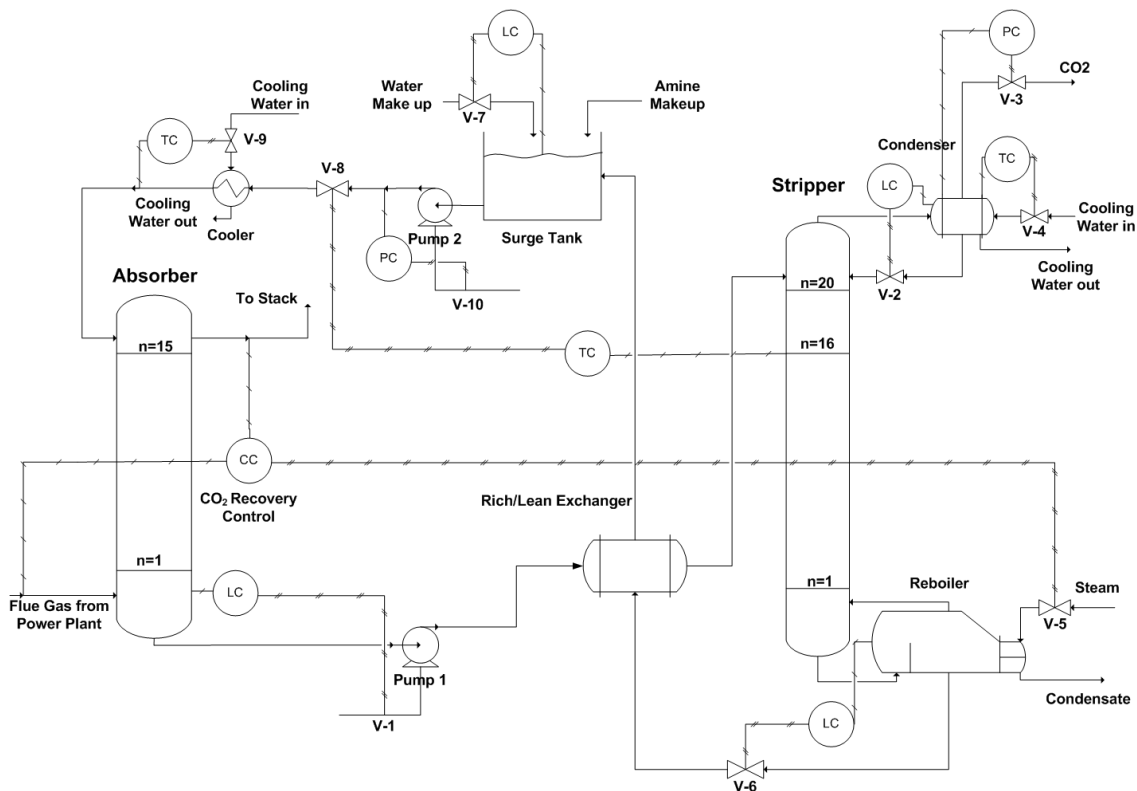


Figure 5.3 Alternative 2, reverse pairing for region I, and also close to the optimal structure for region II

The pairing in Figure 5.1, where  $y_1$  is controlled using  $u_1$  and  $y_2$  is controlled using  $u_2$  is referred to as the “diagonal” pairing (Alternative 1). We will also consider the reverse “off-diagonal” pairing (Alternative 2; see Figure 5.3).

**Pairing issues.** Alternative 1 may seem to be an “obvious” pairing choice but a more careful analysis shows that this is not so clear. A useful tool for selecting pairings is the relative gain array (RGA) and two main pairing rules are (Skogestad and Postlethwaite 2005):

RGA-rule 1: Prefer pairings such that the rearranged system, with the selected pairings along the diagonal, has an RGA matrix close to identity at frequencies around the closed-loop bandwidth. This may be quantified by selecting pairings with a small RGA number:

$$\text{RGA number} = \|\text{RGA}(G) - \mathbf{I}\|_{\text{sum}} \quad (5.1)$$

RGA-rule 2: Avoid pairing on negative steady-state RGA elements.

The second rule states that pairing on a negative RGA provides a potential unstable response when individual loops are malfunctioning, as it is the case of input saturation. To compute the RGA we need a dynamic model. Using the dynamic UniSim simulator and “Profit Design Studio” (PDS) (PDS 2007), we identified the following linear model:

$$G_{\text{dyn.}}(s) = \begin{bmatrix} \frac{6.85s+1.74}{19.7s^2+11.4s+1} & \frac{-0.76s+0.038}{2400s^2+107s+1} \\ \frac{(-9.51s-1.02)e^{-2s}}{218s^2+17.3s+1} & \frac{0.45s+0.0754}{205s^2+18.8s+1} \end{bmatrix} \quad (5.2)$$

The steady-state RGA computed from this model is

$$\text{RGA}_{\text{dyn.}}(s=0) = \begin{bmatrix} 0.77 & 0.23 \\ 0.23 & 0.77 \end{bmatrix} \quad (5.3)$$

Since all elements are positive one cannot eliminate any of the pairings using RGA-rule 2. The RGA-number as a function of frequencies is plotted for the two alternative pairings in Figure 5.4. As expected, we find that the diagonal pairing is the best with the RGA-number close to 0 at all frequencies.

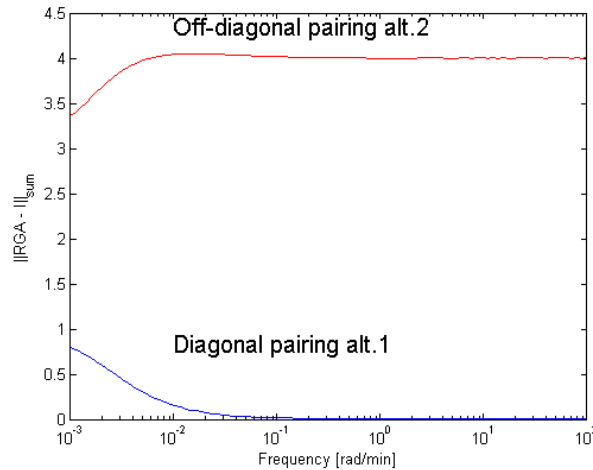


Figure 5.4 RGA number of two different alternatives in pairing

To check the model obtained from the dynamic simulator, we compute the steady-state gains using the steady-state UniSim model and this gave a very surprising result. By making 5% perturbations in the inputs, the following steady-state model was identified:

$$G_{\text{ss}} = 10^{-2} \times \begin{bmatrix} -0.5232 & 1.48 \\ -8.47 & 5.17 \end{bmatrix} \quad (5.4)$$

with the corresponding RGA matrix:

$$RGA_{ss} = \begin{bmatrix} -0.27 & +1.27 \\ +1.27 & -0.27 \end{bmatrix} \quad (5.5)$$

Note that steady-state RGA for the diagonal pairing is negative. The reason is that the sign of the 1,1-element of the gain matrix (5.4) is negative, whereas we found from the dynamic model in (5.2) that the diagonal elements are dominant at higher frequencies correspond to having a positive gain at steady state. The sign change can be explained by Figure 5.5, where we see that  $y_1$  ( $CO_2$  recovery) initially increases in response to a step increase in  $u_1$  (recycle amine flowrate). This agrees with the dynamic model  $G_{dyn}$ . The reason for the initial increase in the  $CO_2$  recovery is an initial decrease in the  $CO_2$  vapor mole fraction in the top of the absorber, which is expected. However, on a longer time scale, with an increased feedrate to the stripper column ( $u_1$ ) and a constant reboiler duty ( $u_2$ ), the  $CO_2$  concentration in the bottom of the stripper increases and starts “filling up” the absorption column with  $CO_2$ . This takes a long time because of the large holdup in the absorber (see Figure 5.6).

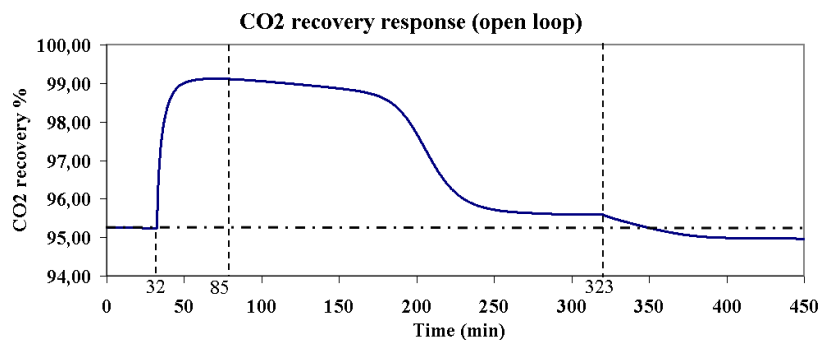


Figure 5.5 Response in  $CO_2$  recovery ( $y_1$ ) to step change in recycle amine flowrate ( $u_1$  by 5%)

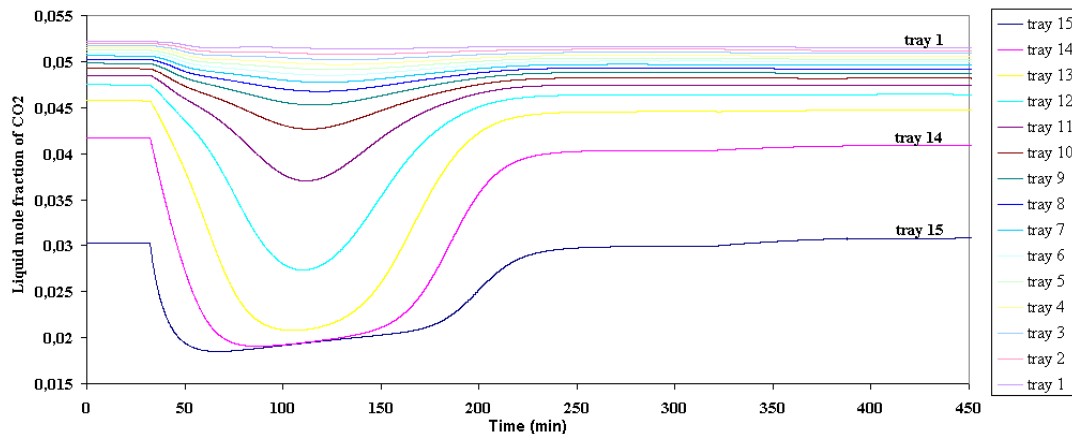


Figure 5.6 Sluggish dynamic response of the  $CO_2$  mole fraction due to large holdup on absorber trays

Finally, the  $CO_2$  “breaks through” at the top of the absorber column and after almost 170 minutes the  $CO_2$  recovery ( $y_1$ ) starts decreasing and keeps decreasing until about 250 minutes. There is a second smaller decrease in  $y_1$  about 70 minutes later. To actually get a negative gain for  $y_1$ , we need the change in recycle amine flowrate ( $u_1$ ) to be sufficiently large, so this is partly a nonlinear effect. The dynamic model  $G_{dyn}$  is based on simulations on an intermediate time

scale and this is why the reversal of the sign of the gain was not identified. The steady-state RGA suggests “reverse pairing” which is referred to as Alternative 2. Based on pairing rule 2 and the model  $G_{ss}$ , we would conclude that the diagonal pairing (Alternative 1) should not be used. However, recall that the reason for RGA rule 2 is to avoid instability if one of the loops is no longer working, which in this case will occur when the reboiler duty saturates.

In summary, the diagonal pairing (“Alternative 1”) should be used in region I because the CVs and the MVs are close, but we need to reconfigure the loops if the reboiler duty reaches its maximum (region II). Alternative 2, on the other hand would work in both regions without any reconfiguration. However compared to Alternative 1 the dynamic performance in region I will be poorer as the associated MVs are not close-by. This is confirmed by dynamic simulations later.

### 5.3.2 Operation in region II (Alternative 3)

Let us next consider operation in region II. The “optimal” solution for region II, is to let the reboiler duty stay at its maximum, “give up” controlling the CO<sub>2</sub> recovery, and move the stripper temperature from tray 16 to tray 13 (Alternative 3, Figure 5.7) (Panahi and Skogestad 2011). Similar to Alternative 2, the stripper temperature is controlled using the recycle flow which is the only available “free” MV in region II.

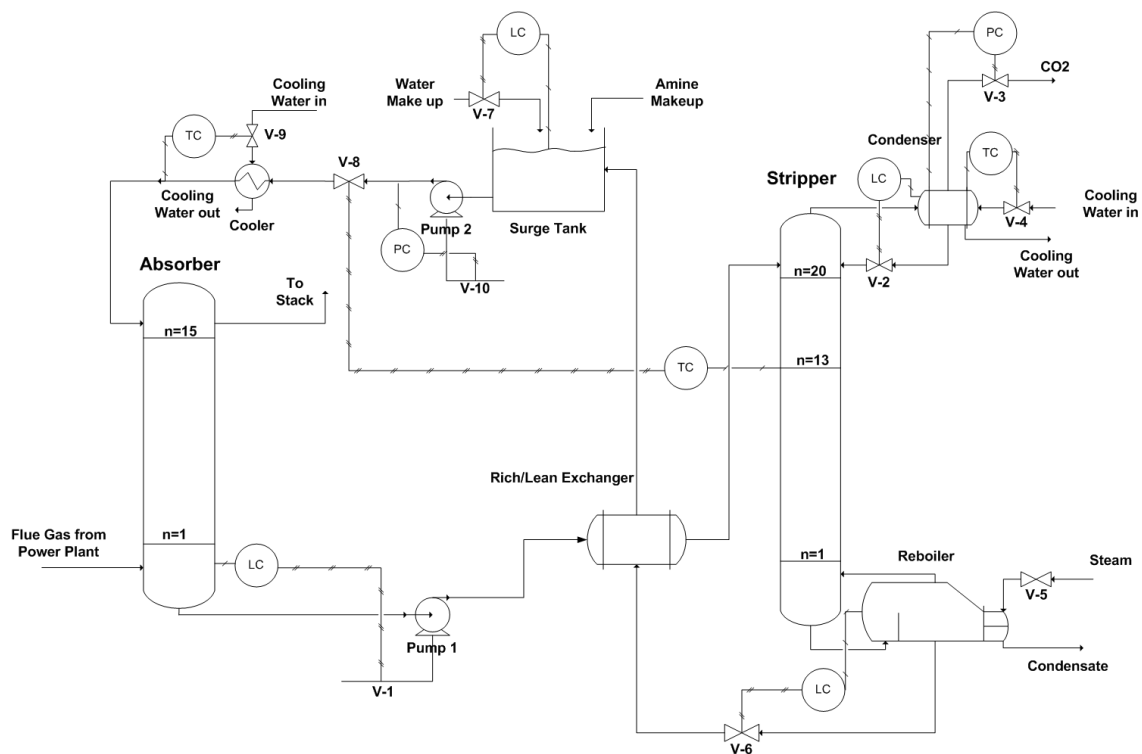


Figure 5.7 Alternative 3, proposed decentralized control structure for region II (Panahi and Skogestad 2011)

For strictly optimal operation in both regions I and II, one could use same supervisory logic that switches between Alternatives 1 and 3. It would switch from Alternative 1 to Alternative 3 when the reboiler duty saturates and it would switch back from Alternative 3 to Alternative 1 when CO<sub>2</sub> recovery passes 95.26%. However, note that Alternative 3 (region II) is actually very close to the “reverse pairing” (Alternative 2) for region I. This suggests that Alternative 2 could also be used to handle region II, although it would involve a small loss because the stripper

temperature is not at its optimal location in region II. With Alternative 2, switching between regions I and II would simply be to give up control of CO<sub>2</sub> recovery when the reboiler duty saturates.

### 5.3.3 Alternative 4 (regions I and II)

So far Alternative 2 is the best structure for the combined regions I and II, and we want to improve on it. In Alternative 2, the recycle amine flowrate (V-8) is manipulated to control the stripper temperature. However, this control loop has a large effective delay so performance is relatively poor (see dynamic simulations later). In Alternative 2, the liquid inflow to the stripper, which actually has a much more direct effect on the stripper temperature, is manipulated to control the level of the absorber. A modification (Alternative 4) is to change the pairings for these two loops, which can be viewed as moving the location of the given flow in the recycle loop from the inlet to the outlet of the absorber (Figure 5.8).

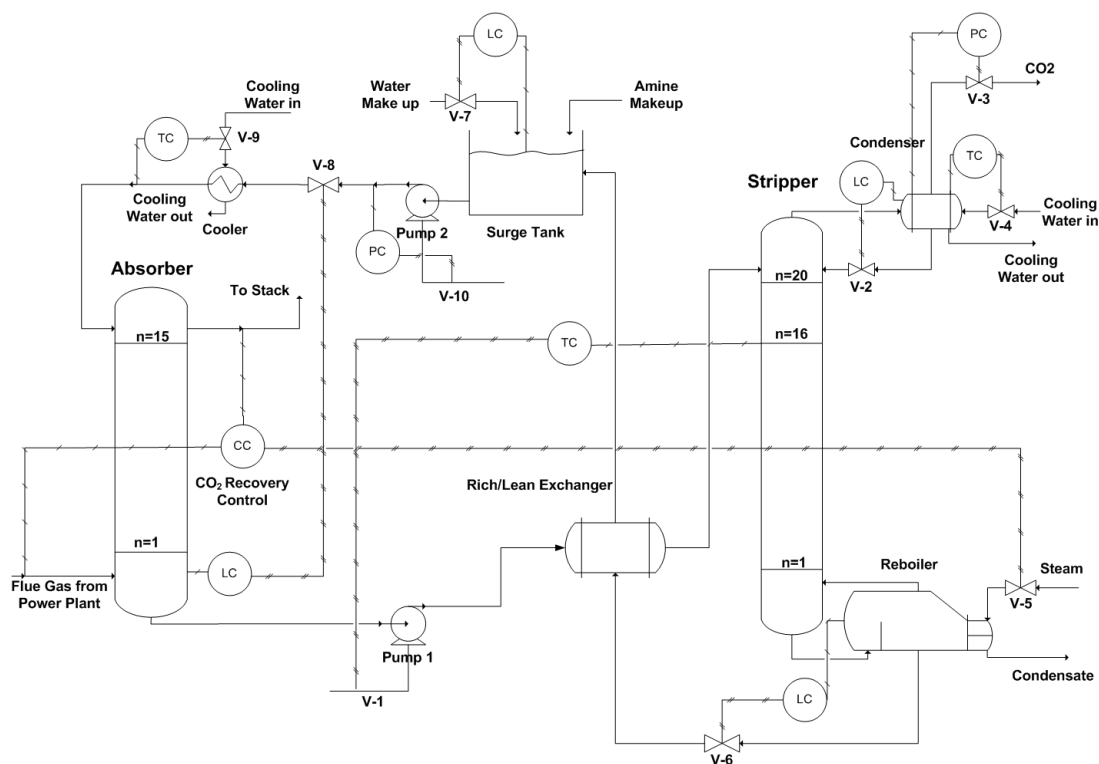


Figure 5.8 Alternative 4, proposed structure for combined regions I and II (modified of alternative 2)

## 5.4 Performance of alternative control structures

In this section we analyse the four alternatives, as well as multivariable control (MPC), using dynamic simulation. We observed some discrepancy in the nominal steady-state in dynamic mode versus the steady-state mode. For example, for the same nominal steady state CV values, the reboiler duty in the dynamic mode is 1074 kW while in the steady state mode the reboiler duty is 1161 kW. This is partly due to the dynamic simulation being pressure driven so that the column pressure profiles are slightly different. In addition, the UniSim dynamics solver may be using approximate thermodynamic models. Fortunately, from a control structure synthesis

perspective, the difference in the nominal steady states is not very important as the first constraint to become active (reboiler duty) as throughput increases, remains unchanged in both modes. As in part I, there are maximum capacities compared to nominal values for the reboiler duty (+20%), cooler (+50%) and pumps (+40%). These constraints are even more important in the present dynamic study.

### 5.4.1 Alternative 1(region I)

We first consider the diagonal pairing for region I (Figure 5.1) and look at the performance (dynamic behavior) when there are large disturbances.

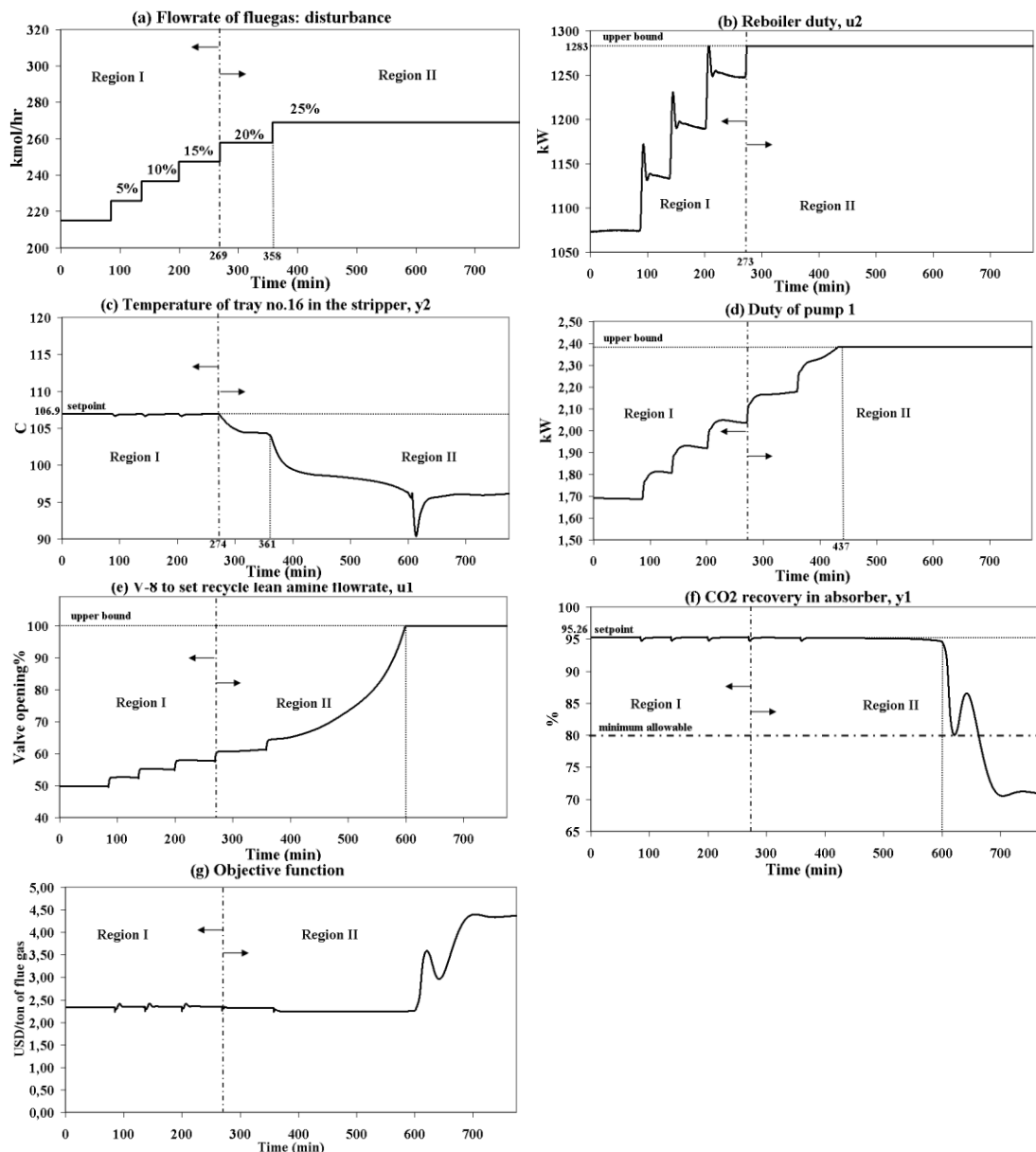


Figure 5.9 Dynamic simulation of pairing alternative 1 (Figure 5.1). The structure handles increase in flue gas flowrates of up to +20% (region I)

All the controllers were tuned using SIMC method (Skogestad 2003) with tuning parameters in Table 5.3.

Table 5.3 tuning parameters (Alt.1)

| Control loop   | Closed loop time constant, $\tau_c$ (min) | Kc    | $\tau_I$ (min) |
|--|---|-------|----------------|
| CO <sub>2</sub> recovery ( $y_1$ ) with recycle amine flowrate ( $u_1$ ) | 0.38                                      | 0.315 | 3.04           |
| Temp. 16 in the stripper ( $y_2$ ) with reboiler duty ( $u_2$ )          | 0.30                                      | 10.53 | 2.4            |

The flowrate of flue gas is increased gradually in steps of 5% from 0% to +25% compared to the nominal flowrate (Figure 5.9a). From Figure 5.9 we see that the control structure behaves very well in region I (up to +20%) with tight control of the CO<sub>2</sub> recovery and stripper temperature. When the flowrate of flue gas increases +20% (at t=269min), the reboiler duty saturates at t=273min (Figure 5.9b), signifying a transition to region II. Initially, it seems that the system is stable although the temperature of tray no. 16 (Figure 5.9c) in the stripper is not controlled in its setpoint, but with a further increase in the flue gas flowrate (at t=358min), the stripper temperature drops further (t=361min) resulting in insufficient CO<sub>2</sub> stripping which builds up in the amine recirculation loop. This necessitates the more amine flow in the absorber to meet the desired CO<sub>2</sub> recovery which saturates the pump 1 (Figure 5.9d) at t=437min. At t≈600min the recycle valve V-8 ( $u_1$ ) becomes fully open (Figure 5.9e) and we get an unstable system where the CO<sub>2</sub> recovery can no longer be maintained at 95.26% (Figure 5.9f) resulting in large objective function value (Figure 5.9g). This is as expected from the earlier RGA analysis. In summary, pairing Alternative 1 can only handle increased flue gas flowrates of up to +20% (region I), at which point the reboiler duty ( $u_2$ ) saturates.

#### 5.4.2 Alternative 3 (region II)

We here consider the “optimal” structure for region II. (“Alternative 3”, Figure 5.7). In the simulation, for a closed loop  $\tau_c=2.33$ min, SIMC method gives Kc=0.314,  $\tau_I=14$ min as PI tuning parameters. Figure 5.10 shows how this structure handles feed flowrate changes with operation within region II, starting from 20% above the nominal (where the process enters region II) with steps of +5%. In this case, we do not attempt to control CO<sub>2</sub> recovery and it drops gradually from 95.26% to 80%, which is the minimum allowable CO<sub>2</sub> recovery. This happens when the feed flowrate increase is +43% (Figure 5.10a). As shown in Figure 5.10c, the stripper temperature is well controlled and hardly affected by the feed flow disturbance.

In general, any active constraint should be considered as a disturbance (Skogestad 2004), thus we changed the fixed (saturated) reboiler duty by  $\pm 10\%$  and the dynamic responses in Figure 5.11 shows that also this disturbance is handled well with stripper temperature deviation of less than 3°C.

#### 5.4.3 Alternative 2 (regions I and II)

The simulations in Figure 5.12 show that this alternative can handle increase of the flue gas starting from the nominal value (0%) and up to +42% (Figure 5.12a).

The reboiler duty ( $u_2$ ) saturates (Figure 5.12b) when the flue gas flowrate increase is +20%, at which point the CO<sub>2</sub> recovery control is given up, and at +42% the minimum CO<sub>2</sub> recovery of 80% (Figure 5.12f) is met. Note that we in both regions control  $y_2$  (temperature of tray no. 16 in the stripper). This is the best choice in region I, and in region II it is close to the best self-optimizing variable which is  $y_3$  (temperature of tray no. 13 in the stripper). Thus, it is not surprising that if Alternative 2 can handle changes of +42% which is close to the region II optimal at +43% (using Alternative 3).

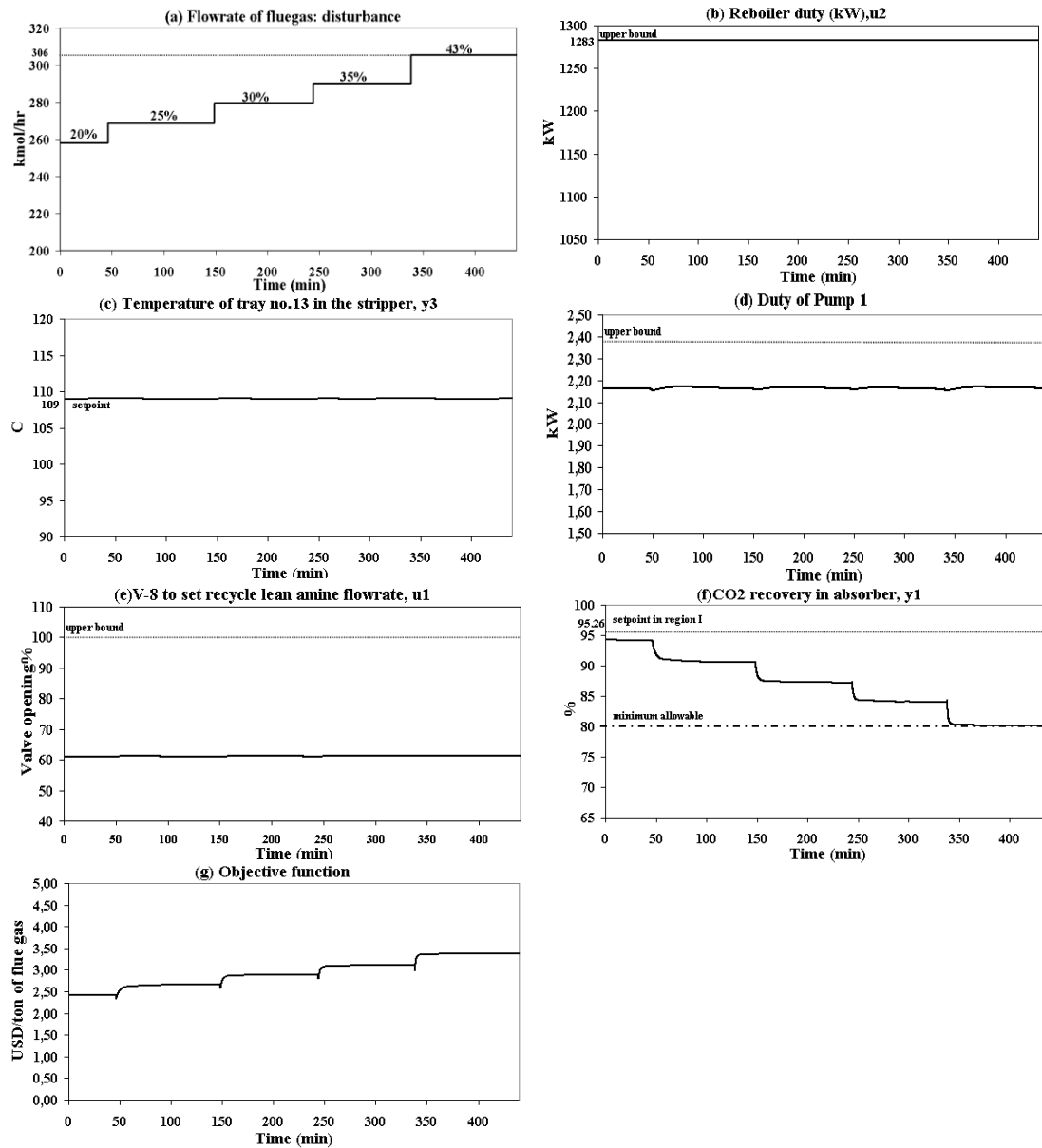


Figure 5.10 Region II: Alternative 3 (Figure 5.7) handles increase in flue gas flowrate to +43%, but it does not cover region I

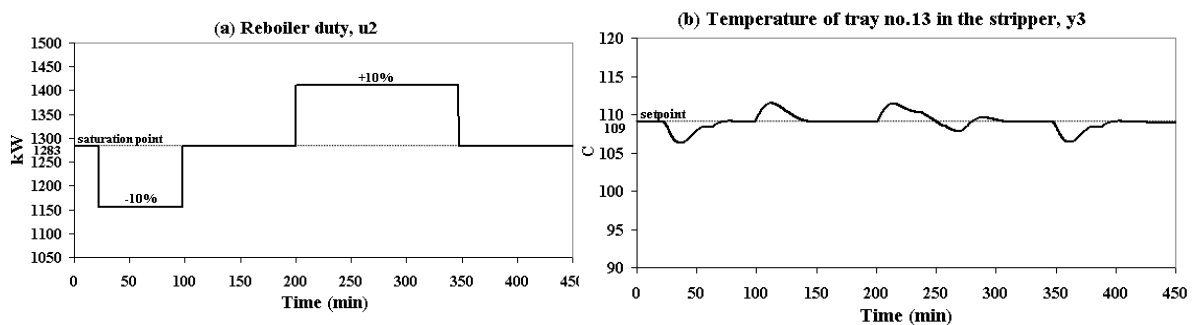


Figure 5.11 Region II: The structure in Figure 5.7 also handles disturbance in reboiler duty which is the active constraint

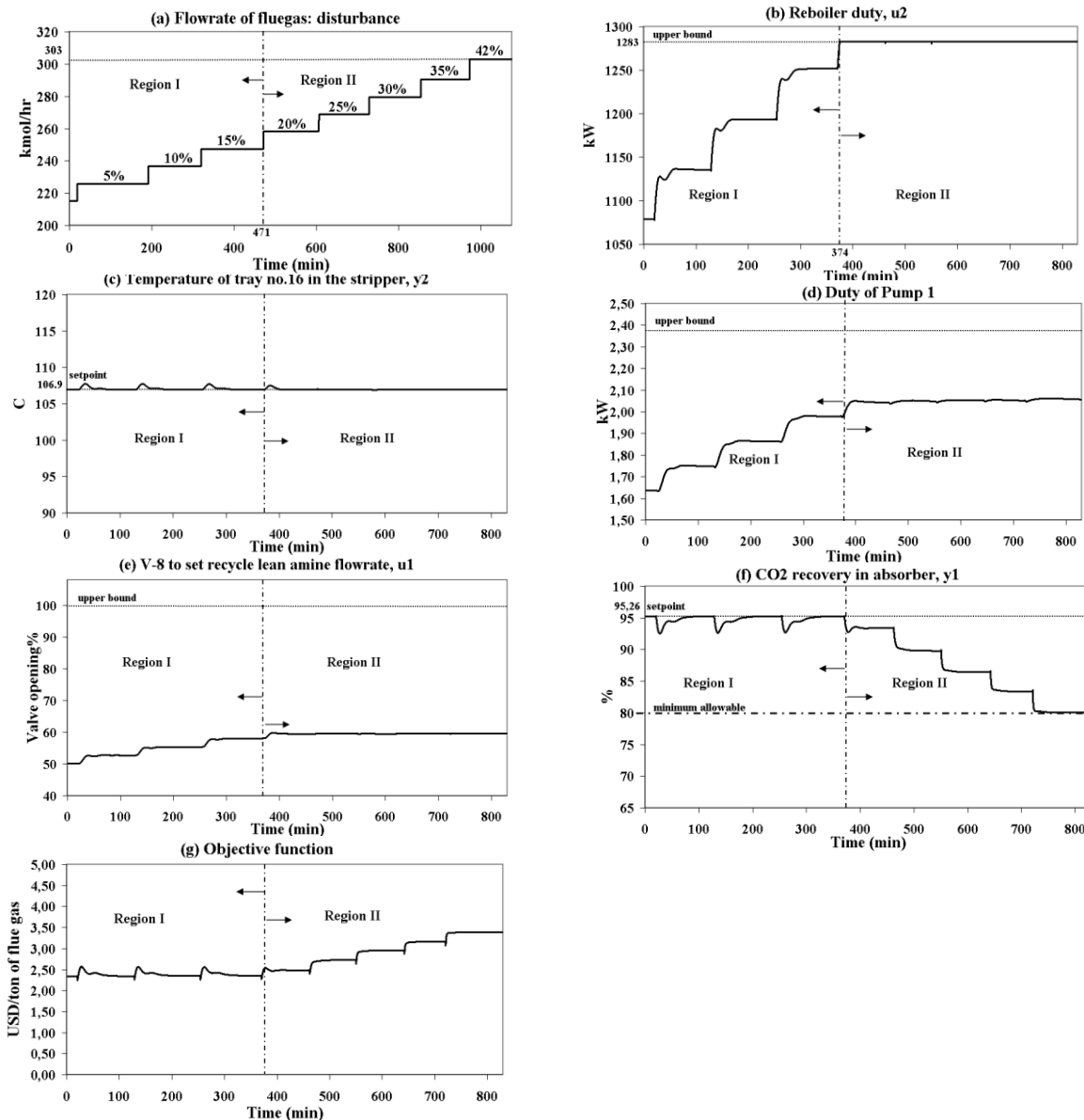


Figure 5.12 Dynamic simulation of alternative 2 (reverse pairings) in combined regions I and II. The structure handles the increase in flowrates of flue gas to +42%

The advantage of Alternative 2 compared to optimal structure (which is to use Alternative 1 in region I and Alternative 3 in region II) is that we do not need switching of CVs. The main disadvantage is that we have more interactions than Alternative 1 in region I. This is seen by comparing the simulations in Figure 5.9 (Alt.1) and Figure 5.12 (Alt.2) in region I. The CO<sub>2</sub> recovery is not as tightly controlled (compare the max. deviation of 0.4% in Figure 5.9f with 3% in Figure 5.12f) and also the stripper temperature shows larger variations (compare max. deviation of 0.3°C in Figure 5.9c with 1°C in Figure 5.12c). In region II, using Alternative 2, there is a minor loss compared to Alternative 3 (compare Figure 5.10g and Figure 5.12g) and also here the temperature control is comparable (compare Figure 5.10c and Figure 5.12c).

### 5.4.4 Alternative 4 (regions I and II)

Alternative 4 (Figure 5.8) involves repairing the absorber level control. As shown in Figure 5.13, this structure handles increase in flue gas flowrate up to +42% like in Alternative 2 but with tighter control of stripper temperature. By comparing Figure 5.12c and Figure 5.13c, we see that the stripper temperature deviation decreases from 1°C to 0.2°C while control of CO<sub>2</sub> recovery remains the same. Therefore, Alternative 4 may be the best structure for practical implementation.

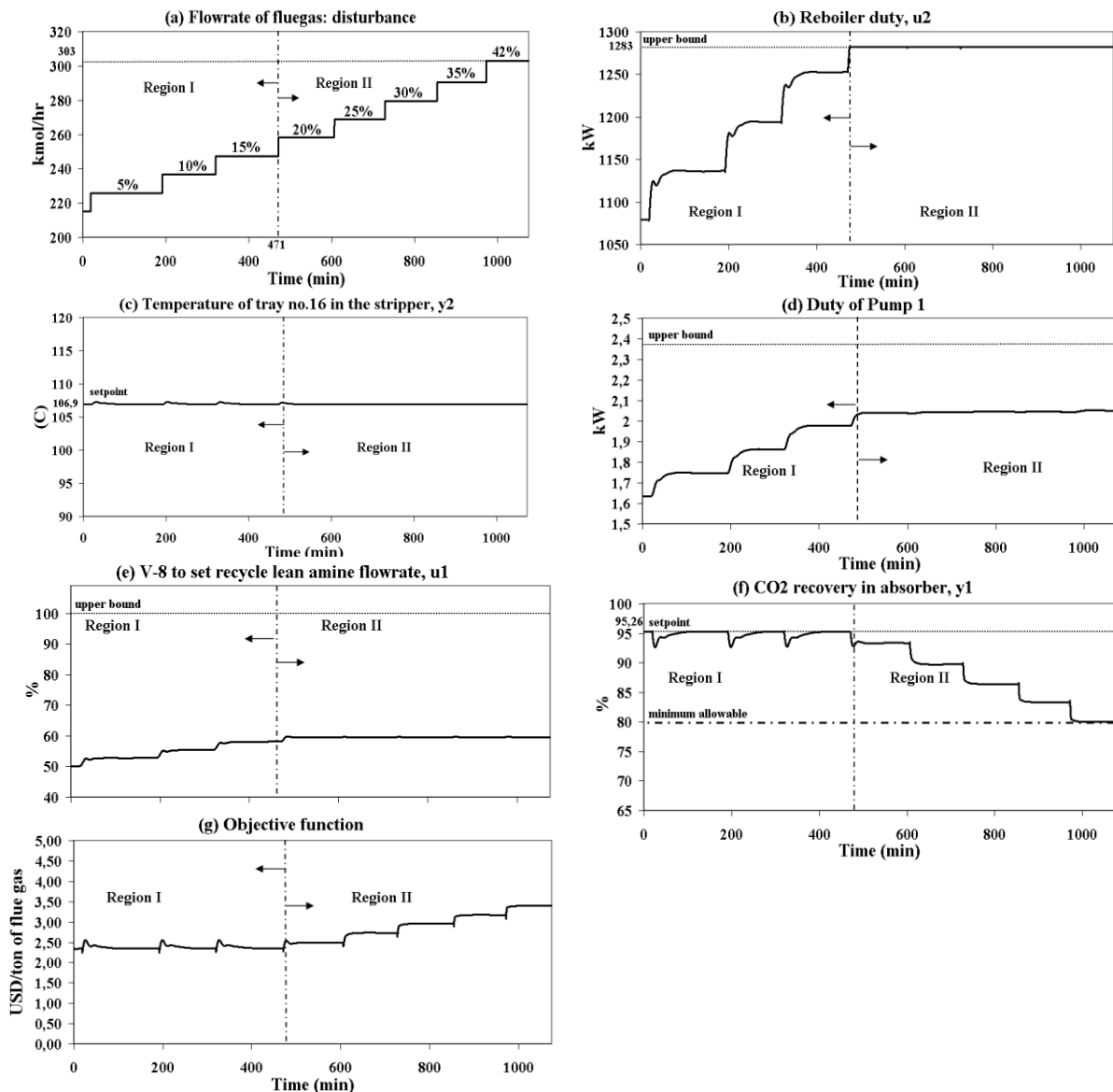


Figure 5.13 Dynamic simulation of pairings alternative 4 (modified of alternative 2) in combined regions I and II

### 5.4.5 Multivariable Controller (regions I and II)

Finally, we consider a multivariable controller (MPC) obtained using the RMPCT (Robust Model Predictive Controller) from Honeywell (UniSim 2008). The aim is to compare its performance with the previous decentralized PI controllers. This MPC includes 2 CVs ( $y_1$  and

$y_2$ ), 2 MVs (recycle lean amine flowrate,  $u_1$  and reboiler duty,  $u_2$ ) and 2 disturbances (flowrate of flue gas and its  $\text{CO}_2$  composition). We used Honeywell's Profit Design Studio to identify the dynamic models and the final responses with MPC are shown in Figure 5.14. For feed values greater than +20%, when the reboiler duty saturates (region II), instead of controlling the  $\text{CO}_2$  recovery at its setpoint value (95.26%), we put less emphasis on controlling the  $\text{CO}_2$  recovery by introducing a range with a lower bound of 80% for this CV. The result is that RMPCT controls the temperature of tray no. 16 at its setpoint and gives up controlling the  $\text{CO}_2$  recovery. When the flue gas flowrate reaches +42% the minimum allowable  $\text{CO}_2$  recovery of 80% is met and there are no degrees of freedom left and further increase of flue gas flowrate is infeasible.

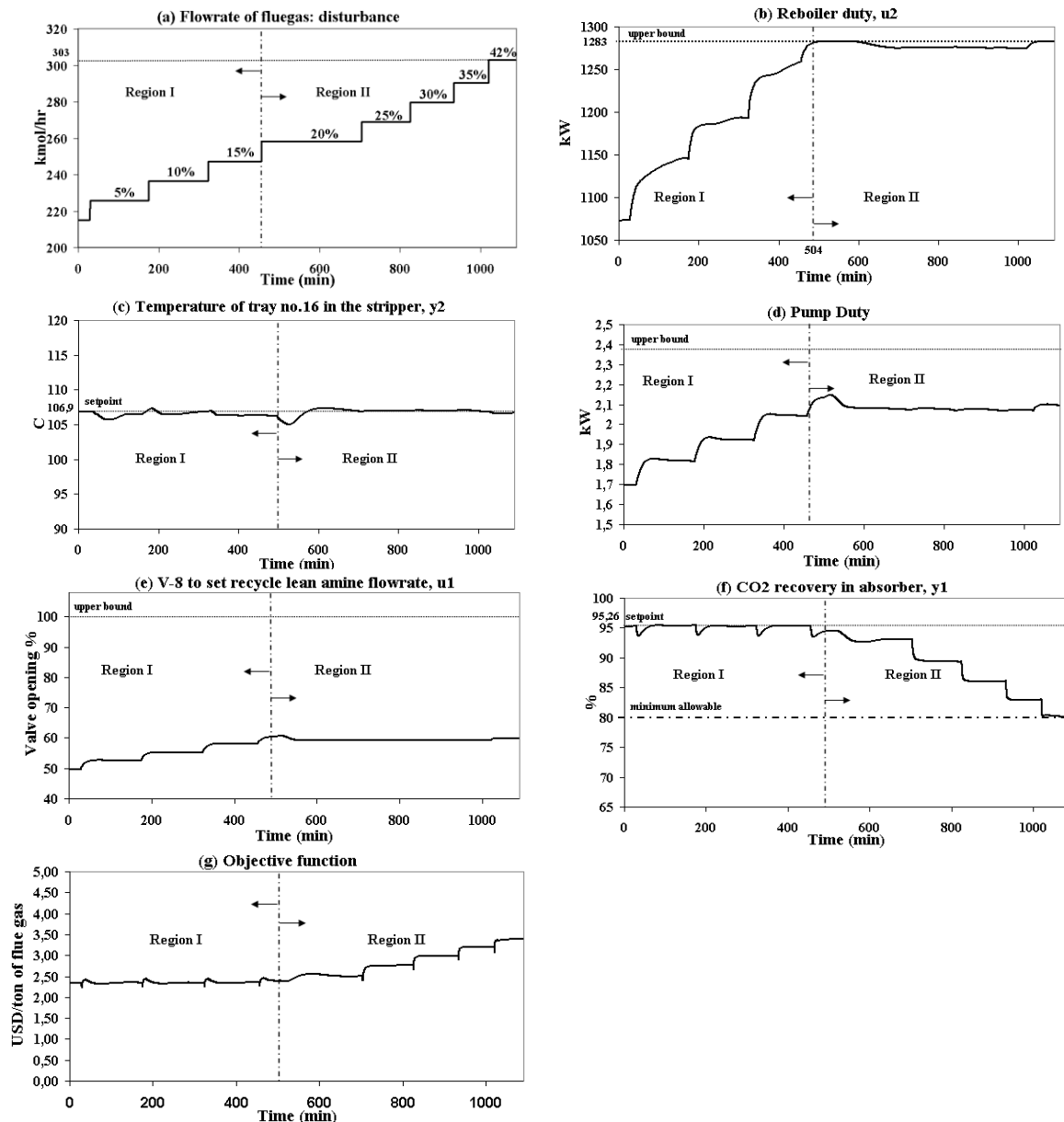


Figure 5.14 Performance of RMPCT tuned in region I, when extended to region II, the structure handles increase in flue gas flowrates of +42%

We finally compare the economic performance of all the structures. From the objective function in Figures: Figure 5.10g (Alt.3), Figure 5.12g (Alt.2), Figure 5.13g (Alt.4) and Figure 5.14g (MPC) we find that there is only a small difference. At the final steady state, the objective function values are 3.38, 3.39, 3.39 and 3.39 (USD/ton of flue gas) respectively. This implies that we can use both Alternative 2, Alternative 4 or MPC to control the system even in the presence of large flowrates of flue gas. Note that the design and implementation of reverse pairings with decentralized controllers are simpler and cheaper than MPC which needs model identification etc. although responses time are comparable.

Of all the alternatives considered, Alternative 4 is proposed as the best structure for the CO<sub>2</sub> capturing process, studied here.

## 5.5 Conclusions

Using the bottom-up part of the plantwide control procedure, we obtained alternative control structures that implement the optimal controlled variables (CO<sub>2</sub> recovery in the absorber and the temperature of tray 16 in the stripper) from part I. Alternative 1 (diagonal pairing of the best CVs found in region I with close-by MVs: recycle amine flowrate and reboiler duty) can handle flue gas flowrates of up to +20% (region I). The reverse pairings (Alternative 2) or MPC handle flow values up to +42%. Due to the large delay between the paired MVs and CVs in Alternative 2, a modified structure (Alternative 4) is proposed where the recycle amine flow manipulator is moved from the inflow to the outflow of the absorber. This simple structure (Alternative 4) has dynamic performance comparable to MPC, and is proposed as the best alternative because of its much simpler implementation.

## Chapter 6

# A Natural Gas to Liquids (GTL) Process Model for Optimal Operation

This chapter is based on the submitted paper “A Natural Gas to Liquids (GTL) Process Model for Optimal Operation” to the journal of Industrial and Engineering Chemistry Research

The design and optimization of a natural gas to hydrocarbon liquids (GTL) process is considered, mainly from the view of maximizing the variable income during operation. Auto-thermal reforming (ATR) is used for synthesis gas production. The kinetic model for Fischer-Tropsch (FT) reactions is the one given by Iglesia et al. for a Cobalt based FT reactor. For the product distribution, three alternative expressions for the chain growth factor  $\alpha$  are compared.

### 6.1 Introduction

A GTL (gas to liquids) plant consists of three main sections (Figure 6.1): Synthesis gas production, Fischer-Tropsch (FT) reactor and FT products upgrading (Rostrup-Nielsen et al. 2000). In this process, natural gas is first converted to synthesis gas (“syngas”; a mixture of hydrogen and carbon monoxide) which is further converted to a range of hydrocarbons in an FT reactor. There are different routes for syngas production: auto-thermal reforming (ATR), steam reforming, combined reforming and gas heated reforming (Steynberg and Dry 2004). We have considered ATR which to be claimed the most economical route for syngas production (Aasberg-Petersen et al. 2003; Bakkerud 2005).

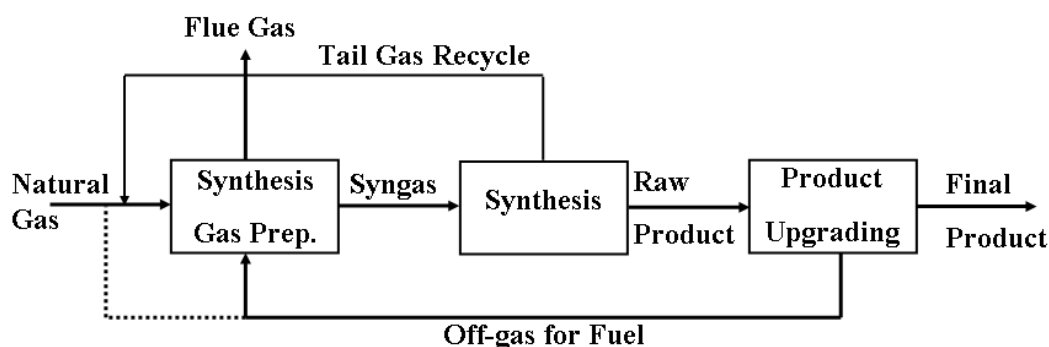


Figure 6.1 A simple Flowsheet of a GTL process (Rostrup-Nielsen et al. 2000)

FT reactions can take place on either iron or Cobalt catalysts in four different types of reactor (Steynberg and Dry 2004); fixed bed, slurry bubble column (SBCR), fluidized bed and circulating fluidized bed reactor.

The currently largest operating GTL plant is the Oryx plant in Qatar with a production capacity of 34,000 bbl/day liquid fuels. This plant includes two parallel trains with two Cobalt based slurry bubble column reactors, each with the capacity of 17,000 bbl/day operating at low temperature FT conditions. Shell is also commissioning a world scale GTL plant (Pearl GTL plant) in 2011 with the capacity of 260,000 bbl/day; 120,000 bbl/day upstream products and 140,000 bbl/day GTL products (Schijndel et al. 2011). This plant is located close to Oryx GTL plant. Shell uses fixed bed reactor for the FT synthesis. Pearl GTL plant has 24 parallel fixed bed reactors each with the production capacity of 6,000 bbl/day (GTL-Workshop 2010).

In the current study, based on available information in open literatures, we study a single train with a capacity of approximately 17,000 bbl/day. The natural gas feed condition is assumed to be fixed at 8195 kmol/h (164.2 MMSCFD), 3000 kPa and 40°C. The composition of natural gas in mole basis is: CH<sub>4</sub>: 95.5%, C<sub>2</sub>H<sub>6</sub>: 3%, C<sub>3</sub>H<sub>8</sub>: 0.5%, n-C<sub>4</sub>H<sub>10</sub>: 0.4%, N<sub>2</sub>: 0.6%

The upgrading section is not included. The main objective of this work is to develop a detailed model that gives the effect of the main operational decision variables on the variable income while satisfying operational constraints. The decision variables include the H<sub>2</sub>O to hydrocarbon feed ratio to the pre-reformer, the Oxygen to hydrocarbon feed ratio to the ATR, the recycle tail gas fraction to the syngas and FT reactors, the purge fraction and the CO<sub>2</sub> removal fraction. The UniSim commercial process simulator (UniSim 2008) is used to simulate the process. The simulator uses detailed steady-state mass and energy balances, and we chose to use the SRK equation of state for the thermodynamic properties. The UniSim files are available from the authors.

Another modeling and simulation study for a GTL plant was recently published by Bao et al. (Bao et al. 2010) where the focus is on optimal process design. They assume a fixed value for the H<sub>2</sub>/CO ratio of 2 and a fixed chain growth probability ( $\alpha$ ) for the FT reactions. On the other hand, our focus is on optimal operation, and our model allows for varying (optimized) H<sub>2</sub>/CO ratio and uses a model with varying  $\alpha$ .

## 6.2 Modeling and process description

The overall flowsheet for the process studied is shown in Figure 6.2.

### 6.2.1 The synthesis gas section

The syngas part is similar to the configuration proposed by Haldor Topsøe (Aasberg-Petersen et al. 2003) with operating pressure of 3000 kPa and includes a pre-reformer, a fired heater and an ATR:

1. The pre-reformer is used to avoid cracking of heavier hydrocarbons in the subsequent ATR. It is assumed that all hydrocarbons heavier than methane are converted according to (6.1). In addition, the methanation and shift reactions (6.2 and 6.3) are assumed to be in equilibrium (Christensen 1996). In our case, the reactor is assumed to be adiabatic with the feed entering at 455°C (Schanke and Sogge 2010). The reaction scheme is

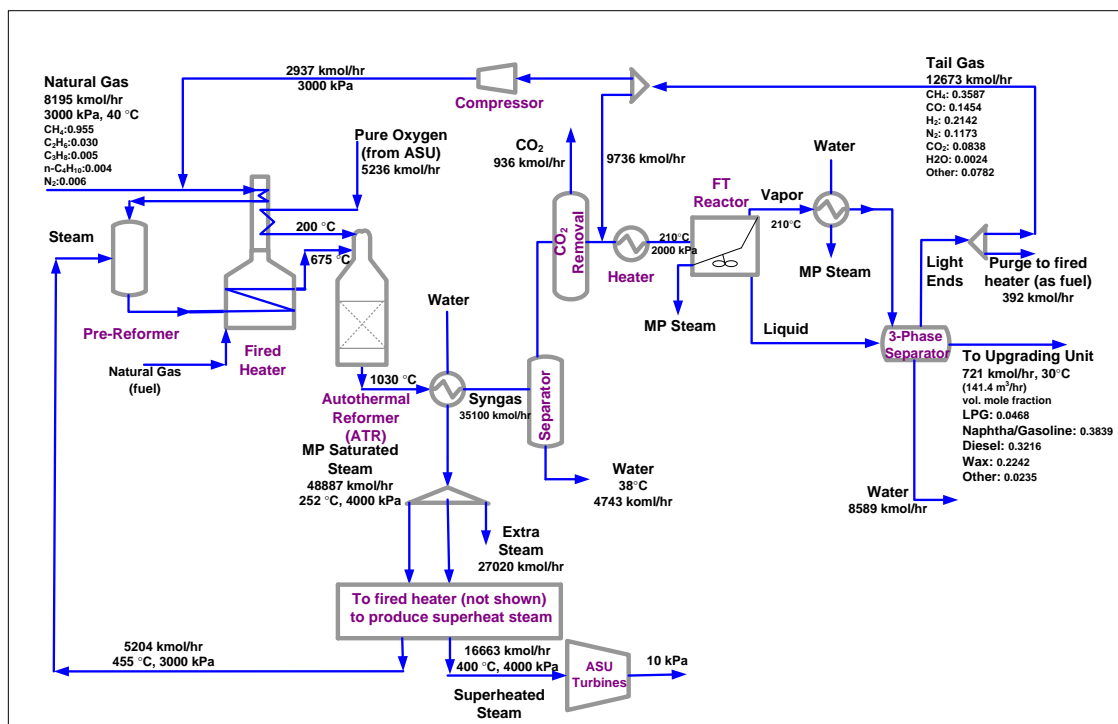
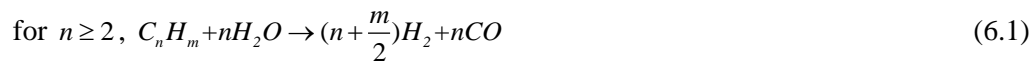


Figure 6.2 Overall process flowsheet with final optimized data ( $\alpha_2$  model, wax price=0.63 USD/kg)

The exit temperature of the adiabatic pre-reformer will depend on the inlet composition and temperature. The exit temperature is between 100 and 300°C lower than the desired ATR inlet temperature, which means that a fired heater is needed.

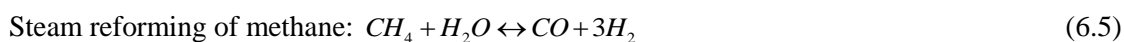
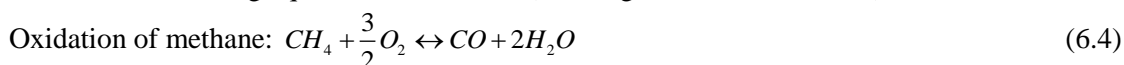
2. The fired heater is used to supply the required energy for:
  - a) Preheating the following streams to 455°C:
    - fresh natural gas (pre-reformer feed)
    - recycle hydrocarbons from FT reactor (pre-reformer feed)
  - b) Superheated process steam (pre-reformer feed) and the superheated steam for driving the turbines of compressor in the oxygen plant and the much smaller

recycled tail gas compressor. Note that saturated steam is first produced in a boiler by heat exchange with the hot outlet stream of the ATR and is then superheated in the fired heater. The energy consumption in the oxygen plant is assumed 400 kWh/ton<sub>O<sub>2</sub></sub> (Schanke and Sogge 2010). This power is supplied by superheated steam from the fired heater, which is expanded from 400 bar and 400°C to 0.1 bar in the ASU turbine (75% efficiency assumed).

- c) Preheating the outlet gas from the pre-reformer to 675°C (optimized value, see below)
- d) Preheating oxygen to 200°C (Aasberg-Petersen et al. 2003)
- e) 10% of the total fired heater duty is assumed to be used to supply superheated steam for other mechanical equipment in the process.

The required fuel for the fired heater is supplied by the combustible components in the purge stream plus some fresh natural gas. An efficiency of 98% is assumed for the combustion of fuels (Cohen et al. 2009).

3. The ATR converts methane in the stream from the fired heater to syngas by reacting it with steam and oxygen. It is modeled as an adiabatic equilibrium reactor according to the following equilibrium reactions (Aasberg-Petersen et al. 2001);



The oxygen is supplied by the air separation unit (ASU) and is blown into the ATR. For GTL applications with a Cobalt based Fischer Tropsch reactor, a typical H<sub>2</sub> to CO ratio in the fresh syngas is about 2 (Aasberg-Petersen et al. 2003) but the exact value will be obtained as a part of the optimization of the process. The hot syngas leaving the ATR is cooled down to ambient temperature for water removal before going to the CO<sub>2</sub> capture unit.

Note that large amounts of water is produced in the subsequent FT reactor, so there is no strict limitation on the water content of cooled syngas, but it is removed for economic reasons to reduce the flow to the FT reactor. The CO<sub>2</sub> removal plant is modeled as a component splitter, where only CO<sub>2</sub> is removed.

With our natural gas feed rate, the hot syngas from the ATR is used to produce about 49000 kmol/hr medium pressure saturated steam (40bar, 252°C) in the boiler. 34% of this MP steam is superheated in the fired heater to be used in the Oxygen plant, and 11% is superheated in the fired heater to be used as the process steam into the pre-reformer. The remaining “extra” 55% of the saturated MP steam is a byproduct of the plant (These values correspond to the optimal model mentioned further in Table 5)

### 6.2.2 Fischer Tropsch section

The syngas is sent to the Fischer-Tropsch (FT) reactor where the highly exothermic FT reactions take place (Yates and Satterfield 1991). The reactor is assumed isothermal with a temperature of 210°C (483K). The reactions are typically written in the following form



where  $(-CH_2-)_n$  denote the olefin and paraffin main products. In addition, CH<sub>4</sub> formation is unavoidable



The FT product distribution can be described by the well-known Anderson-Schulz-Flory (ASF) model

$$w_n = n(1-\alpha)^2 \alpha^{n-1} \tag{6.9}$$

where  $w_n$  ( $n>1$ ) is the weight fraction of  $C_n$  and  $\alpha$  is chain growth probability. The water- gas shift reaction is negligible because it is not catalyzed on Cobalt catalyst (Yates and Satterfield 1991). Figure 6.3 illustrates the meaning of the chain growth graphically. The probability of chain termination is  $1-\alpha$ . Three different methods for calculating the chain growth probability  $\alpha$  are described in section 3. To simulate the reaction scheme, we use the reaction rates for CO consumption and CH<sub>4</sub> formation proposed by Iglesia et al. (1993) together with the carbon mass balance as given by the ASF distribution model.

Iglesia's reaction rates on Cobalt catalyst are valid at 473 to 483 K, 100 to 3000 kPa and H<sub>2</sub>/CO=1-10, and described as below.

$$r_{CH_4} = \frac{7.334 \times 10^{-10} P_{H_2} P_{CO}^{0.05}}{1 + 3.3 \times 10^{-5} P_{CO}} \left( \frac{kmol_{CH_4}}{m^3_{reactor} \cdot s} \right) \tag{6.10}$$

$$r_{CO} = \frac{1.331 \times 10^{-9} P_{H_2}^{0.6} P_{CO}^{0.65}}{1 + 3.3 \times 10^{-5} P_{CO}} \left( \frac{kmol_{CO}}{m^3_{reactor} \cdot s} \right) \tag{6.11}$$

where pressure is in Pa.

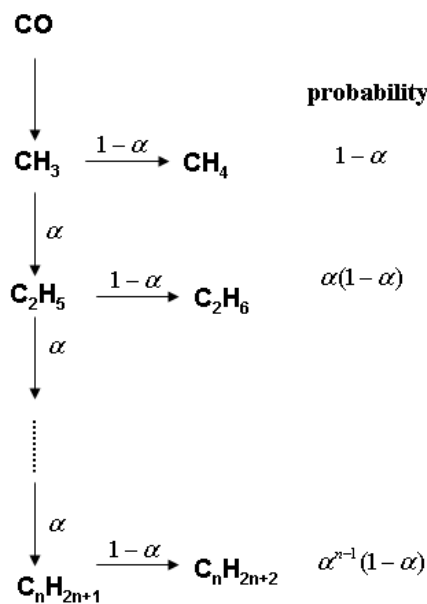


Figure 6.3 Probability of chain growth to different hydrocarbons in FT reactions (GTL-Workshop 2010)

The simulated reactor is a slurry bubble column reactor (SBCR), which is well-known for good heat removal. The following lumps are defined as FT products in our model (Spath and Dayton 2003): C<sub>1</sub>, C<sub>2</sub>, LPG (C<sub>3</sub>-C<sub>4</sub>), Gasoline/Naphtha (C<sub>5</sub>-C<sub>11</sub>), Diesel (C<sub>12</sub>-C<sub>20</sub>) and Wax (C<sub>21+</sub>). Note that for each carbon number, both olefins and paraffins are produced and the factor  $\gamma$  determines the olefins/paraffins ratio (see Appendix of this chapter for details).

An equilibrium three-phase separator operating at 38°C and 20 bar is used for the FT products separation. As for the other units, the SRK equation of state is used for the thermodynamic equilibrium. In all cases, the H<sub>2</sub>O mole fraction in the raw product (outlet hydrocarbon stream of the separator) is less than 0.07% .

The pressure drop in the individual equipment of the syngas and FT units is ignored. This assumption has the same effect on all the three alpha-cases, because the relative change of objective function in different price scenario is important and not the absolute value.

### 6.3 Calculation of chain growth probability $\alpha$

Three different methods for obtaining  $\alpha$  have been considered. Note that in all cases, the ASF model using  $\alpha$  is applied for  $n>1$ , whereas methane ( $n=1$ ) is found from the reaction rate by Iglesias.

#### 6.3.1 Using rates of Iglesias ( $\alpha_1$ )

From the proposed reaction rates for CO (6.10) and CH<sub>4</sub> (6.11), the selectivity of CH<sub>4</sub> as a function of partial pressures of H<sub>2</sub> and CO in FT reactor can be found (left hand side of 6.12). Next, from (A-9) in the Appendix, the selectivity  $r_{CH_4} / r_{CO}$  can be found as a function of  $\alpha$  (right hand side of 6.12).

$$\frac{r_{CH_4}}{r_{CO}} = 0.55 \frac{P_{H_2}^{0.4}}{P_{CO}^{0.6}} = \frac{w_1 \times 2000}{16 \times [\frac{w_1}{16} + 2w_2(\frac{1}{1+\gamma} \frac{1}{30} + \frac{\gamma}{1+\gamma} \frac{1}{28}) + \dots + 25w_{25}(\frac{1}{1+\gamma} \frac{1}{352} + \frac{\gamma}{1+\gamma} \frac{1}{350})]}{(1-\alpha)^2 \times 2000} = \frac{16 \times [\frac{(1-\alpha)^2}{16} + 2(2\alpha(1-\alpha)^2)(\frac{1}{1+\gamma} \frac{1}{30} + \frac{\gamma}{1+\gamma} \frac{1}{28}) + \dots + 25(1-2\alpha-3\alpha^2 - \dots - 20\alpha^{19})(1-\alpha)^2(\frac{1}{1+\gamma} \frac{1}{352} + \frac{\gamma}{1+\gamma} \frac{1}{350})]}{(1-\alpha)^2 \times 2000} \quad (6.12)$$

In spite of the complicated appearance of equation 6.12, it can be easily solved for  $\alpha$ . We call this solution  $\alpha_1$  in the rest of the paper. From its definition,  $\alpha$  is in the range of 0-1 and interestingly 6.12 has only one real root in this range. Figure 6.4 shows the value of the real roots for a wide range of variation in the selectivity. Out of 19 roots, 16 are always imaginary and 2 out of 3 real ones are always greater than 1.

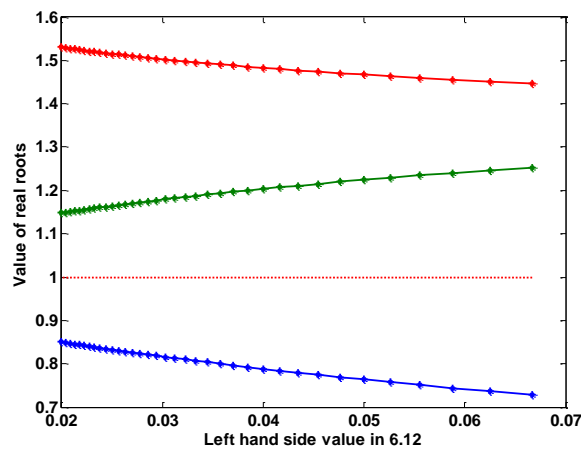


Figure 6.4 Real roots  $\alpha$  as a function of the selectivity ( $1.2 \leq H_2/CO \leq 2.15$ )

### 6.3.2 Using modified function of Yermakova and Anikeev ( $\alpha_2$ )

The following function has been proposed by Yermakova and Anikeev (2000) and modified by Song et al. (2004).

$$\alpha = (0.2332 \frac{y_{CO}}{y_{CO} + y_{H_2}} + 0.633)[1 - 0.0039(T - 533)] \quad (6.13)$$

Here  $y_{CO}$  and  $y_{H_2}$  are mole fractions in the FT reactor and T is reactor temperature (K). The given range of operating conditions are H<sub>2</sub>/CO ratio from 0.5 to 4 and temperature from 423 K to 803 K (Song et al. 2004). In the rest of this paper this value for  $\alpha$  is denoted  $\alpha_2$ .

### 6.3.3 Constant $\alpha$ ( $\alpha_3$ )

A constant  $\alpha$  of 0.9 is frequently proposed in the literature at typical operating conditions of a low temperature Cobalt based FT slurry bubble column reactor (Satterfield et al. 1989; Jager and Espinoza 1995). We call this value  $\alpha_3=0.9$ .

## 6.4 Single-pass Fischer Tropsch reactor

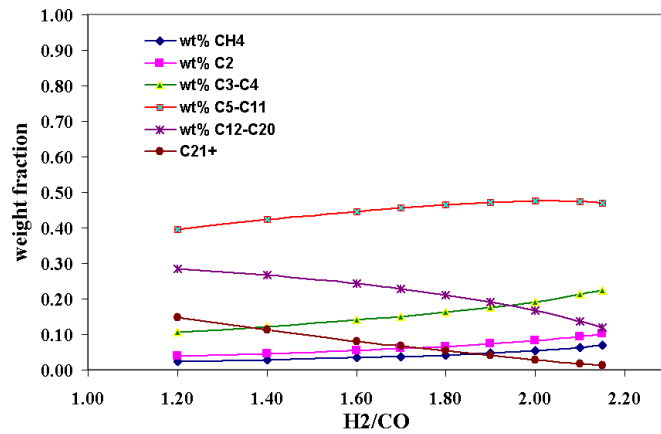
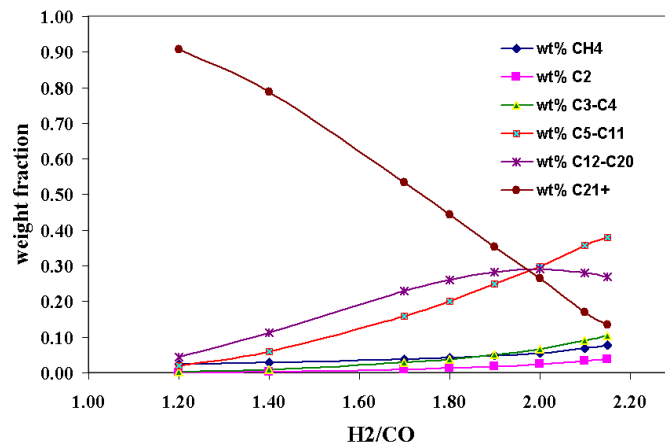
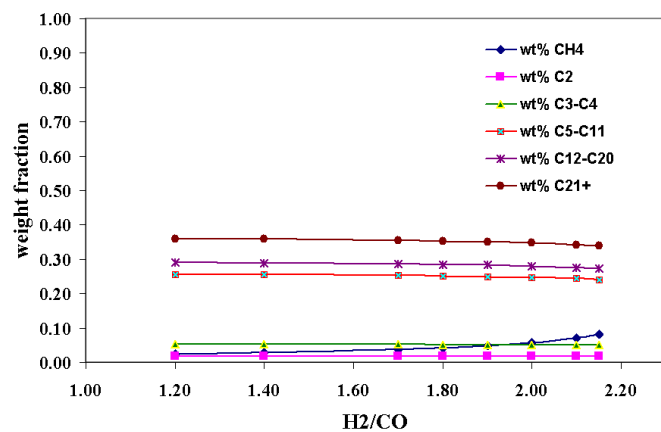
We simulated the FT reactor individually (single pass) with only CO and H<sub>2</sub> in the feed, and show in Figures 6.5, 6.6 and 6.7 how the product distribution depends on the feed H<sub>2</sub>/CO ratio with models  $\alpha_1$ ,  $\alpha_2$  and  $\alpha_3$  for the chain growth probability. The operating pressure and temperature for the reactor are assumed to be 2000 kPa and 210°C.

Table 6.1 shows the corresponding conversion rates of CO, H<sub>2</sub> and production rates of methane and other hydrocarbons for H<sub>2</sub>/CO=2.

Table 6.1 FT reactor performance at H<sub>2</sub>/CO=2 feed when  $\alpha_1$ ,  $\alpha_2$  or  $\alpha_3$  is used

| parameter                                  | $\alpha_1$ | $\alpha_2$ | $\alpha_3$ |
|--|------------|------------|------------|
| CO conversion, %                           | 83.56      | 86.52      | 86.97      |
| H <sub>2</sub> conversion, %               | 90.98      | 91.82      | 91.97      |
| CH <sub>4</sub> formation (kg/kgcat.hr)    | 0.0106     | 0.011      | 0.011      |
| Other hydrocarbons formation (kg/kgcat.hr) | 0.1877     | 0.1924     | 0.1924     |

In Figure 6.8, the value of  $\alpha$  ( $\alpha_1$ ,  $\alpha_2$  and  $\alpha_3$ ) is given as a function of H<sub>2</sub>/CO. We see that  $\alpha_2$  is generally significantly higher than  $\alpha_1$ .  $\alpha_2$  is closest to the commonly used value of  $\alpha_3=0.9$  and in addition the trend in Figure 6.6 ( $\alpha_2$ ) seems more realistic than Figure 6.5 ( $\alpha_1$ ).

Figure 6.5 FT reactor product distribution with  $\alpha_1$  from Iglesia reaction ratesFigure 6.6 FT reactor product distribution with  $\alpha_2$  from Yermakova and AnikeevFigure 6.7 FT reactor product distribution with  $\alpha_3 = 0.9$ 

However, we will use both functions and also the constant  $\alpha$  assumption in the following optimization.

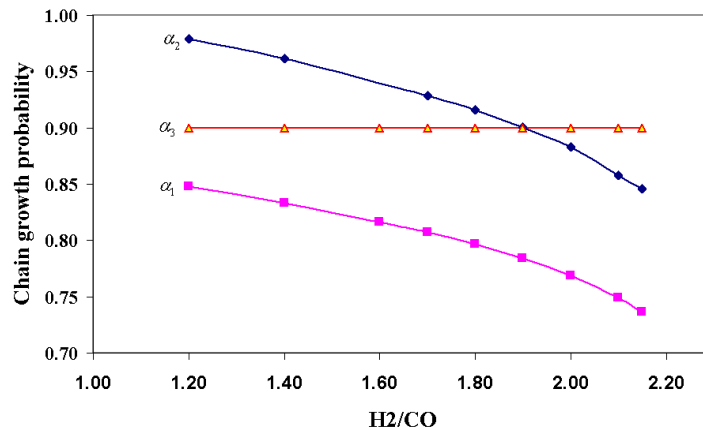


Figure 6.8 Chain growth probability ( $\alpha$ ) as a function of H<sub>2</sub>/CO (feed) for different  $\alpha$  models

## 6.5 Definition of optimal operation for overall process

The operational objective is to maximize the variable income (operational profit) with respect to the operational degrees of freedom subject to satisfying the constraints. Each of these is defined next.

### 6.5.1 Objective function

The objective function to be maximized is:

$$\text{Variable income (P)} = \text{sales revenue} - \text{variable cost} \quad (6.14)$$

The natural gas feedrate to the process side is fixed at 8195 kmol/h, but note that the natural gas used as fuel in the fired heater will vary, mainly depending on the amount and composition of the purged tail gas.

#### Sales revenue

We use the average price over the last 4 years in the Rotterdam market for Gasoline, Diesel and Fuel oil (OPEC 2009). The wax price is set equal to the fuel oil price. For LPG there is a large price variation depending on specifications and location, and an average price of the selling prices in different countries has been assumed. This gives the following prices: LPG (C<sub>3</sub>-C<sub>4</sub>) = 0.9 USD/kg, Gasoline/Naphtha (C<sub>5</sub>-C<sub>11</sub>) = 0.73 USD/kg, Diesel (C<sub>12</sub>-C<sub>20</sub>) = 0.71 USD/kg, Wax (C<sub>21+</sub>) = 0.39 USD/kg.

#### Variable cost

$$\text{Variable cost} = \text{cost of raw materials} + \text{cost of energy} + \text{cost of CO}_2 \text{ removal} \quad (6.15)$$

The raw materials are natural gas, water (steam) and oxygen.

- Natural gas price: 0.5 USD/MMBtu (Halstead 2006) with our gas composition this corresponds to 0.023 USD/kg.
- CO<sub>2</sub> removal cost: 50 USD/ton CO<sub>2</sub> (ZEPReport 2011)
- Water: cost set to zero.
- Energy: cost set to zero (assume excess energy available). Also, we did not include any credit for the “extra” saturated medium-pressure steam generated by the ATR hot effluent.

- Oxygen: It is assumed that the GTL plant must supply the required superheated steam for the oxygen plant, and in addition pay for the used oxygen with a price that decreases somewhat with increased oxygen usage.

$$P_{O_2} = P_{O_2}^o \left( \frac{\dot{m}_{O_2}}{\dot{m}_{O_2}^{ref.}} \right)^{-0.3}, \quad P_{O_2}^o = 0.11 \text{ USD / kg O}_2 \quad (6.16)$$

The price policy makes the income for the O<sub>2</sub> plant less dependent on the operation in the GTL plant and also encourages the GTL plant to use more oxygen. The exponent of -0.3 implies that the oxygen price decreases by a factor of 2 if we use ten times more oxygen. The capacity of the reference oxygen plant at 43.82 kg/sec is estimated based on the data from Holdor Topsøe (Aasberg-Petersen et al. 2003; Dybkjær 2006).

### 6.5.2 Operational Degrees of freedom (steady-state)

The overall plant has 6 operational degrees of freedom at steady-state which can be chosen as the following. The chosen degrees of freedom are the ones, which have significant effect on objective function value and their optimal value is not clear from process understanding. The temperature for the FT reactor is assumed fixed at 210°C. The FT reactor operating pressure is assumed constant at 20 bar, which is the assumed maximum pressure for the reactor due to material constraints.

1-  $\frac{H_2O}{C(\text{hydrocarbon})}$  (fresh + recycled),

2-  $\frac{O_2}{C(\text{hydrocarbon})}$  (into ATR),

3- Fired heater duty,

4- CO<sub>2</sub> recovery percentage,

5- Purge ratio,

6- Recycle ratio to FT reactor

### 6.5.3 Operational constraints

We consider the following constraints during the optimization;

1. Molar ratio  $H_2O/C \geq 0.3$  in feed to syngas unit. This is to avoid soot formation in the ATR. Haldor Topsøe reports (Aasberg-Petersen et al. 2003) soot free pilot operation at  $H_2O/C$  ratios even as low as 0.2 but we conservatively use a lower bound of 0.3.
2. ATR exit temperature  $\leq 1030^\circ C$ . This temperature is an average of some the reported operating outlet ATR temperatures by Haldor Topsøe that ensures soot-free operation (Aasberg-Petersen et al. 2003).
3. Inlet temperature to ATR  $\leq 675^\circ C$ . This is a material constraint (Bakkerud 2009).
4. The purge ratio is optimally around 2% but for simulation purposes (avoid convergence problem) it has bounded at a higher value (5% for  $\alpha_1$  model and 3% for  $\alpha_2$  and  $\alpha_3$  models).

## 6.6 Optimization results

The optimization (maximize P with respect to the degrees of freedom and constraints) was repeated using the three different  $\alpha$  models (6.12, 6.13 and constant  $\alpha$ ). For each  $\alpha$  model, two price scenarios for the final products are considered. The first is the one mentioned earlier and the second is when the price of the wax is assumed to be twice as high i.e. 0.78 USD/kg.

The UniSim “Mixed” method is used for optimization. This method initially uses the BOX method which is based on the Downhill Simplex algorithm and then a SQP method to locate the final solution (UniSim 2008). The results are reported in Tables 6.2, 6.3 and 6.4.

For models  $\alpha_1$  and  $\alpha_3$  there is almost no effect of the wax price. The results with  $\alpha_2$  model seem more reasonable because a quite large sensitivity to the wax prices is expected. The H<sub>2</sub> to CO ratio (both in fresh syngas and in inlet stream into the FT reactor) are compared as these usually are considered the main parameters in determining the product distribution of GTL processes. The carbon efficiency in the Tables is defined as the ratio of carbon in the products and carbon in the natural gas feed, including natural gas used as fuel in the fired heater.

In all cases we get the following three optimally active constraints:

- The purge ratio is active at its minimum (5% for  $\alpha_1$  model and 3% for  $\alpha_2$  and  $\alpha_3$ ).
- The fired heater outlet temperature is active at the maximum, 675°C.
- The ATR outlet temperature is active at the maximum, 1030°C. Since the outlet temperature of ATR is quite high (1030°C), the equilibrium assumption is reasonable.

Table 6.2 Optimal operation when model  $\alpha_1$  is used

| Wax price scenario                  | $\frac{\text{H}_2\text{O}}{\text{C}}$<br>(fresh+recycle) | $\frac{\text{O}_2}{\text{C}}$<br>(into ATR) | CO <sub>2</sub> recovery | Recycle to FT | Purge of tail gas | $\frac{\text{H}_2}{\text{CO}}$ fresh | $\frac{\text{H}_2}{\text{CO}}$ into FT | $\alpha_1$ | Carbon efficiency | Objective function (USD/hr) |
|-------------------------------------|--|---|--------------------------|---------------|-------------------|--------------------------------------|--|------------|-------------------|-----------------------------|
| 0.39 $\frac{\text{USD}}{\text{kg}}$ | 0.9080   | 0.5185                                      | 97.51%                   | 82.00%        | 5%                | 2.06                                 | 1.80                                   | 0.77       | 70.00%            | 41667                       |
| 0.78 $\frac{\text{USD}}{\text{kg}}$ | 0.8059   | 0.5150                                      | 93.24%                   | 84.90%        | 5%                | 2.02                                 | 1.67                                   | 0.78       | 70.33%            | 43037                       |

Table 6.3 Optimal operation when model  $\alpha_2$  is used (recommended)

| Wax price scenario                  | $\frac{\text{H}_2\text{O}}{\text{C}}$<br>(fresh+recycle) | $\frac{\text{O}_2}{\text{C}}$<br>(into ATR) | CO <sub>2</sub> recovery | Recycle to FT | Purge of tail gas | $\frac{\text{H}_2}{\text{CO}}$ fresh | $\frac{\text{H}_2}{\text{CO}}$ into FT | $\alpha_2$ | Carbon efficiency | Objective function (USD/hr) |
|-------------------------------------|--|---|--------------------------|---------------|-------------------|--------------------------------------|--|------------|-------------------|-----------------------------|
| 0.39 $\frac{\text{USD}}{\text{kg}}$ | 0.8036   | 0.5226                                      | 93.00%                   | 73.50%        | 3%                | 2.19                                 | 2.22                                   | 0.83       | 72.23%            | 44292                       |
| 0.78 $\frac{\text{USD}}{\text{kg}}$ | 0.5100   | 0.5283                                      | 46.00%                   | 86.00%        | 3%                | 1.88                                 | 1.39                                   | 0.92       | 75.94%            | 54795                       |

Table 6.4 Optimal operation with fixed  $\alpha_3=0.9$

| Wax price scenario                  | $\frac{\text{H}_2\text{O}}{\text{C}}$<br>(fresh+recycle) | $\frac{\text{O}_2}{\text{C}}$<br>(into ATR) | CO <sub>2</sub> recovery | Recycle to FT | Purge of tail gas | $\frac{\text{H}_2}{\text{CO}}$ fresh | $\frac{\text{H}_2}{\text{CO}}$ into FT | $\alpha_3$ | Carbon efficiency | Objective function (USD/hr) |
|-------------------------------------|--|---|--------------------------|---------------|-------------------|--------------------------------------|--|------------|-------------------|-----------------------------|
| 0.39 $\frac{\text{USD}}{\text{kg}}$ | 0.441  | 0.5047                                      | 90.78%                   | 79.08%        | 3%                | 2.08                                 | 1.98                                   | 0.90       | 75.92%            | 38470                       |
| 0.78 $\frac{\text{USD}}{\text{kg}}$ | 0.4406   | 0.5076                                      | 91.00%                   | 77.08%        | 3%                | 2.07                                 | 1.97                                   | 0.90       | 75.87%            | 54680                       |

One can imagine that the fired heater outlet temperature is set by the fired heater duty, and the ATR outlet temperature is set by the oxygen feedrate. This leaves three unconstrained optimization degrees of freedom ( $H_2O/C$  feed ratio, recycle ratio to FT reactor, and  $CO_2$  recovery fraction), for which, the optimal values result from the optimization. For each of these three degrees of freedom, controlled variables need to be identified. This will be the topic of a future study. We now use the  $\alpha_2$  model in a more detailed study using an average wax price of 0.63 USD/kg. The results of the optimization for this case are shown in Table 6.5.

Table 6.5 Optimal nominal values ( $\alpha_2$  model), wax price=0.63 USD/kg

| $\frac{H_2O}{C}$<br>(fresh+recycle) | $\frac{O_2}{C}$<br>(into ATR) | $CO_2$<br>recovery | Recycle<br>to FT | Purge<br>of tail<br>gas | $\frac{H_2}{CO}$<br>fresh | $\frac{H_2}{CO}$<br>into FT | $\alpha_2$ | Carbon<br>efficiency | Objective<br>function<br>(USD/hr) |
|-------------------------------------|-------------------------------|--------------------|------------------|-------------------------|---------------------------|-----------------------------|------------|----------------------|-----------------------------------|
| 0.6389                              | 0.5233                        | 75.76%             | 76.83%           | 3%                      | 2.1                       | 2.01                        | 0.87       | 74.24%               | 48402                             |

Figure 6.9 shows the dependency of the profit function with respect to the six degrees of freedom around the nominal optimal point. It shows that the profit value is sensitive to change in the active constraints: purge ratio (Figure 6.9d), ATR inlet and outlet temperatures (Figures 6.9e and 6.9f). The unconstrained degrees of freedom; The  $H_2O/C$  (Figure 6.9a) and tail gas recycle ratio to FT (Figure 6.9b) have also significance effect on the objective function while the objective function is almost flat with respect to the change in  $CO_2$  recovery (Figure 6.9c).

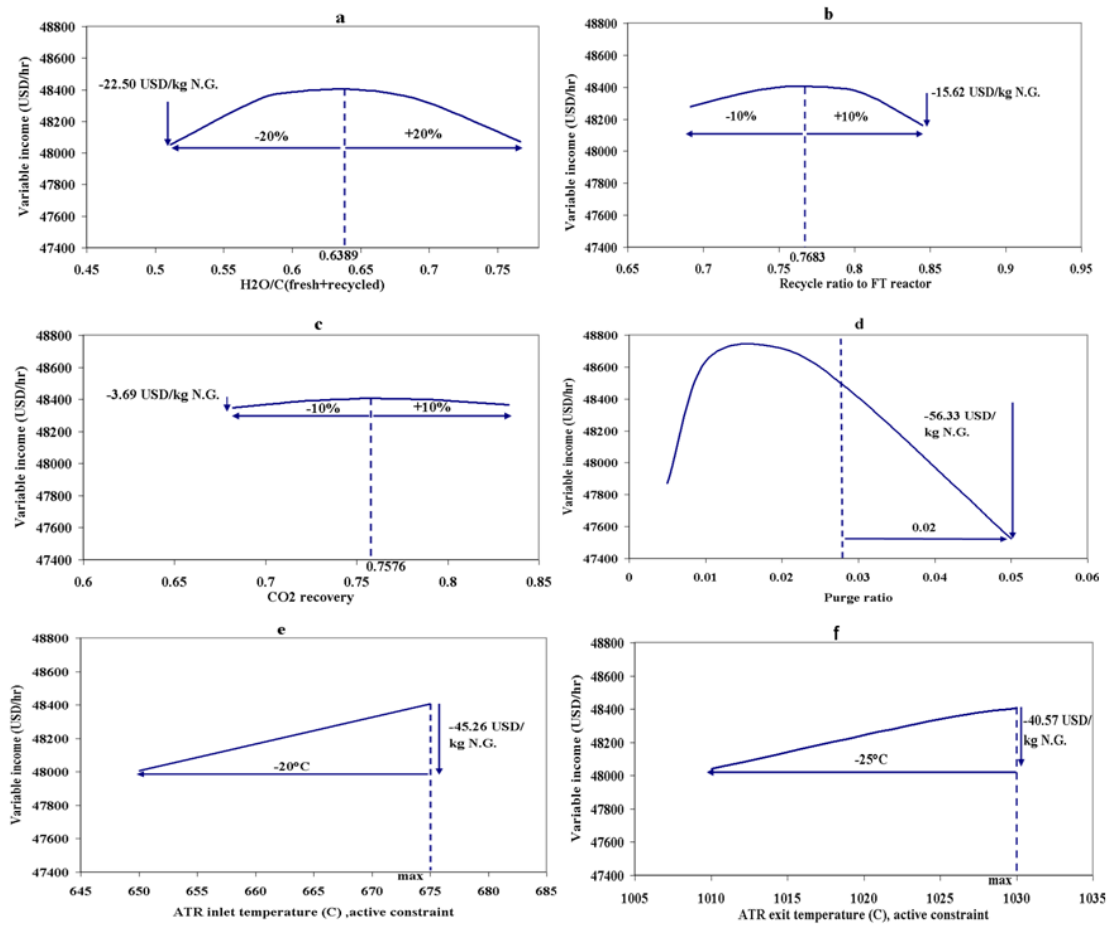


Figure 6.9 Dependency of the variable income with respect to the decision variables and active constraints around optimal nominal point (nominal data from Table 6.5)

The amount of light hydrocarbons carried along with the recycle vapor stream leaving the three-phase separator depends on the conversion in the FT reactor, the H<sub>2</sub>/CO ratio at the outlet of syngas unit and chain growth probability. For example, in the nominal case the tail gas composition on molar basis is: CH<sub>4</sub>: 35.87%, H<sub>2</sub>:21.42%, CO: 14.54%, N<sub>2</sub>: 11.73%, CO<sub>2</sub>: 8.38%, H<sub>2</sub>O: 0.24% and other hydrocarbons: 7.82%.

The CH<sub>4</sub> in the tail gas should be recycled to the syngas unit, whereas the un-reacted CO and H<sub>2</sub> should be recycled to FT reactor for further conversion, while the inert N<sub>2</sub> should be purged. The optimal values for recycle and purge are determined by the optimization as shown in Table 6.5. Note that there is no constraint on the inert fraction. The recycled tail gas to the syngas unit needs to be compressed to 30 bar (Compressor in Figure 6.2). The compressor work duty is only 1.15 MW, which is small compared to the fired heater duty of 326 MW (thermodynamically, the equivalent work is about 54 MW).

We will use this model in the next chapter to find the best controlled variables and propose control structure in a systematic manner for different operational regions.

## 6.7 Conclusions

A gas to liquids process (GTL) has been simulated and optimized to describe the effect of decision variables on the plant variable income. Auto-thermal reforming (ATR) was chosen for syngas production and a Cobalt based slurry bubble column reactor was simulated using proposed Fischer-Tropsch reaction rates by Iglesia et al. Three different criteria for Fischer-Tropsch products distribution have been considered and the one proposed by Yermakova and Anikeev can very well describe dependencies in the overall process. The achieved model will be used for further control and economic studies.

### Acknowledgment

The authors gratefully thank Dr. Dag Schanke (GTL specialist) at Statoil R&D center in Trondheim for his valuable discussions, comments and helping in design and simulation of the process.

### Appendix

The proposed reaction rates by Iglesia et al. are as below (Iglesia et al. 1993):

$$r_{CH_4} = \frac{1.08 \times 10^{-8} P_{H_2} P_{CO}^{0.05}}{1 + 3.3 \times 10^{-5} P_{CO}} \left( \frac{mol_{CH_4}}{\text{g-atom surface metal. s}} \right) \quad (\text{A-1})$$

$$r_{CO} = \frac{1.96 \times 10^{-8} P_{H_2}^{0.6} P_{CO}^{0.65}}{1 + 3.3 \times 10^{-5} P_{CO}} \left( \frac{mol_{CO}}{\text{g-atom surface metal. s}} \right) \quad (\text{A-2})$$

To convert these values to more common units, the following assumptions are made (Schanke 2010);

- The catalyst density is 2000 kg/m<sup>3</sup>,
- The weight fraction of Cobalt in the catalyst is 20% and 10% of the Cobalt is exposed as surface atoms,
- The catalyst volume fraction in the reactor is 10 %.

This gives the following values for  $r_{CO}$  and  $r_{CH_4}$  :

$$r_{CO} = \frac{1.96 \times 10^{-8} P_{H_2}^{0.6} P_{CO}^{0.65}}{1 + 3.3 \times 10^{-5} P_{CO}} \left( \frac{mol_{CO}}{g\text{-atom surface metal. s}} \right) \times \left( \frac{0.1g\text{-atom surface metal}}{mol_{CO\text{-total}}} \right) \times \left( \frac{1mol_{CO\text{-total}}}{58.9gr_{CO\text{-total}}} \right) \times \left( \frac{0.2gr_{CO\text{-total}}}{gr.Cat.} \right) \times \left( \frac{2000 \times 10^3 gr_{cat.}}{m^3} \right) \times \left( \frac{0.10m^3}{m_{reactor}^3} \right) \times \left( \frac{1kmol_{CO}}{1000mol_{CO}} \right) = \frac{1.331 \times 10^{-9} P_{H_2}^{0.6} P_{CO}^{0.65}}{1 + 3.3 \times 10^{-5} P_{CO}} \left( \frac{kmol_{CO}}{m_{reactor}^3 \cdot s} \right) \quad (A-3)$$

$$r_{CH_4} = \frac{1.08 \times 10^{-8} P_{H_2} P_{CO}^{0.05}}{1 + 3.3 \times 10^{-5} P_{CO}} \left( \frac{mol_{CH_4}}{g\text{-atom surface metal. s}} \right) \times \left( \frac{0.1g\text{-atom surface metal}}{mol_{CO\text{-total}}} \right) \times \left( \frac{1mol_{CO\text{-total}}}{58.9gr_{CO\text{-total}}} \right) \times \left( \frac{0.2gr_{CO\text{-total}}}{gr.Cat.} \right) \times \left( \frac{2000 \times 10^3 gr_{cat.}}{m^3} \right) \times \left( \frac{0.10m^3}{m_{reactor}^3} \right) \times \left( \frac{1kmol_{CH_4}}{1000mol_{CH_4}} \right) = \frac{7.334 \times 10^{-10} P_{H_2} P_{CO}^{0.05}}{1 + 3.3 \times 10^{-5} P_{CO}} \left( \frac{kmol_{CH_4}}{m_{reactor}^3 \cdot s} \right) \quad (A-4)$$

Selectivity to different hydrocarbons in FT reactions is described by well-known ASF ideal model as (A-5):

$$w_n = n(1 - \alpha)^2 \alpha^{n-1} \quad (A-5)$$

where  $w_n$  is the weight fraction of  $C_n$  and  $\alpha$  is chain growth probability. Note that  $w_n$  is fraction of carbon atoms reacted totally which ends up in product with n C-atoms. This is almost (which is assumed here) but not completely the same as weight fraction (Schanke 2010).

Based on mass balance:

mass of consumed carbon as CO = mass of produced carbons ( $C_n$ ) as FT products

The rate of CO consumption is correlated with weight fraction of the produced hydrocarbons as (A-6).

$$r_{CO} \left( \frac{kmol_{CO}}{m_{reactor}^3 \cdot hr} \right) \times \frac{12kg_C}{1kmol_{CO}} \times FT \text{ reactor volume}(m^3) = w_1 \left( \frac{kg_{CH_4}}{kg_{total \text{ hydrocarbons}}} \right) \times W_{total} (kg_{total \text{ hydrocarbons}} / hr) \times \frac{12kg_C}{16kg_{CH_4}} + W_{total} (kg_{total \text{ hydrocarbons}} / hr) \times \left[ w_2 \left( \frac{kg_{C_2H_6}}{kg_{total \text{ hydrocarbons}}} \right) \times \frac{1}{1+\gamma} \times \frac{2 \times 12kg_C}{30kg_{C_2H_6}} + w_2 \left( \frac{kg_{C_2H_4}}{kg_{total \text{ hydrocarbons}}} \right) \times \frac{\gamma}{1+\gamma} \times \frac{2 \times 12kg_C}{28kg_{C_2H_4}} \right] + W_{total} (kg_{total \text{ hydrocarbons}} / hr) \times \left[ w_3 \left( \frac{kg_{C_3H_8}}{kg_{total \text{ hydrocarbons}}} \right) \times \frac{1}{1+\gamma} \times \frac{3 \times 12kg_C}{44kg_{C_3H_8}} + w_3 \left( \frac{kg_{C_3H_6}}{kg_{total \text{ hydrocarbons}}} \right) \times \frac{\gamma}{1+\gamma} \times \frac{3 \times 12kg_C}{42kg_{C_3H_6}} \right] + \dots + W_{total} (kg_{total \text{ hydrocarbons}} / hr) \times \left[ w_{20} \left( \frac{kg_{C_{20}H_{42}}}{kg_{total \text{ hydrocarbons}}} \right) \times \frac{1}{1+\gamma} \times \frac{20 \times 12kg_C}{282kg_{C_{20}H_{42}}} + w_{20} \left( \frac{kg_{C_{20}H_{40}}}{kg_{total \text{ hydrocarbons}}} \right) \times \frac{\gamma}{1+\gamma} \times \frac{20 \times 12kg_C}{280kg_{C_{20}H_{40}}} \right] + W_{total} (kg_{total \text{ hydrocarbons}} / hr) \times \left[ w_{25} \left( \frac{kg_{C_{25}H_{52}}}{kg_{total \text{ hydrocarbons}}} \right) \times \frac{1}{1+\gamma} \times \frac{25 \times 12kg_C}{352kg_{C_{25}H_{52}}} + w_{25} \left( \frac{kg_{C_{25}H_{50}}}{kg_{total \text{ hydrocarbons}}} \right) \times \frac{\gamma}{1+\gamma} \times \frac{25 \times 12kg_C}{350kg_{C_{25}H_{50}}} \right] \quad (A-6)$$

$$\text{where } w_{25} = (1 - w_1 - w_2 - \dots - w_{20}) \quad (A-7)$$

and  $\gamma$  is Olefin to Paraffin ratio. 20 reactions ( $C_1$ - $C_{20}$ ) for paraffins and 19 reactions for Olefins ( $C_2$ - $C_{20}$ ) are defined with weight fraction of  $w_n$  and the rest of the hydrocarbons are estimated with  $C_{25}$  as Wax ( $C_{21+}$ ) with weight fraction of  $w_{25}$ . Simplification of eq.(A-6) yields weight of total hydrocarbons ( $kg_{total \text{ hydrocarbons}} / hr$ ) in the product as eq.(A-8). We choose reactor volume=2000m<sup>3</sup> which gives reasonable CO and H<sub>2</sub> conversion in our model.

$$W_{total} (kg_{total \text{ hydrocarbons}} / hr) = \frac{r_{CO} \times 2000}{\left[ \frac{w_1}{16} + 2w_2 \left( \frac{1}{1+\gamma} \frac{1}{30} + \frac{\gamma}{1+\gamma} \frac{1}{28} \right) + \dots + 25w_{25} \left( \frac{1}{1+\gamma} \frac{1}{352} + \frac{\gamma}{1+\gamma} \frac{1}{350} \right) \right]} \quad (A-8)$$

By having  $W_{total}$ , production rates of all hydrocarbons (paraffins and olefins) can be described as below.

$$r_{CH_4} = \frac{w_1 \times W_{total}}{16} \times \frac{1}{1+\gamma} = \frac{w_1}{30 \times \left[ \frac{w_1}{16} + 2w_2 \left( \frac{1}{1+\gamma} \frac{1}{30} + \frac{\gamma}{1+\gamma} \frac{1}{28} \right) + \dots + 25w_{25} \left( \frac{1}{1+\gamma} \frac{1}{352} + \frac{\gamma}{1+\gamma} \frac{1}{350} \right) \right]} \times \frac{1}{1+\gamma} \times r_{CO} \times 2000 \quad (A-9)$$

$$r_{C_2H_6} = \frac{w_2 \times W_{total}}{30} \times \frac{1}{1+\gamma} = \frac{w_2}{30 \times \left[ \frac{w_1}{16} + 2w_2 \left( \frac{1}{1+\gamma} \frac{1}{30} + \frac{\gamma}{1+\gamma} \frac{1}{28} \right) + \dots + 25w_{25} \left( \frac{1}{1+\gamma} \frac{1}{352} + \frac{\gamma}{1+\gamma} \frac{1}{350} \right) \right]} \times \frac{1}{1+\gamma} \times r_{CO} \times 2000 \quad (A-10)$$

$$r_{C_2H_4} = \frac{w_2 \times W_{total}}{28} \times \frac{\gamma}{1+\gamma} = \frac{w_2}{28 \times \left[ \frac{w_1}{16} + 2w_2 \left( \frac{1}{1+\gamma} \frac{1}{30} + \frac{\gamma}{1+\gamma} \frac{1}{28} \right) + \dots + 25w_{25} \left( \frac{1}{1+\gamma} \frac{1}{352} + \frac{\gamma}{1+\gamma} \frac{1}{350} \right) \right]} \times \frac{\gamma}{1+\gamma} \times r_{CO} \times 2000 \quad (A-11)$$

...

$$r_{C_{25}H_{52}} = \frac{w_{25} \times W_{total}}{352} \times \frac{1}{1+\gamma} = \frac{(1 - w_1 - w_2 - \dots - w_{25})}{352 \times \left[ \frac{w_1}{16} + 2w_2 \left( \frac{1}{1+\gamma} \frac{1}{30} + \frac{\gamma}{1+\gamma} \frac{1}{28} \right) + \dots + 25w_{25} \left( \frac{1}{1+\gamma} \frac{1}{352} + \frac{\gamma}{1+\gamma} \frac{1}{350} \right) \right]} \times \frac{1}{1+\gamma} \times r_{CO} \times 2000 \quad (A-12)$$

$$r_{C_{25}H_{50}} = \frac{w_{25} \times W_{total}}{350} \times \frac{\gamma}{1+\gamma} = \frac{(1 - w_1 - w_2 - \dots - w_{25})}{350 \times \left[ \frac{w_1}{16} + 2w_2 \left( \frac{1}{1+\gamma} \frac{1}{30} + \frac{\gamma}{1+\gamma} \frac{1}{28} \right) + \dots + 25w_{25} \left( \frac{1}{1+\gamma} \frac{1}{352} + \frac{\gamma}{1+\gamma} \frac{1}{350} \right) \right]} \times \frac{\gamma}{1+\gamma} \times r_{CO} \times 2000 \quad (A-13)$$

$\gamma$  (Olefins to Paraffins ratio) is assumed to be in average value of 0.35 for all hydrocarbons (Iglesia et al. 1993).



## Chapter 7

# Selection of the Controlled Variables for a GTL Process

This chapter is based on the paper “Selection of Controlled Variables for a Natural Gas to Liquids (GTL) Process Using Self-Optimizing Method” planned for submission to Industrial & Engineering Chemistry Research Journal

In this chapter, selection of the best individual and combined controlled variables (CVs) for a natural gas to hydrocarbon liquids (GTL) process is considered using self-optimizing method. The objective function is to maximize the variable income of the plant and two modes of operation are studied. In mode I, where natural gas flowrate is given, there are three unconstrained degrees of freedom (DOFs) and the corresponding individual self-optimizing CVs are CO<sub>2</sub> recovery in fresh synthesis gas (syngas), CO mole fraction in fresh syngas and CO mole fraction in recycle tail gas from the Fischer Tropsch (FT) reactor. This set of CVs gives the minimum worst-case loss of 1393 USD/hr. Adding one, two and three more measurements, to control combinations of measurements decrease the worst-case loss significantly to 184, 161 and 53 USD/hr respectively. In mode II, the natural gas flowrate is a degree of freedom and it is optimal to increase it as much as possible. The variable income increases almost linearly until the oxygen flowrate becomes active. Practically, this is the maximum achievable income. Theoretically, it is possible to increase the natural gas flowrate to improve the objective function but this results in very large recycle flowrates into FT reactor where its volume is the limitation and this causes snowball effect.

## 7.1 Introduction

For large natural gas reservoirs, converting natural gas to transportable liquid fuels (GTL) is economical when the target markets are further away than approx. 2500 km from the resources. Figure 7.1 shows the gas commercialization options and situation of GTL processes comparing to other possibilities of transportation, converting or usages.

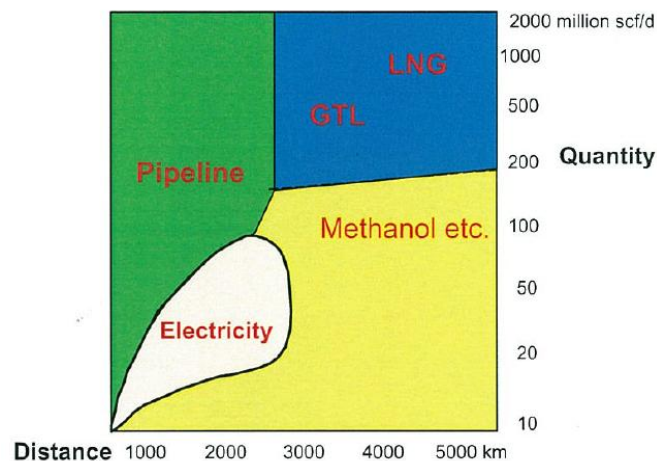


Figure 7.1 Gas commercialization options and situation of GTL processes (GTL-Workshop 2010)

In this chapter, optimal operation of a GTL process is considered using the top-down part of general plantwide control procedure of Skogestad (Skogestad 2004). The emphasis is on self-optimizing method for selection of the best controlled variables (individual and combination of measurements). We want to operate this plant economically efficient in presence of unexpected disturbances. The main issue is “which variables should be controlled?” To select the best controlled variables, the self-optimizing method is applied. Self-optimizing control is when we can achieve an acceptable loss with constant setpoint values for the controlled variables (CVs) without the need to reoptimize when disturbances occur (Skogestad 2004). This means that we use off-line optimization and analysis to design a control structure that can use constant setpoint policy for the CVs. This may completely remove the need for a real time optimization layer (RTO) for updating the setpoints when disturbances occur. But we will need to accept a small loss in objective cost compared to the case when RTO. By using measurements, the loss can be decreased significantly (from engineering point of view approximately to zero). Based on the loss magnitude one can decide on using individual or combination of measurements as self-optimizing CVs.

Generally, self-optimizing method is considered in two modes of operation. In mode I, feedrate to the process is given and in mode II, maximum possible throughput is achieved. The steps of the self-optimizing method are as follows.

1. Step 1: define the objective function and constraints
2. Step 2: identify degrees of freedom (DOFs) for optimization
3. Step 3: identification of important disturbances
4. Step 4: optimization
5. Step 5: identification of candidate controlled variables
6. Step 6: selection of CVs

In section 7.3, the self-optimizing steps are followed in details for the GTL process to select the best controlled variables. The UniSim commercial simulator is used for modeling the process.

## 7.2 Process description

GTL processes include three main steps (see Figure 7.2) to convert natural gas to a range of liquid fuels. In the synthesis gas (syngas) unit, natural gas is reacted with oxygen and steam to “syngas” a mixture of CO and H<sub>2</sub> which is further converted to a range of liquid hydrocarbon fuels by the highly exothermic Fischer-Tropsch (FT) reactions.

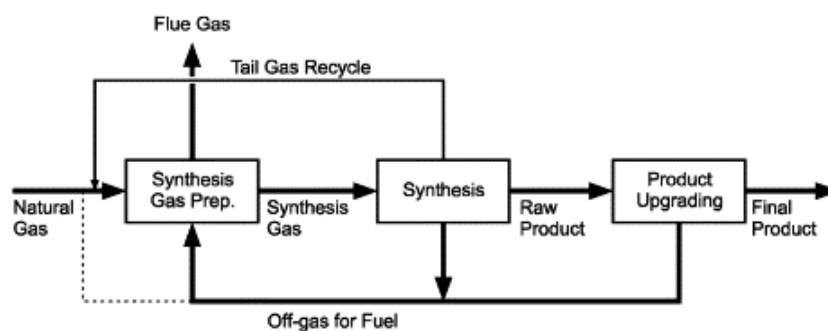


Figure 7.2 A simple flowsheet of GTL process (Rostrup-Nielsen et al. 2000)

The FT hydrocarbon products include mostly paraffins and olefins in the range from light (methane) to heavy hydrocarbons (wax). The heavier products are upgraded in the upgrading unit to clean fuels and light hydrocarbons are recycled back to the syngas unit or used as fuel inside the plant.

In the current chapter, the process model is taken from previous chapter (Panahi et al. 2011) where the details of modeling and optimization of GTL process are discussed. Figure 7.3 shows the process flowsheet. The main unit operations in the flowsheet are: pre-reformer, fired heater, auto-thermal reformer (ATR), which is claimed to be the best way for syngas production (Aasberg-Petersen et al. 2003), CO<sub>2</sub> removal of syngas stream and the FT reactor, which in our case is a Cobalt based slurry bubble column reactor (SBCR).

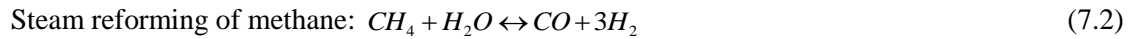
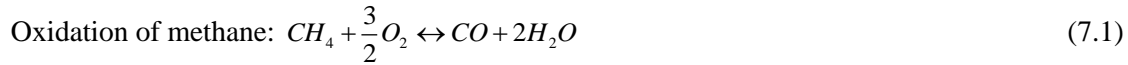
### Fired heater

Natural gas and recycled hydrocarbons from the FT unit are mixed and preheated in the fired heater to 455°C (Schanke and Sogge 2010) and then enter the pre-reformer. In the pre-reformer, all heavier hydrocarbons are converted by reaction with steam to syngas. The advantage of the pre-reformer is that one avoids cracking in the subsequent ATR. The methanation and shift reactions are assumed to be in equilibrium in the pre-reformer (Christensen 1996). The required superheated process steam is supplied by superheating (in the fired heater) the saturated steam that is produced by heat exchange with the ATR's outlet hot stream. The outlet of the pre-reformer is preheated in fired heater and then enters the ATR. Oxygen, which is supplied by the air separation unit (ASU) is also preheated to 200°C (Aasberg-Petersen et al. 2003) in the fired heater and is then blown into the ATR. Note that, turbines (to drive the compressors) in the ASU are the main consumers of superheated steam. A large portion (approx. 50%) of the fired heater duty is therefore used to supply superheated steam for the ASU. The power consumption in the ASU is assumed to be  $400 \frac{\text{kWh}}{\text{ton}_{\text{O}_2}}$  (Schanke and Sogge 2010).



### Auto-thermal reformer

The following reactions take place in the ATR (Aasberg-Petersen et al. 2001):



Whereas the outlet of the ATR is more than 1000°C, the FT reactor is operating at very much lower temperatures around 210°C. The heat from the syngas is used in a reboiler to generate saturated steam. Syngas is then further cooled down to separate out associated water. In the next unit, the CO<sub>2</sub> contents is reduced (amine absorption/stripping process can be an option). The prepared syngas, which we call the fresh syngas, has a H<sub>2</sub> to CO ratio of around 2-2.1. The exact ratio is decided by the optimizer. Syngas unit is assumed to operate at 30bar and we nominally assume a 3bar pressure drop between the syngas unit and FT reactor (Schanke and Sogge 2010). This is simulated using a valve (see V-1 in Figure 7.3) with variable pressure drop as function of flowrate. Therefore, the pressure of fresh syngas to the FT reactor is 27bar.

### Fischer Tropsch (FT) reactor

The highly exothermic FT reactions are described by Yates and Satterfield reactions (Yates and Satterfield 1991).



where  $n \geq 2$ .

The products are paraffins and olefins. Methane formation is also unavoidable. We use the proposed reaction rates of (Iglesia et al. 1993) for Cobalt based FT reactions to simulate the slurry bubble column FT reactor (SBCR).

$$r_{CH_4} = \frac{1.08 \times 10^{-8} P_{H_2} P_{CO}^{0.05}}{1 + 3.3 \times 10^{-5} P_{CO}} \left( \frac{mol_{CH_4}}{g\text{-atom\_surface metal. s}} \right) \quad (7.5)$$

$$r_{CO} = \frac{1.96 \times 10^{-8} P_{H_2}^{0.6} P_{CO}^{0.65}}{1 + 3.3 \times 10^{-5} P_{CO}} \left( \frac{mol_{CO}}{g\text{-atom\_surface metal. s}} \right) \quad (7.6)$$

The details of the reaction rates and reactor simulation is given in chapter 6 (Panahi et al. 2011). The following lumps are assumed to describe the FT products: C<sub>1</sub>, C<sub>2</sub>, LPG (C<sub>3</sub>-C<sub>4</sub>), Gasoline/Naphtha (C<sub>5</sub>-C<sub>11</sub>), Diesel (C<sub>12</sub>-C<sub>20</sub>) and Wax (C<sub>21+</sub>). Light ends (mostly C<sub>1</sub> and C<sub>2</sub>) are either recycled to the syngas unit or purged to be used as fuel for the fired heater.

The FT reactor operates at 27bar and 210°C. The pressure drop in the FT reactor is assumed to be 2 bar. The FT reactions are as mentioned highly exothermic, but an advantage of slurry reactors is their excellent heat removal properties. Therefore, it is easy to control the reactor temperature at almost constant temperature. Boiling water is used as the cooling medium. By controlling the boiling water pressure, the reactor temperature can indirectly be controlled. A compressor (Compressor II in the flowsheet) was added in the FT recycle loop to compensate for the 2bar pressure drop in the FT reactor. The ASF model is used to describe the distribution of the products.

$$w_n = n(1-\alpha)^2 \alpha^{n-1} \quad (7.7)$$

Here  $w_n$  is the weight fraction of hydrocarbons (C<sub>n</sub>) and  $\alpha$  is the chain growth probability. Figure 7.4 illustrates the meaning of chain growth probability.

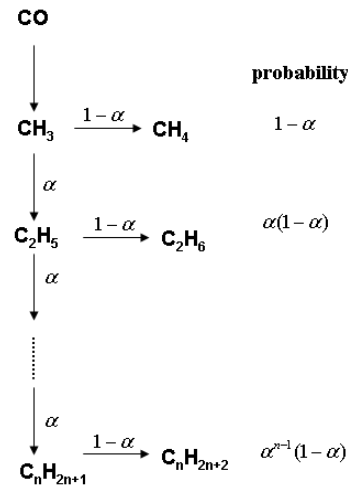


Figure 7.4 Probability of the chain growth to hydrocarbons in FT reactions

As Figure 7.4 shows the selectivity to hydrocarbons is a function of the chain growth probability. The factor  $\alpha$  is a function of the hydrogen to carbon monoxide ratio. In previous chapter we discussed these dependencies (Panahi et al. 2011) and showed that how significance is this ratio. We use the function proposed by Yermakova and Anikeev (2000) and modified by Song et al. (2004) to calculate chain growth probability:

$$\alpha = (0.2332 \frac{y_{CO}}{y_{CO} + y_{H_2}} + 0.633)[1 - 0.0039(T - 533)] \quad (7.8)$$

Here,  $y_{CO}$  and  $y_{H_2}$  are mole fractions in the FT reactor and T is reactor temperature (K).

In the next section, we apply the self-optimizing method (Skogestad 2004) to select the best individual and combined self-optimizing CVs for this process.

## 7.3 Top-down analysis for operation of the GTL process

We perform the analysis in two modes of operation; in mode I, the natural gas feed flowrate is given (disturbance) and in mode II, the natural gas feed flowrate is a degree of freedom for optimization. Achieving maximum possible profit where bottleneck of the process is met is the target in mode II.

### 7.3.1 Mode I: natural gas flowrate is given

The steps of the top-down analysis are as follow.

#### 7.3.1.1 Step 1. Define the objective function and constraints

We define variable income (profit) as the objective function to be maximized.

$$\text{Variables income} = \text{sales revenue} - \text{variable cost} \quad (7.9)$$

$$\text{Variable cost} = \text{cost of raw materials} + \text{cost of energy} + \text{cost of CO}_2 \text{ removal} \quad (7.10)$$

The prices for raw materials, products and other costs are given in Table 7.1 (Panahi et al. 2011).

Table 7.1 Assumed prices cost (Panahi et al. 2011)

Raw materials:

- natural gas: 0.5 USD/MMBtu
- water/steam: 0
- oxygen: oxygen is supplied by the ASU unit and we assume that the GTL plant supplies the required steam for the oxygen plant. The price we need to pay decreases somewhat with increased oxygen usage;  $P_{O_2} = P_{O_2}^o \left( \frac{\dot{m}_{O_2}}{\dot{m}_{O_2}^{ref.}} \right)^{-0.3}$ ,  $P_{O_2}^o = 0.11$  USD/kg (7.11)

Energy: 0

CO<sub>2</sub> removal: 50 USD/ton CO<sub>2</sub>

Products:

- LPG (C<sub>3</sub>-C<sub>4</sub>) = 0.9 USD/kg
- Gasoline/Naphtha (C<sub>5</sub>-C<sub>11</sub>) = 0.73 USD/kg
- Diesel (C<sub>12</sub>-C<sub>20</sub>) = 0.71 USD/kg
- Wax (C<sub>21+</sub>) = 0.63 USD/kg

The inequality constraints are as follows.

1. Feed syngas molar ratio H<sub>2</sub>O/C ≥ 0.3 to ensure soot free conditions. Carbon in this ratio includes fresh and recycled hydrocarbons. Note that Holdor Topsøe reports soot free operations at even lower values (Aasberg-Petersen et al. 2003) but we choose 0.3 as the lower bound.
2. Inlet temperature of ATR (outlet of fired heater) ≤ 675°C. The reason for this limit is piping material constraint (Bakkerud 2009).
3. Outlet of ATR ≤ 1030°C. This temperature is an average of several ATR temperatures reported by Holdor Topsøe (Dybkjær and Christensen 2001) which ensures soot free operation.
4. To avoid convergence problem, for simulation purposes, purge ratio of tail gas is bounded at 3% although the optimal is in lower value at around 2%.
5. In addition, there are capacity constraints on the variable units; fired heater (duty +40% compared to nominal), CO<sub>2</sub> recovery unit (+20% feedrate), oxygen plant (+20% oxygen flowrate).

The equality constraints, most of which were explained in process description are:

1. fresh natural gas + recycle hydrocarbons temperature to pre-reformer is kept at 455°C,
2. steam temperature to pre-reformer is kept at 455°C
3. Oxygen feed temperature to ATR is kept at 200°C,
4. Feed enters into syngas unit at 30 bar. Note that the pressure of the fresh streams are set in other units which are out of the our flowsheet boundary,
5. Fresh Syngas from ATR (after passing the boiler) is cooled down to 38°C for separation of water content,
6. Syngas enters into the FT reactor at 210°C,
7. Boling water pressure (cooling medium of FT reactor) is kept at 12.5 bar. This gives a gradient of 20°C between FT desired temperature (210°C) and the coolant (190°C).
8. FT products are cooled down to 30°C in a 3-phase separator to separate liquid fuels, water and tail gas,
9. Recycle tail gas to FT reactor is compressed to 27 bar,

### 7.3.1.2 Step 2. Identify degrees of freedom (DOFs) for optimization

The steady-state degrees of freedom which can be adjusted during the operation can be selected to be:

1. H<sub>2</sub>O (superheat steam) feedrate to pre-reformer (this can be viewed also as H<sub>2</sub>O/C),

2. Superheat steam bypass stream flowrate,
3. Natural gas feedrate as fuel (make up) to the fired heater,
4. Natural gas + recycle hydrocarbons bypass stream flowrate,
5. Oxygen feedrate to ATR,
6. Oxygen bypass stream flowrate,
7. Separator duty for separation of water content in fresh syngas,
8. CO<sub>2</sub> recovery%,
9. Syngas pre-heater duty (the flow stream entering into the FT reactor),
10. Outlet medium pressure (MP) steam flowrate of steam drum,
11. 3-Phase separator duty for separation of FT products,
12. Tail gas recycle ratio to FT reactor and syngas unit,
13. Compressor II duty (the recycle tail gas flow to FT reactor),
14. Recycle tail gas purge ratio,
15. Compressor I duty (the recycle tail gas flow to syngas unit),

### 7.3.1.3 Step 3. Identification of important disturbances

The main disturbances (d) are natural gas feedrate, natural gas composition, natural gas price and FT “kinetic parameter”. In general, the value of all active constraints may be considered as disturbances. We determine the maximum expected value for each disturbance in step 6.

### 7.3.1.4 Step 4. Optimization

We first did the optimization for the nominal case. The “Mixed method” in UniSim is used. This method tries to combine the advantage of global optimization of the BOX method and the efficiency of SQP method. Initially, it uses the BOX method with a very loose convergence tolerance and then switches to the SQP method to locate the final solution with the desired tolerance (UniSim 2008). Figure 7.1 shows the optimal nominal flowsheet. Table 7.2 shows the optimal nominal values of some of the important parameters.

We find three active constraints during optimal nominal operation;

1. the outlet temperature of the fired heater is active at the maximum (675°C),
2. the outlet temperature of the ATR is active at the maximum (1030°C),
3. purge ratio is active at the specified minimum which is to purge 3% of the tail gas.

Since change at any of these active constraints has a significant effect on objective function value (Panahi et al. 2011), we included all of them as disturbances during analysis.

Table 7.2 optimal nominal values

| $\frac{H_2O}{C}$ | $\frac{O_2}{C}$ | CO <sub>2</sub><br>Recovery | Recycle<br>ratio to FT | Purge of<br>tail gas | $\frac{H_2}{CO}$<br>fresh | $\frac{H_2}{CO}$<br>into FT | CO conversion |         | H <sub>2</sub> conversion |         | $\alpha$ | Carbon<br>Efficiency | Objective<br>function<br>(USD/hr) |
|------------------|-----------------|-----------------------------|------------------------|----------------------|---------------------------|-----------------------------|---------------|---------|---------------------------|---------|----------|----------------------|-----------------------------------|
|                  |                 |                             |                        |                      |                           |                             | per pass      | overall | per pass                  | overall |          |                      |                                   |
| 0.6010           | 0.5233          | 75.73%                      | 73.79%                 | 3%                   | 2.1                       | 2.03                        | 85.74%        | 95.50%  | 89.93%                    | 96.92%  | 0.87     | 74.59%               | 49293                             |

We have 15 steady-state degrees of freedom, 9 equality constraints and 3 active constraints which each needs one degree of freedom for control. Therefore we have 15-9-3=3 remaining unconstrained degrees of freedom. Some suggested pairings of the active and equality constraints with appropriate degrees of freedom are shown in Table 7.3. Note that we didn't include the levels in Table 7.3 because they have no steady-state effect.

Table 7.3 possible pairings of steady-state degrees of freedom with equality/active controlled variables

| <u>Degree of freedom (DOF)</u>   | <u>Controlled variable (CV)</u>                                     |
|--|---|
| 1- Superheat steam bypass stream flowrate                                | Superheat steam temperature to pre-reformer                         |
| 2- Natural gas feedrate as fuel (make up) to the fired heater            | Outlet temperature of the fired heater (active constraint)          |
| 3- Natural gas + recycle hydrocarbons bypass stream flowrate             | Natural gas + recycle hydrocarbons feed temperature to pre-reformer |
| 4- Oxygen feedrate to ATR  | ATR outlet temperature (active constraint)                          |
| 5- Oxygen bypass stream flowrate   | Oxygen feed temperature to ATR                                      |
| 6- Separator duty for separation of water content in fresh syngas        | Separator temperature   |
| 7- Syngas pre-heater duty (the flow stream entering into the FT reactor) | FT reactor inlet temperature  |
| 8- Outlet medium pressure (MP) steam flowrate of steam drum              | Steam drum pressure   |
| 9- Duty of 3-phase separator for separation of FT products               | 3-phase separator temperature                                       |
| 10- Compressor II duty (the recycle tail gas flow to FT reactor),        | Compressor II outlet pressure                                       |
| 11-Recycle tail gas purge ratio,   | Purge ratio (active constraint)                                     |
| 12- Compressor I duty (the recycle tail gas flow to syngas unit),        | Compressor I outlet pressure  |

### Unconstrained CVs in mode I

With the suggested pairings presented in Table 7.3, we are left with the following unconstrained degrees of freedom:

$u_1$ :  $H_2O/C$ ,

$u_2$ :  $CO_2$  recovery %

$u_3$ : recycle ratio to the FT reactor.

The objective is now to select the best self-optimizing CVs to pair with these DOFs. Note that we could have used three other DOFs and obtained equivalent results in the subsequent analysis (although  $G^y$ ,  $G_d^y$ ,  $J_{uu}$  and  $F$  matrices would be different)

#### 7.3.1.5 Step 5. Identification of candidate controlled variables

We consider 18 candidate measurements including the three unconstrained degrees of freedom:

1.  $O_2/C$  ( $y_1$ )
2.  $H_2O/C$  ( $y_2$ )
3.  $CO_2$  recovery% ( $y_3$ )
4. recycled tail gas ratio to FT reactor ( $y_4$ )
5.  $H_2/CO$  in fresh syngas ( $y_5$ )
6.  $H_2/CO$  in tail gas ( $y_6$ )
7.  $H_2/CO$  into FT reactor ( $y_7$ )

8. H<sub>2</sub> mole fraction in fresh syngas (y<sub>8</sub>)
9. CO mole fraction in fresh syngas (y<sub>9</sub>)
10. CH<sub>4</sub> mole fraction in fresh syngas (y<sub>10</sub>)
11. H<sub>2</sub> mole fraction in tail gas (y<sub>11</sub>)
12. CO mole fraction in tail gas (y<sub>12</sub>)
13. CH<sub>4</sub> mole fraction in tail gas (y<sub>13</sub>)
14. H<sub>2</sub> mole fraction into FT reactor (y<sub>14</sub>)
15. CO mole fraction into FT reactor (y<sub>15</sub>)
16. fresh syngas flowrate (y<sub>16</sub>)
17. tail gas flowrate to syngas unit (y<sub>17</sub>)
18. tail gas flowrate to FT reactor (y<sub>18</sub>)

We have 18 candidate measurements and one needs to select 3 individual measurements, CV=Hy where H is the selection matrix, therefore there are  $\binom{18}{3} = \frac{18!}{3!15!} = 816$  possible single measurement candidate sets. The self-optimizing method is applied in the next step to choose the best set.

#### 7.3.1.6 Step 6. Selection of CVs

To find the best set of CVs, we applied the “exact local method” (Halvorsen et al. 2003) which gives the maximum loss imposed by each candidate set in presence of disturbances. The set with the minimum worst-case loss is the best. Expressions 7.12-7.15 give the mathematical formulation of calculating loss.

$$\text{worst-case Loss} = \frac{1}{2} \bar{\sigma}(M)^2 \quad (7.12)$$

$$M = J_{uu}^{1/2} (HG^y)^{-1} (H[FW_d \ W_n]) \quad (7.13)$$

where the optimal sensitivity (F) can be obtained analytically from 7.14 or numerically by re-optimizing the process from 7.15.

$$F = G^y J_{uu}^{-1} J_{ud} - G_d^y \quad (7.14)$$

$$F = \frac{\Delta y^{\text{opt}}}{\Delta d} \quad (7.15)$$

In 7.12,  $\bar{\sigma}$  gives maximum singular value of matrix M,  $J_{uu}$  is Hessian of the objective function with respect to unconstrained DOFs,  $G^y$  is the gain of the selected measurements from the inputs,  $W_d$  is the expected magnitude of the disturbances,  $W_n$  is implementation error,  $J_{ud}$  is second derivative of objective function with respect to DOFs and disturbances and  $G_d^y$  is gain from disturbances to the selected measurements. It is worth knowing that Frobenius norm which gives the average loss could be used instead of worst case loss but both methods give the same results (Kariwala et al. 2008).

We consider 7 disturbances (d) with the following maximum expected magnitude (included in the diagonal matrix,  $W_d$ ):

- d<sub>1</sub>(N.G. flowrate):10%,
- d<sub>2</sub>(N.G. hydrocarbons composition):10%,
- d<sub>3</sub>(fired heater outlet temperature):30°C,
- d<sub>4</sub>(ATR outlet temperature):40°C,

$d_5$ (FT kinetics parameter):10%,  
 $d_6$ (purge ratio):15%,  
 $d_7$ (N.G. price):10%

The implementation error for different candidate measurements is assumed to be (included in the diagonal matrix,  $W_n$ ); compositions: 0.1%, flowrates: 10%, split ratios: 15%.

**Individual measurements as CVs**

A branch and bound algorithm (Kariwala and Cao 2009) is applied to find the best set of single measurements with the minimum worst-case loss. The smallest loss is obtained by controlling the CO<sub>2</sub> recovery ( $y_3$ ) in CO<sub>2</sub> removal unit, the CO mole fraction in the fresh syngas ( $y_9$ ) and CO mole fraction in the tail gas ( $y_{12}$ ). Table 7.4 shows the 5 best sets with their corresponding worst case loss.

Table 7.4 Five best set of individual self-optimizing CVs in the optimal nominal case  
 (Mode I of operation)

| no. | Sets   |  |  | Loss (USD/hr) |
|-----|--|--|--|---------------|
| 1   | $y_3$ : CO <sub>2</sub> recovery                         | $y_9$ : CO mole fraction in fresh syngas | $y_{12}$ : CO mole fraction in tail gas    | 1393          |
| 2   | $y_3$ : CO <sub>2</sub> recovery                         | $y_2$ : H <sub>2</sub> O/C               | $y_6$ : H <sub>2</sub> /CO in tail gas     | 1457          |
| 3   | $y_3$ : CO <sub>2</sub> recovery                         | $y_2$ : H <sub>2</sub> O/C               | $y_5$ : H <sub>2</sub> /CO in fresh syngas | 1698          |
| 4   | $y_3$ : CO <sub>2</sub> recovery                         | $y_6$ : H <sub>2</sub> /CO in tail gas   | $y_5$ : H <sub>2</sub> /CO in fresh syngas | 2594          |
| 5   | $y_{10}$ : CH <sub>4</sub> mole fraction in fresh syngas | $y_6$ : H <sub>2</sub> /CO in tail gas   | $y_5$ : H <sub>2</sub> /CO in fresh syngas | 2643          |

We pair the CVs of the best set with the close-by manipulated variables; control CO mole fraction in outlet of the ATR using H<sub>2</sub>O/C and control CO mole fraction in tail gas using recycle tail ratio). Note that the other self-optimizing CV, CO<sub>2</sub> recovery%, which was unconstrained degree of freedom itself, is set by the CO<sub>2</sub> plant. The resulting control structure is given in Figure 7.5.

**Measurement combinations as CVs**

As the loss of the best individual sets of measurements in Table 7.4 is fairly high (compared to the objective function value in the optimal nominal point), we consider measurement combinations as CVs, CV=Hy where H is a “full matrix” in terms of the selected measurements, to get a smaller loss (Alstad et al. 2009). The optimal H is obtained by solving the following optimization problem.

$$\begin{aligned} \min_H & \|HY\|_F^2 \\ \text{s.t. } & HG^y = J_{uu}^{1/2} \end{aligned} \tag{7.16}$$

where  $Y=[FW_d W_n]$ . An analytical solution (Alstad et al. 2009) for 7.16 is:  $H^T = (YY^T)^{-1}G^y(G^{yT}(YY^T)^{-1}G^y)^{-1}J_{uu}^{1/2}$ .

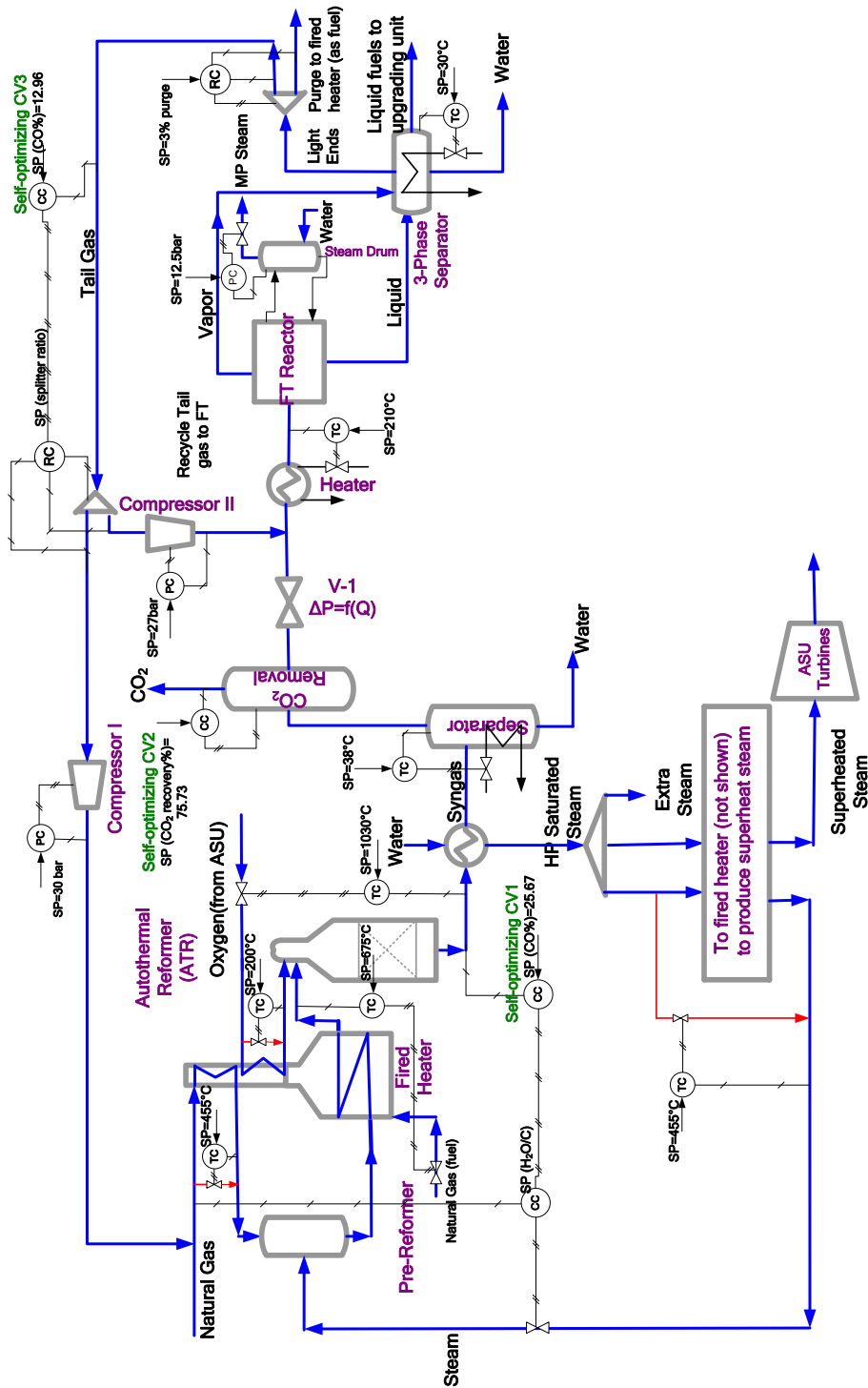


Figure 7.5 control structure for mode I of operation with proposed CVs and possible pairings with MVs (red lines are by-pass streams)

A partial branch and bound algorithm (Kariwala and Cao 2010) is applied to find the best set of CVs with more measurements than 3. Figure 7.6 and Table 7.5 show the results of Solving 7.12 and 7.16 for different number of measurements.

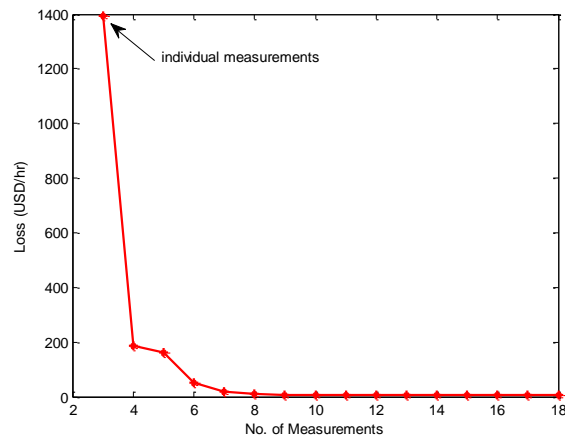


Figure 7.6 Minimum worst case loss with different number of measurements (mode I)

Table 7.5 The best set of combination measurements and their corresponding losses in comparison with the best individual measurements set (mode I)

| no. of the best measurements | set of combinatorial CVs   | the minimum worst-case loss (USD/hr) |
|------------------------------|--|--------------------------------------|
| 3                            | CV1= $y_3$<br>CV2= $y_9$<br>CV3= $y_{12}$  | 1393                                 |
| 4                            | CV1= $0.0979y_2 - 7.8012y_6 + 6.0855y_{14} - 14.0955y_{15}$<br>CV2= $0.5675y_3 + 1.7998y_8 + 1.4682y_{14} - 4.4740y_{15}$<br>CV3= $-1.3208y_3 + 18.8916y_8 + 0.0933y_{14} - 6.9939y_{15}$  | 184                                  |
| 5                            | CV1= $0.1051y_3 + 0.4706y_6 - 7.8432y_8 - 1.9028y_{11} + 2.2211y_{15}$<br>CV2= $0.5991y_3 + 0.1158y_6 + 1.4006y_8 - 0.8808y_{11} + 0.0283y_{15}$<br>CV3= $-1.3865y_3 + 0.0022y_6 + 19.7495y_8 + 0.9013y_{11} - 7.9914y_{15}$   | 161                                  |
| 6                            | CV1= $-1.2398y_3 + 5.4289y_6 - 16.6155y_7 + 8.2854y_8 - 16.7099y_{11} + 40.2823y_{15}$<br>CV2= $-0.4956y_3 + 0.4974y_6 - 1.2787y_7 + 2.6418y_8 - 2.0204y_{11} + 2.9575y_{15}$<br>CV3= $-1.7597y_3 + 1.3781y_6 - 4.6106y_7 + 24.2249y_8 - 3.2075y_{11} + 2.5700y_{15}$                                    | 53                                   |
| 7                            | CV1= $-2.0063y_2 - 2.2283y_3 + 6.1392y_6 - 22.7731y_7 + 6.2647y_8 - 17.2959y_{11} + 22.1873y_{14}$<br>CV2= $-1.4081y_2 - 0.0565y_3 + 1.2053y_6 - 3.2276y_7 - 0.3196y_8 - 3.1263y_{11} + 3.6418y_{14}$<br>CV3= $1.4675y_2 - 1.2323y_3 + 0.6431y_6 - 3.3250y_7 + 27.8493y_8 - 2.0504y_{11} - 0.9377y_{14}$ | 17                                   |

The results show that by having 4 measurements the loss decreases significantly to 184 USD/hr and by having 5 and 6 measurements the loss decreases to 161 USD/hr and 53 USD/hr respectively. By combining 7 measurements the minimum worst case loss is 17 USD/hr that is almost zero from a practical point of view. Measurement  $y_3$  (CO<sub>2</sub> recovery) is always included, but other optimal measurement set varies.

### 7.3.2 Model II: natural gas is a degree of freedom for optimization

From an economical point of view with the given prices, it is optimal to increase the amount of natural gas as much as possible to get more products. Therefore, we consider the natural gas flowrate as a degree of freedom in optimization and try to find the maximum achievable profit. Since the work duty of the compressors in the optimal nominal case are small (compressor I: 0.47 MW, compressor II: 0.55 MW) compared with the equivalent work duty of the fired heater (energy duty: 328.6 MW), we don't define an upper bound for their capacities. Instead, based on optimization results, the design capacity of the compressors can be obtained. The profit increases almost linearly with the natural gas flowrate (see Figure 7.7) up to the point when the first capacity constraint is reached, which is when oxygen flowrate reaches the maximum (point A in Figure 7.7): +23.18% in natural gas feedrate). The reason that it does not increase completely linearly is because of the fixed volume of the FT reactor which implies that the optimal values of the intensive variables change somewhat the maximum throughput is at a feedrate increase of +33.32% (compared to the nominal point) where the profit increase is +21.6% (point B in Figure 7.7). Note that profit increases by only 0.6% from the point A where oxygen flowrate reached its maximum which indicates that there may not be adjustable in practice to operate in this region with the current prices.

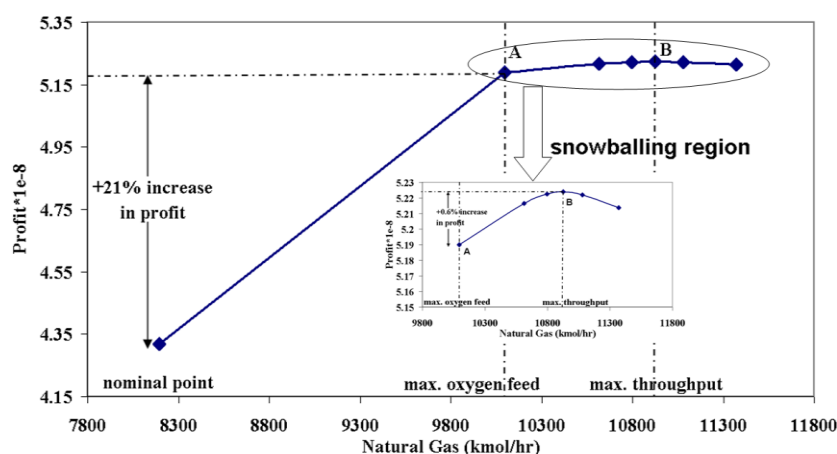


Figure 7.7 Optimal profit as function of natural gas flowrate

Point A: near max. profit (recommended operating point), Point B: max. achievable profit (max throughput)

Figure 7.8 shows the optimal flowsheet at the maximum throughput. Table 7.6 summarizes the optimal values of the main parameters. In mode II, in addition to the oxygen flowrate, outlet temperature of fired heater (at maximum), outlet temperature of ATR (at maximum) and purge ratio (at minimum) are also active, which they are the same active constraints as the nominal case. A comparison of the optimal values of nominal point (mode I) with the point A (oxygen flowrate at maximum) and point B (maximum throughput in mode II) gives the optimal decrease in  $H_2O/C$  from 0.6010 to 0.4084, optimal increase in tail gas recycled ratio to the FT reactor from 73.79% to 97.13% and almost no change in  $CO_2$  recovery percentage. Interestingly, the ratio  $H_2/CO$  in the fresh syngas has almost the same optimal value in all three points. These numbers explain the optimal change in the two modes of operation. In mode II, recycled tail gas ratio to the FT reactor has increased significantly and this is because the oxygen flowrate has reached the maximum and a large recycle tail gas flowrate to syngas unit can result in lower ATR temperature and consequently lower methane conversion.

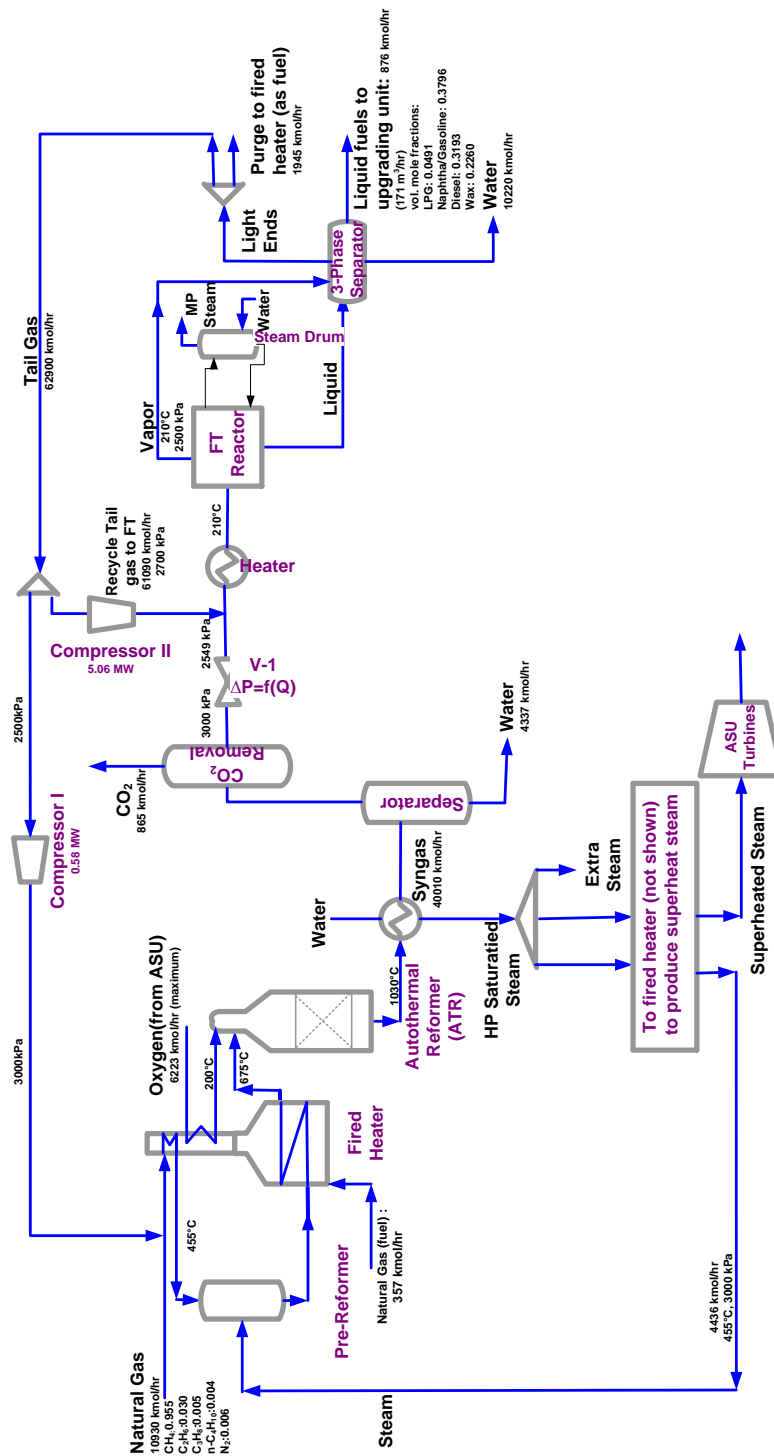


Figure 7.8 Process flowsheet of GTL process with data for maximum throughput

Figure 7.9 shows that as the feed natural gas flowrate increases, CO and H<sub>2</sub> conversion rates decrease (constant volume of FT reactor) and purge flowrate increases as it is optimal to recycle

more to the FT reactor. This is snowballing effect (Luyben 1994) which should be avoided in practice. Therefore the FT reactor volume may be viewed as the bottleneck of the process. Actually, the bottleneck for operation is the active constraints, but in terms of redesign it may be better to increase the reactor volume.

Table 7.6 Optimal values at maximum throughput

|                 | $\frac{H_2O}{C}$ | $\frac{O_2}{C}$ | CO <sub>2</sub> recovery | Recycle ratio to FT | Purge of tail gas | $\frac{H_2}{CO}$ fresh | $\frac{H_2}{CO}$ into FT | CO conversion |         | H <sub>2</sub> conversion |         | $\alpha$ | Carbon efficiency | Objective function (USD/hr) |
|-----------------|------------------|-----------------|--------------------------|---------------------|-------------------|------------------------|--------------------------|---------------|---------|---------------------------|---------|----------|-------------------|-----------------------------|
|                 |                  |                 |                          |                     |                   |                        |                          | per pass      | overall | per pass                  | overall |          |                   |                             |
| opt. nominal    | 0.6010           | 0.5233          | 75.73%                   | 73.79%              | 3%                | 2.1                    | 2.03                     | 85.74%        | 95.50%  | 89.93%                    | 96.92%  | 0.8707   | 74.59%            | 49293                       |
| max. oxygen     | 0.5357           | 0.5160          | 76.80%                   | 90%                 | 3%                | 2.092                  | 1.91                     | 67.08%        | 94.14%  | 74.705                    | 95.88%  | 0.8692   | 74.30%            | 59246                       |
| max. throughput | 0.4084           | 0.5040          | 76.04%                   | 97.13%              | 3%                | 2.095                  | 1.80                     | 51.25%        | 94.79%  | 60.69%                    | 96.39%  | 0.8701   | 74.31%            | 59634                       |

### Unconstrained CVs in Mode II

In mode II, there are 16 DOFs (one extra compared to mode I), 4 active constraints and the same 9 equality constraints as mode I. Note that in this mode, to select the self-optimizing CVs, whereas oxygen flowrate is active, we use natural gas flowrate to control ATR exit temperature (active constraint). The other pairings are as mode I. Therefore we are again left with 3 unconstrained degrees of freedom ( $16-9-4=3$ ) which are: H<sub>2</sub>O/C, CO<sub>2</sub> recovery % and recycle ratio to FT (the same sets as the nominal case). Self-optimizing analysis is repeated to find the best set of CVs. Compare to the nominal case we add a new disturbance which is change in the maximum oxygen flowrate ( $d_8:5\%$ ).

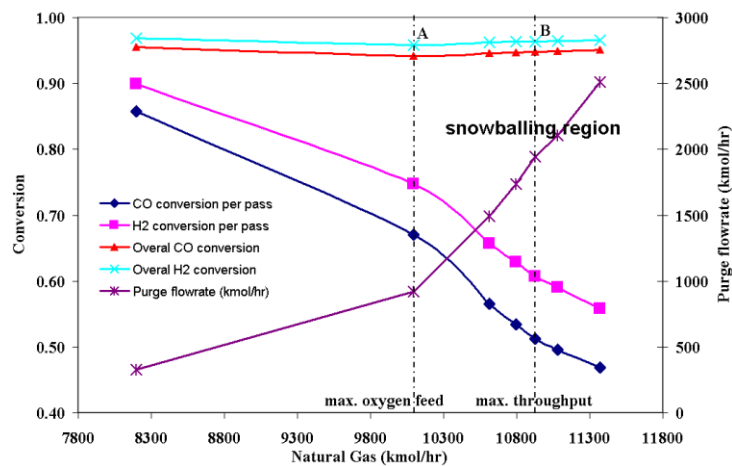


Figure 7.9 Optimal values of CO, H<sub>2</sub> conversion (single pass and overall) in FT reactor and purge flowrate as natural gas increases

### Individual measurements

By applying the exact local method we find the best individual measurements. The best five sets are presented in Table 7.7.

In mode II, two of the unconstrained degrees of freedom are self-optimizing CVs (CO<sub>2</sub> recovery and H<sub>2</sub>O/C) and the third CV is H<sub>2</sub>/CO into FT reactor which should be paired with the only remained degree of freedom, which is recycle tail gas ratio. The resulting control structure is

shown in Figure 7.11. Note that the objective of this work is to select controlled variables (CVs) and the shown pairings with the manipulated variables (MVs) is only a suggestion.

Table 7.7 Five best sets of individual self-optimizing CVs in the maximum throughput case (Mode II of operation)

| no. | Sets                                      |   |   | Loss (USD/hr) |
|-----|---|---|---|---------------|
| 1   | y <sub>3</sub> : CO <sub>2</sub> recovery | y <sub>2</sub> : H <sub>2</sub> O/C               | y <sub>7</sub> : H <sub>2</sub> /CO into FT reactor | 3022          |
| 2   | y <sub>3</sub> : CO <sub>2</sub> recovery | y <sub>2</sub> : H <sub>2</sub> O/C               | y <sub>6</sub> : H <sub>2</sub> /CO in tail gas     | 3316          |
| 3   | y <sub>3</sub> : CO <sub>2</sub> recovery | y <sub>2</sub> : H <sub>2</sub> O/C               | y <sub>5</sub> : H <sub>2</sub> /CO in fresh syngas | 3495          |
| 4   | y <sub>3</sub> : CO <sub>2</sub> recovery | y <sub>2</sub> : H <sub>2</sub> O/C               | y <sub>17</sub> : tail gas flowrate to syngas unit  | 4179          |
| 5   | y <sub>3</sub> : CO <sub>2</sub> recovery | y <sub>9</sub> : CO mole fraction in fresh syngas | y <sub>15</sub> : CO mole fraction into FT reactor  | 4419          |

By comparing of the best sets of individual measurements for the two modes of operation we find one common set which is the third set in Tables 7.4 and 7.7, and interestingly, we see that two measurements; y<sub>3</sub> (CO<sub>2</sub> recovery) and y<sub>5</sub> (H<sub>2</sub>/CO in fresh syngas) have almost the same setpoint values (see the optimal values in Table 7.6). The setpoint of the third measurement, H<sub>2</sub>O/C changes from 0.6010 in the nominal case to 0.4084 in the maximum throughput case. This means that when the oxygen flowrate reaches its maximum, it is close to optimal to control the outlet temperature of the ATR using natural gas flowrate and decrease H<sub>2</sub>O/C setpoint. Therefore in this case, one can view H<sub>2</sub>O/C setpoint as throughput manipulator (TPM). From a practical point of view, operation in snowballing region is not recommended therefore saturation point of oxygen flowrate is suggested for operation.

**Measurement combinations as CVs**

In addition to individual measurements, we considered also combinations of CVs in mode II. Figure 7.10 and Table 7.8 illustrate the results. By combining 4, 5, 6 and 7 measurements, worst-case loss decreases significantly to 520, 153, 112 and 61 USD/hr respectively.

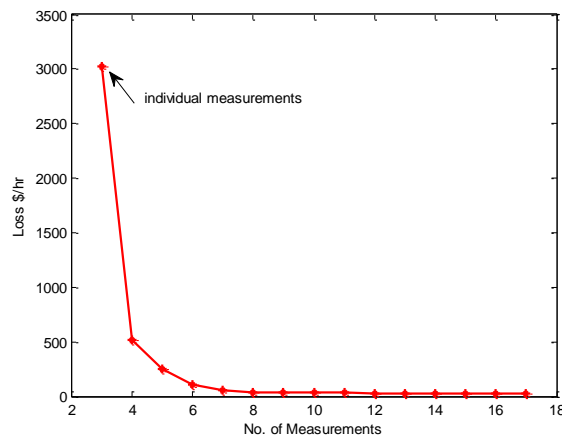


Figure 7.10 Minimum worst-case loss with different number of measurements (mode II)



Table 7.8 The best set of combination measurements and their corresponding losses in comparison with the best individual measurements set (mode II)

| no. of measurements | the best set of combinatorial CVs   | the minimum worst-case loss (USD/hr) |
|---------------------|---|--------------------------------------|
| 3                   | $CV1 = y_2$<br>$CV2 = y_3$<br>$CV3 = y_7$   | 3022                                 |
| 4                   | $CV1 = 1.2265y_2 - 3.9023y_6 + 26.5645y_{11} - 44.1699y_{12}$<br>$CV2 = -1.4168y_2 - 3.8972y_6 + 27.4781y_{11} - 43.8481y_{12}$<br>$CV3 = -0.1675y_2 + 6.5306y_6 - 44.4148y_{11} + 63.5875y_{12}$   | 520                                  |
| 5                   | $CV1 = -3.2704y_6 - 11.0752y_{10} + 23.9689y_{11} - 39.4867y_{12} + 0.0001y_{17}$<br>$CV2 = -5.6662y_6 + 9.1168y_{10} + 37.8373y_{11} - 59.4219y_{12} - 0.0002y_{17}$<br>$CV3 = 6.1857y_6 + 0.5967y_{10} - 42.2267y_{11} + 60.4177y_{12} - 0.0000y_{17}$  | 153                                  |
| 6                   | $CV1 = -1.5199y_6 - 2.5054y_7 - 10.0711y_{10} + 18.6901y_{11} - 44.9909y_{12} + 14.1532y_{15}$<br>$CV2 = -14.6808y_6 + 15.4651y_7 + 0.8535y_{10} + 46.1202y_{11} - 11.2275y_{12} - 66.6206y_{15}$<br>$CV3 = 4.9366y_6 + 2.0426y_7 - 0.4327y_{10} - 40.3465y_{11} + 66.3164y_{12} - 9.4631y_{15}$                        | 112                                  |
| 7                   | $CV1 = 4.3020y_2 + 0.7874y_3 - 3.1178y_6 + 1.4389y_7 + 12.1582y_{11} - 12.3659y_{12} - 13.6128y_{15}$<br>$CV2 = 0.7497y_2 + 0.2475y_3 - 13.2986y_6 + 14.2588y_7 + 39.8464y_{11} - 5.0080y_{12} - 63.7779y_{15}$<br>$CV3 = 0.0725y_2 + 0.0196y_3 + 5.3032y_6 + 1.5697y_7 - 41.2960y_{11} + 66.0941y_{12} - 7.6749y_{15}$ | 61                                   |

## 7.4 Conclusions

The steady-state Top-down part of the general plantwide control procedure was applied for selection of the best controlled variables (CVs) for GTL process in two modes of operation. In mode I, the natural gas feedrate is given and in mode II, the natural gas feedrate is degree of freedom for optimization in order to achieve the maximum possible profit. The transition from mode I to mode II happens when the oxygen flowrate reaches its maximum. In both modes of operation, we have 3 remained unconstrained steady-state degrees of freedom and among the best corresponding individual measurement CV sets, we found for both modes two CVs with almost the same setpoint value ( $H_2/CO$  in fresh syngas and  $CO_2$  recovery%) and a third one ( $H_2O/C$  feed) where the setpoint decreases from 0.6010 (the nominal case) to 0.4084 (the maximum throughput) and this choice gives a simple transition. The setpoint of the steam to carbon feed ratio ( $H_2O/C$ ) can be chosen as the throughput manipulator (TPM) from the nominal case to max. throughput.

Use combinations of measurements reduces significantly the worst-case loss. In both modes, we reach almost zero loss by combining 7 measurements. In mode II, where the oxygen flowrate saturates, the optimal recycle flowrate to the FT reactor increases significantly as we further increase the feedrate and therefore the purge flow also increases. This is snowballing effect which should be avoided. In addition, the economic benefit of increasing the feedrate is small. Therefore we recommend operation in mode II at the feedrate where oxygen flowrate becomes active (point A in Figure 7.7).



# Chapter 8

## Conclusions and future work

### 8.1 Concluding remarks

In this thesis, the general plantwide procedure of Skogestad has been used in order to design efficient control structures for two processes. Post-combustion CO<sub>2</sub> capturing and natural gas to liquids (GTL) processes are the case studies which have been studied in details here. One of the main conclusions is the high efficiency of this method in selection of the right controlled variables using top-down analysis and in addition design the regulatory layer for implementing (validation) the control structures using bottom-up analysis. The results of the work can be used to be implemented in practice. UniSim/Hysys linked with Matlab has also shown to be a good tool to design control structure using this procedure.

In chapter 3, the objective is to operate the CO<sub>2</sub> plant efficiently close to minimum required energy in presence of disturbances while CO<sub>2</sub> recovery of 90% is met. There is one unconstrained degree of freedom which is reboiler duty. The corresponding self-optimizing CV was found to be temperature of tray no. 17 in the stripper. The stability of the proposed structure is considered against the large variations in the load from the power plant. The control structure becomes unstable when reboiler duty of the stripper saturates which is the case when flue gas feedrate is increased by +25%. With saturation of reboiler duty where the heat input is insufficient for stripping the CO<sub>2</sub> content from rich amine solvent, CO<sub>2</sub> is accumulating in the process and this causes an unstable control system. To solve the problem, the idea is to give up controlling the CO<sub>2</sub> recovery in the other side of the plant (absorber) and stabilize the stripper temperature profile using the only available degree of freedom which is recycle amine flowrate. The proposed structure is stable although self-optimizing is necessary to be repeated in the new operating region (after saturation of reboiler duty). In chapters 4 and 5 the CO<sub>2</sub> plant is studied more in details where a more realistic objective function is introduced.

In chapters 4 and 5, we introduce tax on the released CO<sub>2</sub> (this is equivalent to sell CO<sub>2</sub> with the same price) to the air which makes it optimal to remove more CO<sub>2</sub>. This scenario for cost function results in two unconstrained degrees of freedom which are recycle amine flowrate and reboiler duty. The corresponding self-optimizing CVs were found to be CO<sub>2</sub> recovery in the absorber and temperature of tray no.16 in the stripper. When the flue gas feedrate is increased by +20%, reboiler duty saturates which means the process has been entered into region II. By repeating the self-optimizing analysis, temperature of tray no. 13 in the stripper is found as the best controlled variable to be controlled using the only available degree of freedom (recycle amine flowrate). We tried to consider the possibility of combining the regions to remove the need for switching the control loops. We followed the bottom-up part of the procedure and first identify the stabilizing controlled variables (CV2) and paired them with proper manipulated variables. Then we found the steady-state and dynamic RGA matrices in order to pair the supervisory controlled variables (CV1) with remaining degrees of freedom which are reboiler duty and recycle amine flowrate. Steady-state and dynamic RGA matrices result in two different pairings. The control structure using diagonal pairing (alternative 1: control of CO<sub>2</sub> recovery using recycle amine and control of stripper tray no.16 temperature using reboiler duty) suggested by dynamic RGA fails when reboiler duty saturates while the structure using off-diagonal pairing (alternative 2) proposed by steady-state RGA can handle large variations in flue gas feedrate. Since in alternative 2, CVs and MVs are far, the dynamic response is relatively poor and we try to improve on it by reconfiguration of two control loops. We used the stripper inflow, which earlier was manipulated to control absorber bottom level, to control the stripper temperature and instead used recycle amine flowrate to control bottom level of the absorber (alternative 4). Note that the optimal in region II is to reconfigure the loops; giving up control of CO<sub>2</sub> recovery and control temperature of tray no.13 using recycle amine flowrate (alternative 3), but dynamic simulations show that there is a minor difference between the objective function values of the optimal one in region II (alternative 3) and other alternatives (alt. 2 or alt. 4). Therefore alternative 4 is recommended in practice.

In chapters 6, a detailed model is developed for a GTL process. The simulated model is similar to one train of the Oryx GTL plant which has two parallel trains each with the daily production capacity of 17,000 bbl liquid fuels. ATR technology is used for synthesis gas unit and FT reactor is a Cobalt based slurry bubble column operating in low FT temperature. FT reactions are simulated by combination of the proposed reaction rates by Iglesia, ASF model and an  $\alpha$  model proposed by Yermakova and Anikeev. This obtained model is suitable for optimal operation studies.

In chapter 7, self-optimizing method is applied to the GTL process in two modes of operation. In mode I, natural gas feedrate is given and we find three unconstrained degrees of freedom which are H<sub>2</sub>O/C, CO<sub>2</sub> recovery and tail gas recycle ratio. The best set of self-optimizing CVs are found to keep constant CO mole fraction in fresh syngas, CO mole fraction in tail gas and CO<sub>2</sub> recovery. Since the magnitude of the worst-case loss is fairly high we go for selection of combination of measurements where combining 7 measurements results in practically almost zero loss. In mode II, we include natural gas flowrate as a degree of freedom and reoptimize the process. As natural gas increases, the profit also increases almost linearly until oxygen flowrate reaches the maximum. From this point the linear trend does not follow anymore and just a small improvement happens in objective function. Actually after saturation of oxygen feedrate, optimal is to recycle more to the FT reactor which also results in purging more (snowballing effect) and since the volume of the reactor is fixed the conversion per pass start decreasing. Therefore FT reactor is the bottleneck of the process. Snowballing region, which appears in our case after saturation of oxygen plant capacity is not recommend in practice for operation. Therefore we should stop making more profit at the maximum oxygen capacity. Self-optimizing is also applied in mode II of operation when we have a new degree of freedom (natural gas

feedrate) and also a new active constraint (oxygen flowrate). We choose to use natural gas feedrate to control ATR temperature (active constraint). Therefore we have again the same set of unconstrained degrees of freedom as mode I.  $\text{CO}_2$  recovery,  $\text{H}_2\text{O}/\text{C}$  and  $\text{H}_2/\text{CO}$  into FT reactor are found as the best CVs set with the minimum worst-case loss. Interestingly we find a common set in both modes (the set that ranks three in both modes) where two CVs ( $\text{CO}_2$  recovery and  $\text{H}_2/\text{CO}$  in fresh syngas) have almost the same setpoint values and the setpoint for the third one ( $\text{H}_2\text{O}/\text{C}$ ) decreases from 0.601 to 0.4084. The setpoint of  $\text{H}_2\text{O}/\text{C}$  can be viewed as throughput manipulator.

## 8.2 Directions for future work

For future studies the followings are suggested:

- Implementation of the final proposed control structure for  $\text{CO}_2$  capturing process on a pilot plant.
- Dynamic simulation of the GTL process in order to validate the proposed structures and dynamic applicability of combination of the measurements.
- In the plantwide control procedure, the optimization of the flowsheet in UniSim and similar simulators is very time consuming, especially when we have iterating blocks like recycle, adjust etc. This is much more significant for optimal operation studies, where we need a model with very small tolerances. Developing more efficient and robust methods for optimization and flowsheet convergence can help a lot for the progress of optimal operation studies.
- The application of the systematic plantwide procedure is strongly recommended to other newer energy-intensive processes. The aim is to control the right controlled variables and design economically efficient control structures to operate those plants with the minimum energy requirements. In spite of what engineers often think, control structures are not always straightforward especially when large numbers of measurements are available for control. The final control structure for  $\text{CO}_2$  capture process in this thesis showed that without following this systematic method, we may not be able to reach a good structure.
- Self-optimizing analysis needs to be repeated when a new operational constraint appears in the process and this makes the approach time consuming. Challenges for development a systematic method for arriving at a simple and single control structure, which can handle all operational regions can be an interesting topic for future works in this area.

## Bibliography

- Aasberg-Petersen, K., J. H. Bak Hansen, T. S. Christensen, I. Dybkjaer, P. S. Christensen, C. Stub Nielsen, S. E. L. Winter Madsen and J. R. Rostrup-Nielsen (2001). "Technologies for large-scale gas conversion." Applied Catalysis A: General 221(1-2): 379-387.
- Aasberg-Petersen, K., T. S. Christensen, C. Stub Nielsen and I. Dybkjær (2003). "Recent developments in autothermal reforming and pre-reforming for synthesis gas production in GTL applications." Fuel Processing Technology 83(1-3): 253-261.
- Alstad, V., S. Skogestad and E. S. Hori (2009). "Optimal measurement combinations as controlled variables." Journal of Process Control 19(1): 138-148.
- Aske, E. M. B. and S. Skogestad (2009). "Consistent Inventory Control." Industrial & Engineering Chemistry Research 48(24): 10892-10902.
- Bakkerud, P. K. (2005). "Update on synthesis gas production for GTL." Catalysis Today 106(1-4): 30-33.
- Bakkerud, P. K. (2009). Personal Communication.
- Bao, B., M. M. El-Halwagi and N. O. Elbashir (2010). "Simulation, integration, and economic analysis of gas-to-liquid processes." Fuel Processing Technology 91(7): 703-713.
- Bedelbayev, A., T. Greer and B. Lie (2008). Model Based Control of Absorption Tower for CO<sub>2</sub> Capturing. Conference of Scandinavian Simulation Society (SIMS 2008).
- Christensen, T. S. (1996). "Adiabatic prereforming of hydrocarbons -- an important step in syngas production." Applied Catalysis A: General 138(2): 285-309.
- Cohen, H., G. F. C. Rogers and H. I. H. Saravanamuttoo (2009). Gas turbine theory.
- Davis, J. and G. Rochelle (2009). "Thermal degradation of monoethanolamine at stripper conditions." Energy Procedia 1(1): 327-333.
- De Araújo, A. C. B., M. Govatsmark and S. Skogestad (2007). "Application of plantwide control to the HDA process. I--steady-state optimization and self-optimizing control." Control Engineering Practice 15(10): 1222-1237.
- Dybkjær, I. (2006). Synthesis Gas Technology. Reprinted from hydrocarbon engineering July 2006. [http://www.topsoe.com/business\\_areas/synthesis\\_gas/~media/PDF%20files/Heat\\_exchange\\_reforming/Topsoe\\_synthesis\\_gas\\_technology.ashx](http://www.topsoe.com/business_areas/synthesis_gas/~media/PDF%20files/Heat_exchange_reforming/Topsoe_synthesis_gas_technology.ashx).
- Dybkjær, I. and T. S. Christensen (2001). Syngas for large scale conversion of natural gas to liquid fuels. Studies in Surface Science and Catalysis. Eds J. J. S. E. Iglesia and T. H. Fleisch, Elsevier. Volume 136: 435-440.
- Goldstein, H. S. (2010). A green certificate market in Norway and its implications for the market participants. Energy Economics and Policy. Zurich, ETH

- 
- GTL-Workshop (2010). "Introduction to GTL Technology, Pre-Symposium Workshop." Organized by Gas Processing Center and Shell Company Doha, Qatar.
- Halstead, K. (2006). Oryx GTL – a case study, details the first new-generation commercial-scale gas-to-liquids plant, Foster Wheeler ,  
[www.fwc.com/publications/tech\\_papers/files/Oryx781fosterwheeler.pdf](http://www.fwc.com/publications/tech_papers/files/Oryx781fosterwheeler.pdf).
- Halvorsen, I. J., S. Skogestad, J. C. Morud and V. Alstad (2003). "Optimal Selection of Controlled Variables†." Industrial & Engineering Chemistry Research 42(14): 3273-3284.
- IEA Report (2008). Energy Technology Perspectives, Scenarios and Strategies to 2050 International Energy Agency (IEA) and Organization for Economic Co-operation and Development.
- Iglesia, E., S. C. Reyes and S. L. Soled (1993). Reaction-Transport selectivity models and the design of fischer-tropsch catalysts. Computer-aided design of catalysts. Eds P. C. J. Becker E. Robert 199-257.
- Jager, B. and R. Espinoza (1995). "Advances in low temperature Fischer-Tropsch synthesis." Catalysis Today 23(1): 17-28.
- Jassim, M. S. and G. T. Rochelle (2005). "Innovative Absorber/Stripper Configurations for CO<sub>2</sub> Capture by Aqueous Monoethanolamine." Industrial & Engineering Chemistry Research 45(8): 2465-2472.
- Jayarathna, S. A., B. Lie and M. C. Melaen (2011). "NEQ rate based modeling of an absorption column for post combustion CO<sub>2</sub> capturing." Energy Procedia 4: 1797-1804.
- Jensen, J. B. (2008). Optimal Operation of Refrigeration Cycles. PhD thesis.
- Kariwala, V. and Y. Cao (2009). "Bidirectional branch and bound for controlled variable selection. Part II: Exact local method for self-optimizing control." Computers & Chemical Engineering 33(8): 1402-1412.
- Kariwala, V. and Y. Cao (2010). "Bidirectional Branch and Bound for Controlled Variable Selection Part III: Local Average Loss Minimization." IEEE Transactions on Industrial Informatics 6(1): 54-61.
- Kariwala, V., Y. Cao and S. Janardhanan (2008). "Local Self-Optimizing Control with Average Loss Minimization." Industrial & Engineering Chemistry Research 47(4): 1150-1158.
- Kim, Y. H., K.-W. Jun, H. Joo, C. Han and I. K. Song (2009). "A simulation study on gas-to-liquid (natural gas to Fischer-Tropsch synthetic fuel) process optimization." Chemical Engineering Journal 155(1-2): 427-432.
- Knudsen, J. N. J., P-J Vilhelmsen, O. Biede (2007). First year operation experience with a 1t/h CO<sub>2</sub> absorption pilot plant at Esbjerg coal-fired power plant. Proceedings of European Congress of Chemical Engineering (ECCE-6), Copenhagen.

- Kvamsdal, H. M., J. P. Jakobsen and K. A. Hoff (2009). "Dynamic modeling and simulation of a CO<sub>2</sub> absorber column for post-combustion CO<sub>2</sub> capture." Chemical Engineering and Processing: Process Intensification 48(1): 135-144.
- Lawal, A., M. Wang, P. Stephenson and O. Obi (2010). "Demonstrating full-scale post-combustion CO<sub>2</sub> capture for coal-fired power plants through dynamic modelling and simulation." Fuel In Press, Corrected Proof.
- Lawal, A., M. Wang, P. Stephenson and H. Yeung (2009). "Dynamic modelling of CO<sub>2</sub> absorption for post combustion capture in coal-fired power plants." Fuel 88(12): 2455-2462.
- Lin, Y.-J., T.-H. Pan, D. S.-H. Wong, S.-S. Jang, Y.-W. Chi and C.-H. Yeh (2010). "Plantwide Control of CO<sub>2</sub> Capture by Absorption and Stripping Using Monoethanolamine Solution." Industrial & Engineering Chemistry Research 50(3): 1338-1345.
- Luyben, W. L. (1994). "Snowball effects in reactor/separator processes with recycle." Industrial & Engineering Chemistry Research 33(2): 299-305.
- OPEC (2009). "OPEC Annual Statistical Bulletin, Website: [www.opec.org](http://www.opec.org)."
- Panahi, M., M. Karimi, S. Skogestad, M. Hillestad and H. F. Svendsen (2010). Self-Optimizing and Control Structure Design for a CO<sub>2</sub> Capturing Plant. Proceedings of the 2nd Annual Gas Processing Symposium. Amsterdam, Elsevier: 331-338.
- Panahi, M., A. Rafiee, S. Skogestad and M. Hillestad (2011). "A Comprehensive Gas to Liquid Process Model for Optimal Design and Operation." submitted to Industrial & Engineering Chemistry Research Journal
- Panahi, M. and S. Skogestad (2011). "Economically efficient operation of CO<sub>2</sub> capturing process part I: Self-optimizing procedure for selecting the best controlled variables." Chemical Engineering and Processing: Process Intensification 50(3): 247-253.
- PDS (2007). Honeywell Profit Design Studio R310.
- Rostrup-Nielsen, J., I. Dybkjaer and K. Aasberg-Petersen (2000). "Synthesis gas for large scale Fischer-Tropsch synthesis." American Chemical Society, Division of Petroleum Chemistry, Preprints 45(2): 186-189.
- Satterfield, C. N., I. C. Yates and C. C. Chanenchuk (1989). DOE Report no. PC79816-6, Contract no. DE-AC22-87PC79816, July-September.
- Schach, M.-O., R. d. Schneider, H. Schramm and J.-U. Repke (2010a). "Techno-Economic Analysis of Postcombustion Processes for the Capture of Carbon Dioxide from Power Plant Flue Gas." Industrial & Engineering Chemistry Research 49(5): 2363-2370.
- Schach, M. O., R. Schneider, H. Schramm and J. U. Repke (2010b). Exergoeconomic Analysis of Post-Combustion CO<sub>2</sub> Capture Processes. Computer Aided Chemical Engineering. Eds S. Pierucci and G. B. Ferraris, Elsevier. Volume 28: 997-1002.

- 
- Schach, M. O., R. Schneider, H. Schramm and J. U. Repke (2011). Plantwide Control Design of a Postcombustion CO<sub>2</sub> Capture Process. 21st European Symposium on Computer Aided Process Engineering (ESCAPE 21).
- Schanke, D. (2010). Personal Communication, Statoil, Research center/Trondheim.
- Schanke, D. and J. Sogge (2010). Personal communication, Statoil, Research center/Trondheim.
- Schijndel, J. v., N. Thijssena, G. Baaka, A. Avhalea, J. Ellepolaa and J. Grievinkb (2011). "Development of a synthesis tool for Gas-To-Liquid complexes." Proceedings of 21st European Symposium on Computer Aided Process Engineering – ESCAPE 21: 417-421.
- Skogestad, S. (2000). "Plantwide control: the search for the self-optimizing control structure." Journal of Process Control 10(5): 487-507.
- Skogestad, S. (2002). Plantwide control: Towards a systematic procedure. Computer Aided Chemical Engineering. Eds G. Johan and S. Jan van, Elsevier. Volume 10: 57-69.
- Skogestad, S. (2003). "Simple analytic rules for model reduction and PID controller tuning." Journal of Process Control 13(4): 291-309.
- Skogestad, S. (2004). "Control structure design for complete chemical plants." Computers & Chemical Engineering 28(1-2): 219-234.
- Skogestad, S. (2011). Plantwide Control. Ullman's Encyclopedia of Process Systems Engineering (In press) Eds R. Gani, G. Sin and K. V. Gernaey.
- Skogestad, S. and I. Postlethwaite (1996). Multivariable Feedback Control Analysis and Design.
- Skogestad, S. and I. Postlethwaite (2005). Multivariable Feedback Control Analysis and Design.
- Song, H.-S., D. Ramkrishna, S. Trinh and H. Wright (2004). "Operating strategies for Fischer-Tropsch reactors: A model-directed study." Korean Journal of Chemical Engineering 21(2): 308-317.
- Spath, P. L. and D. C. Dayton (2003). Preliminary Screening Technical and Economic Assessment of Synthesis Gas to Fuels and Chemicals with Emphasis on the Potential for Biomass-Derived Syngas, [http://www.fischer-tropsch.org/DOE/DOE\\_reports/510/510-34929/510-34929.pdf](http://www.fischer-tropsch.org/DOE/DOE_reports/510/510-34929/510-34929.pdf).
- Steynberg, A. P. and M. E. Dry (2004). Fischer Tropsch Technology.
- Toshiba (2008). Toshiba to Build Pilot Plant to Test CO<sub>2</sub> Capture Technology. <http://www.japanfs.org/en/pages/028843.html>.
- UniSim (2008). UniSim Design Honeywell Company. R380.
- Yates, I. C. and C. N. Satterfield (1991). "Intrinsic kinetics of the Fischer-Tropsch synthesis on a cobalt catalyst." Energy & Fuels 5(1): 168-173.

Yermakova, A. and V. I. Anikeev (2000). "Thermodynamic Calculations in the Modeling of Multiphase Processes and Reactors." Industrial & Engineering Chemistry Research 39(5): 1453-1472.

ZEP Report (2011). CO<sub>2</sub> Capture Costs, ZEP Capture Cost Working Group, European Technology Platform for Zero Emission Fossil Fuel Power Plants.

Ziaii, S., G. T. Rochelle and T. F. Edgar (2009). "Dynamic Modeling to Minimize Energy Use for CO<sub>2</sub> Capture in Power Plants by Aqueous Monoethanolamine." Industrial & Engineering Chemistry Research 48(13): 6105-6111.

## **Appendix A**

Steady State Simulation for Optimal Design and Operation of a GTL Process, Published in book series "Advances in Gas Processing", volume 2, pages 275-284

This appendix is an early work for optimal design and operation of GTL process



## Steady State Simulation for Optimal Design and Operation of a GTL Process

Mehdi Panahi, Sigurd Skogestad, Ramprasad Yelchuru

*Chemical Engineering Department, Norwegian University of Science and Technology (NTNU), 7491, Trondheim, Norway*

### Abstract

This study of gas to liquid (GTL) production uses an autothermal reformer (ATR) for synthesis gas production and a slurry bubble column reactor (SBCR) with Cobalt catalyst for the Fischer-Tropsch (FT) conversion to liquid fuels. The well-known Satterfield kinetics are used for the FT reactor; the remaining reactions are simulated assuming thermodynamic equilibrium. The process also includes high-pressure CO<sub>2</sub> removal. Important process parameters, which are subject to optimization, include feed rates of water and oxygen, inlet ATR temperature and recycle flows. In addition to determining the process and equipment design, optimization is used to find the controlled variables. The aim is to identify “self-optimizing variables” that indirectly give close-to-optimal operation with constant setpoints, in spite of disturbances.

**Keywords:** Gas to liquid process, Optimization, Plantwide control, Self-optimizing control, Process control,

### 1. Introduction

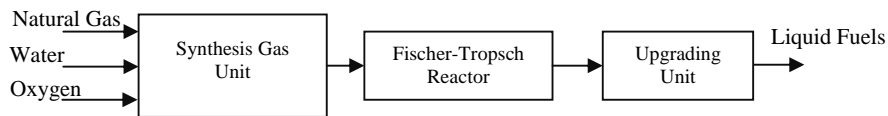


Figure 1: Main parts of GTL process

The GTL process in Fig.1 has 3 main steps (i) production of synthesis gas (syngas), (ii) Fischer-Tropsch (FT) reactor and (iii) upgrading units. (Fig.1). In the syngas unit, a mixture of hydrogen and carbon monoxide is produced and is sent to the Fischer-Tropsch (FT) reactor for converting to liquid fuels. The syngas and FT units make up almost 85% of total investment cost of the plant. In our work, our focus is on these two units.

This paper focuses on the optimal operation of such plants so that we can capture in practice the benefits in terms of energy savings and productivity that are predicted when designing the process. Skogestad (2004) has proposed a systematic method for designing the control structure of a complete chemical plant. The first step of this

procedure is the selection of controlled variables (self-optimizing control) which is the focus of this paper.

## 2. Conceptual design of a GTL process

### 2.1. Feed data

Natural gas feed is assumed at the following conditions:

Flow rate:  $8195 \frac{\text{kmol}}{\text{hr}}$ , Pressure: 73.5 bar, Temperature: 40 °C

Composition: CH<sub>4</sub> (95.5%), C<sub>2</sub>H<sub>6</sub> (3%), C<sub>3</sub>H<sub>8</sub> (0.5%), nC<sub>4</sub>H<sub>10</sub> (0.4%), N<sub>2</sub> (0.6%)

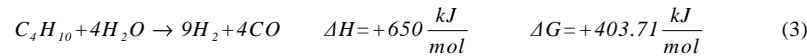
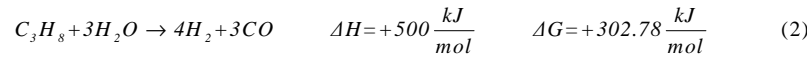
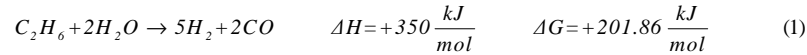
Nominal feed rates of water and oxygen (see Fig. 1):  $\frac{\text{H}_2\text{O}}{\text{Natural Gas}} = 0.53$ ,  $\frac{\text{O}_2}{\text{Natural Gas}} = 0.67$

### 2.2. Syngas unit

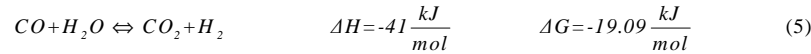
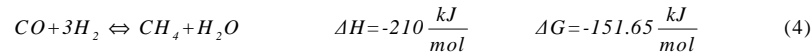
In GTL processes, there are different routes for syngas production from natural gas, including Auto Thermal Reforming (ATR), steam reforming, partial oxidation of methane and CO<sub>2</sub> reforming. ATR is a combination of steam reforming and oxidation of methane. It is claimed to be the best route for syngas production (Bakkerud, 2005) and has been selected for this study.

To avoid the potential problem that the ATR works as a steam cracker, producing olefins from higher hydrocarbons in the feed, an adiabatic pre-reformer is introduced. Here, the temperature is 350-550°C and all higher hydrocarbons are converted (Aasberg-Petersen et al, 2001) according to the following reactions:

Complete conversion reactions (endothermic, so energy is needed):



Equilibrium reactions:

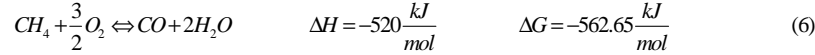


In our case, natural gas and water are preheated to 455°C and fed to the adiabatic pre-reformer. In spite of the exothermic equilibrium reactions the overall reactions are endothermic and the outlet temperature is about 416°C.

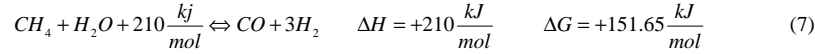
The pre-reformer outlet stream is mixed with recycled flue gas from the FT unit and heated in a fired heater to 675°C before entering the adiabatic autothermal reformer

(ATR). Oxygen is preheated to 200 °C and is also fed to the ATR. The ATR is the main reactor in producing the synthesis gas and the following three main reactions take place:

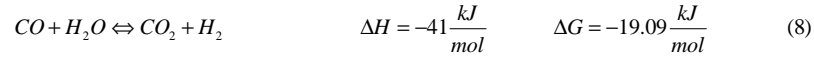
Oxidation of methane (exothermic):



Steam reforming of methane (endothermic):



Shift Reaction (exothermic):



Because of the large heat generated by combustion in reaction (6) the net reactions are exothermic, and the outlet temperature of the ATR is about 1000 °C.

A high-pressure CO<sub>2</sub> capturing process with MDEA as an absorbent is used to remove most of the CO<sub>2</sub> from the syngas. A mixture of hydrogen and carbon monoxide is the main product of ATR and a ratio of  $\frac{H_2}{CO}$  around 2-2.3 is desired to have maximum conversion to liquid fuels in the subsequent FT reactor (see Fig. 2). To set this ratio, a small amount of CO<sub>2</sub> is recycled to the ATR. This avoids that too much CO is shifted to CO<sub>2</sub> according to reaction (8).

### 2.3. FT reactor

The syngas is sent to the FT reactor. The FT synthesis with cobalt catalyst produces mostly n-alkanes and 1-alkenes. The FT reaction and kinetics using cobalt catalyst was taken from Satterfield and Yates (Yates and Satterfield, 1991). The main reaction is



$$-R_{CO} = \frac{aP_{CO}P_{H_2}}{(1+bP_{CO})^2} \quad (10)$$

The a and b are temperature-dependent constants; a representing a kinetic parameter and b an adsorption coefficient (Table 1). The amount of cobalt catalyst is 392.2 kg / m<sup>3</sup><sub>reactor</sub> (based on data from Sehabiague et al, 2008).

Table 1: Kinetic parameter for FT reaction

| Reactor Temperature (°C) | a ( $\frac{\text{mmol}}{\text{min.g of catalyst. Mpa}^2}$ ) | b ( $\frac{1}{\text{MPa}}$ ) |
|--------------------------|---|------------------------------|
| 240                      | 75.76   | 11.61                        |
| 220                      | 53.11   | 22.26                        |

$$a = 8.01368e^{-\frac{37326}{8.31^*T}} \left( \frac{\text{kmol}}{\text{kg}_{\text{cat}} \cdot \text{sec} \cdot \text{MPa}^2} \right), \quad b = 1.248 * 10^{-6} e^{\frac{68402}{8.31^*T}} \left( \frac{1}{\text{MPa}} \right)$$

The product distribution of the hydrocarbons “(-CH<sub>2</sub>)<sub>n</sub>” are assumed to follow an Anderson-Schulz-Flory (ASF) distribution to methane, alkanes and alkenes, which can be expressed as:

$$\frac{W_n}{n} = (1-\alpha)^2 \alpha^{n-1} \quad (11)$$

$$R_{CH_4} = -(1-\alpha)^2 R_{CO} \quad (12)$$

$$R_{C_n H_{2n+2}} = \frac{\alpha^{n-1}}{1+\gamma} R_{CH_4} \quad (13)$$

$$R_{C_n H_{2n}} = \frac{\gamma}{1+\gamma} \alpha^{n-1} R_{CH_4} \quad (14)$$

Here,  $W_n$  is the weight fraction of hydrocarbon molecules containing  $n$  carbon atoms.  $\alpha$  is the chain growth probability, which is determined by the catalyst and the process conditions.  $\alpha$  for  $C_1$  and  $C_{2+}$  were set to 0.45 and 0.85, respectively (Fox III and Tam 1995).  $\gamma$  is the selectivity to olefins which is approximately 4 (Ahón et al 2005). Cobalt is not very active for the water gas shift reaction so the shift reaction is negligible. In total, 59 reactions (to  $CH_4$  and to alkanes and alkenes with number of carbons from 2 to 30) were modelled in a CSTR (SBCR) reactor.

The FT reactions are highly exothermic and the generated heat in the reactor is removed by boiling water at high pressure to generate steam. The FT products at 227 °C are then cooled to 50 °C and separated in a 3-phase separator (water, liquid fuels and flue gas). The flue gas, mostly unreacted  $H_2$  and  $CO$ , is recycled (90%) to the FT reactor, some (9%) is recycled to the ATR reactor, while about 1% is purged.

The effect of reactor volume on liquid fuels production is shown in Fig. 3. From this figure, it can be observed that a volume greater than about 2200 m<sup>3</sup> does not significantly increase liquid fuel production, so the reactor volume was selected to be 2200 m<sup>3</sup>. The final process flowsheet is shown in Fig. 4. All units were modelled using the Unisim flowsheet simulator.

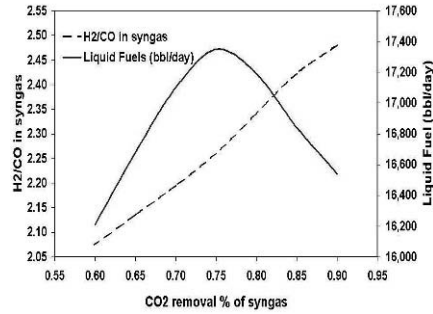


Figure 2: Effect of %CO<sub>2</sub> removal on (1) H<sub>2</sub>/CO in syngas and (2) production of liquid fuels

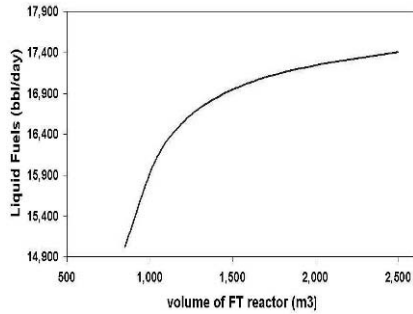


Figure 3: Liquid fuels production as function of volume of FT reactor

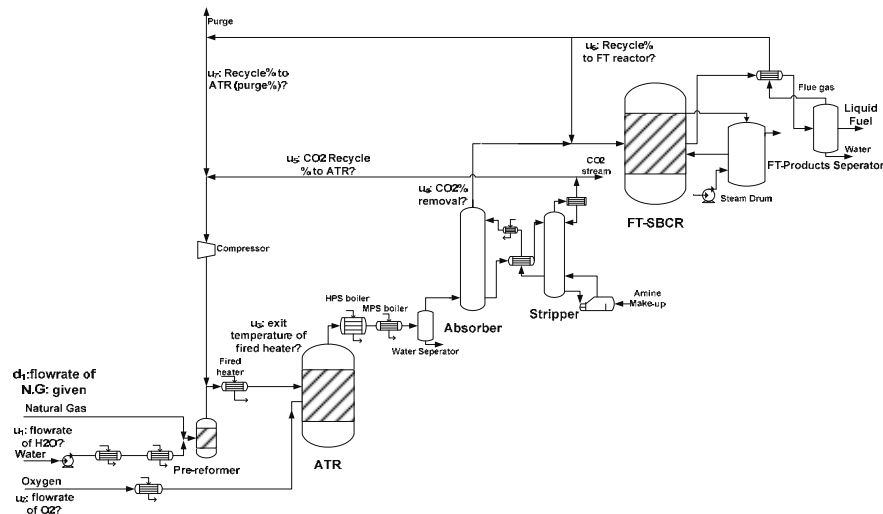


Figure 4: Process flowsheet for GTL process

### 3. Optimal operation and Self-optimizing control

With a given process design the objective is now to study operation and we use the procedure of Skogestad (2004). One important step is to perform optimization to find optimal conditions of the process for various disturbances.

Step 1: Define the objective function

We consider the case where the product price of the liquid product (fuel) is high so it is optimal to maximize the yield. Hence, the objective function is defined as: Maximize the liquid fuels production with a given feed rate of natural gas.

The following operational constraints should be satisfied:

- (a) The  $\frac{\text{H}_2\text{O}}{\text{Natural Gas}}$  ratio should be larger than 0.3 to avoid soot formation in the ATR.
- (b) The fired heater exit temperature should not exceed 675 °C due to limitations on construction material. (Bakkerud, 2009)

### 3.1. Step 2: Degrees of freedom (DOFs)

With a given natural gas feed rate we identify seven degrees of freedom that can be used for optimizing the objective. These were here selected to be:

- 1- Water feed rate ( $u_1$ )
- 2- Oxygen feed rate ( $u_2$ )
- 3- Exit temperature of fired heater ( $u_3$ )
- 4- Fraction CO<sub>2</sub> removed in the CO<sub>2</sub> capturing plant ( $u_4$ )
- 5- Amount of CO<sub>2</sub> recycled to the ATR ( $u_5$ )
- 6- Amount of flue gas recycled to FT reactor ( $u_6$ )
- 7- Amount of flue gas recycled to the ATR ( $u_7$ )

Optimization with respect to these 7 degrees of freedom was performed using the SQP algorithm in UniSim to find the optimal nominal operating point.

Optimal objective function (liquid production): 17,315 bbl/day

There is 1 active constraint (exit temperature of fired heater); leaving 6 unconstrained degrees of freedom at the optimum. The optimal values for the 7 degrees of freedom are as follows

$$u_1(\text{H}_2\text{O}) = 6025 \text{ kmol/hr} \left( \frac{\text{H}_2\text{O}}{\text{Natural Gas}} = 0.735 \right)$$

$$u_2(\text{O}_2) = 5803 \text{ kmol/hr} \left( \frac{\text{O}_2}{\text{Natural Gas}} = 0.708 \right)$$

$$u_3(\text{exit temperature of fired heater}) = 675 \text{ °C (active constraint)}$$

$$u_4(\text{CO}_2 \text{ removal } \%) = 77.8$$

$$u_5(\text{recycled } \% \text{ of removed CO}_2) = 1.34$$

$$u_6(\text{recycled } \% \text{ of flue gas to FT reactor}) = 88.69$$

$$u_7(\text{recycled } \% \text{ of flue gas to ATR}) = 91.53$$

The active constraint (exit temperature of fired heater) should always be controlled, but it is not clear how we should use the remaining 6 unconstrained degrees of freedom. Preferably, we would like to find 6 variables that give close-to-optimal operation with constant setpoints (“self-optimizing” control). To look for potential self-optimizing variables, we may reoptimize the process for different disturbances and look for variables with a small optimal variation. Based on this we may suggest potential CVs, and we can then test alternatives by considering the economic loss when they are kept constant.

### 3.2. Step 3: Disturbances

We consider 4 major disturbances for the GTL process:

- 1- flowrate of natural gas ( $\pm 10\%$ )
- 2- composition of hydrocarbons in natural gas (-10%)
- 3- change in FT kinetics ( $\pm 10\%$  in kinetic parameter  $a$ ),
- 4- change in exit temperature of fired heater ( $\pm 25^\circ\text{C}$ )

Reoptimizing the process for different disturbances show that the constraint on the exit temperature of the fired heater always remains active. This means that 6 CVs associated with the 6 unconstrained DOFs need to be identified.

To keep control simple, we first try whether we can keep some of the original DOFs ( $u_1$ - $u_7$ ) constant at their nominal optimal value and achieve near-optimal operation with small loss in the presence of different disturbances and also implementation errors (which is when we are not able to keep the DOFs constant). The ideal case is when the loss is small so there is no need to reoptimize any of DOFs in presence of disturbances or implementation error.

#### 3.2.1. First disturbance: Change in flowrate of natural gas

The flowrate of natural gas is allowed to change  $\pm 10\%$ . Fig.5 shows the value of reoptimized objective function when we let to all the six unconstrained DOFs vary (solid line), the dotted line shows the value if we keep all DOFs constant at their optimal nominal points. We see that if the flowrate of natural gas increases by 10%, then the simple policy with constant DOFs gives a 20.6% loss in liquid fuel production, which is not acceptable. We also considered the optimal variation in the six DOFs, and found that the largest variation was in the oxygen flowrate (Fig. 6). This suggests that we may attempt to let the other DOFs be constant. Indeed, we see from the dashed line in Fig. 5 that if we keep all DOFs ( $u_i$ ) at their optimal nominal points, except for the oxygen flowrate, then we have an acceptable loss (1.3%) in the worst case. However, there are other disturbances, so it is too early to conclude that we can keep all these DOFs constant.

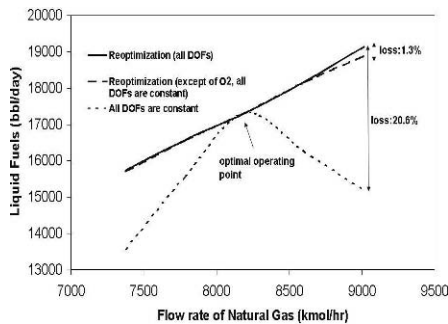


Figure 5: Effect on operation of changes in flowrate of natural gas feed.

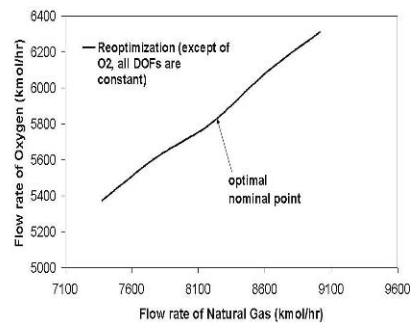


Figure 6: Relation between reoptimized oxygen flowrate and natural gas flowrate

### 3.2.2. Second disturbance: Change in composition of hydrocarbons in feed

The same method was applied to the second disturbance, which is an increase in the  $N_2$  contents in the range from 0.6% to 10%. The results in Fig.7 show that the effect of this disturbance is quite small. In the worst case, the fuel production loss is 3.3%. If we allow for reoptimization of the  $O_2$  feed rate (Fig. 8) then the loss is almost zero (Fig. 7).

### 3.2.3. Third disturbance: Model mismatch in kinetic parameter of FT reactions

This disturbance is not important. Fig.9 shows that a  $\pm 10\%$  change in the kinetic parameter  $a$  gives a loss of less than 1% even with all DOFs kept constant.

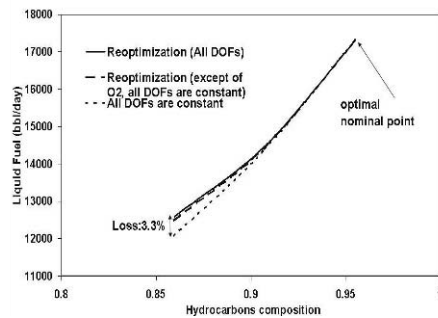


Figure 7: Effect on operation of changes in feed composition

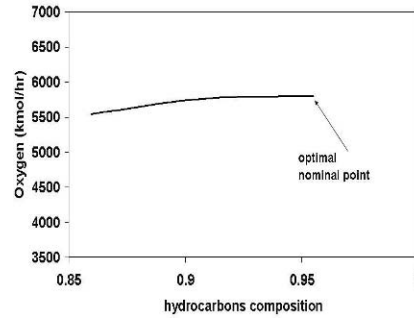


Figure 8: Relation between re-optimized oxygen flowrate and composition of hydrocarbons in feed

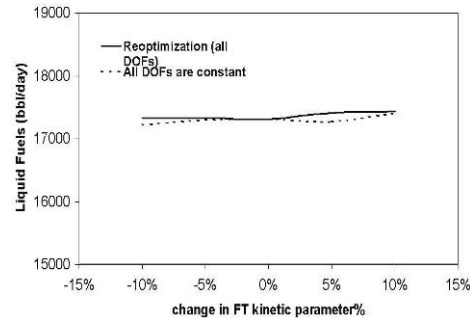


Figure 9: Effect on operation of change in FT kinetic parameter  $a$

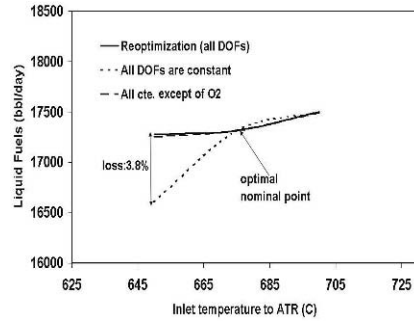


Figure 10: Effect on optimal operation of changes in change to exit fired heater temperature to ATR

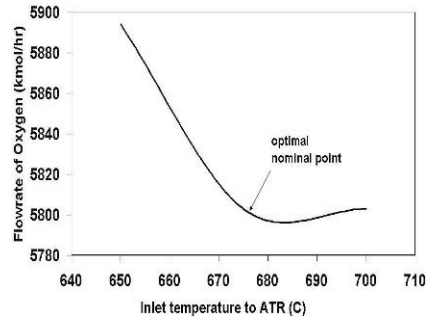


Figure 11: Relation between re-optimized flowrate of oxygen and exit fired heater temperature

#### 3.2.4. Fourth disturbance: Change in fired heater exit temperature

Fig. 10 shows that if the fired heater exit temperature decreases by 25 °C, without reoptimizing, the fuel production loss is 3.8%. If we reoptimize the oxygen feedrate, the loss is almost zero. The reoptimized flowrate of oxygen is shown in Fig. 11.

Table 2: Summary of losses for various disturbances

| no. | disturbance              | worst case of each disturbance |          | Loss (%), if all DOFs are constant except of O <sub>2</sub> flowrate |
|-----|--------------------------|--------------------------------|----------|--|
|     |                          | Change from nominal point      | Loss (%) |  |
| 1   | Flowrate natural gas     | +10%                           | 20.6     | 1.3  |
| 2   | Inlet temperature to ATR | -25 °C                         | 3.8      | 0.1  |
| 3   | Hydrocarbons in the feed | -10%                           | 3.3      | 0.8  |
| 4   | Kinetic FT parameter a   | +5%                            | 0.8      | -  |

Table 3: Effect of CV implementation error on objective function (loss)

| CVs                                    | Implementation error | Loss (%) |
|--|----------------------|----------|
| Recycled flue gas % to ATR (u7)        | -15%                 | 13.55    |
| H <sub>2</sub> O feedrate (u1)         | -10%                 | 1.9      |
| Recycled flue gas % to FT (u6)         | -15%                 | 0.51     |
| CO <sub>2</sub> removal% (u4)          | -5%                  | 0.21     |
| Recycled CO <sub>2</sub> % to ATR (u5) | -15%                 | 0.02     |

The results for all four disturbances are summarized in Table 2. It seems that we can always keep all the DOFs constant, except of the O<sub>2</sub> feedrate. However, in addition to disturbances, we should also examine the effect on the objective function of the implementation errors in the selected controlled variables, for example caused by

measurement errors. From Table 3 we see that objective function is sensitive to implementation errors in recycled flue gas to ATR ( $u_7$ ) and H<sub>2</sub>O feedrate ( $u_1$ ), while its sensitivity to the other CVs ( $u_4$ ,  $u_5$ ,  $u_6$ ) is negligible. Note that the implementation error in the active constraint ( $u_3$ ) has already been considered as a disturbance, while we have already decided that the oxygen feedrate ( $u_2$ ) should not be kept constant.

In summary, we still have 3 unconstrained DOFs (flowrate of oxygen  $u_2$ , flowrate of water  $u_1$  and recycled flue gas to ATR,  $u_7$ ) for which we have not identified good (self-optimizing) controlled variables. Some potential candidates are: H<sub>2</sub>/CO ratio at ATR outlet, temperature at ATR outlet, methane contents in flue gas, oxygen/hydrocarbon feed ratio and water feedrate. For the last two “open-loop” policies one may need good flow measurements to reduce the implementation error. The selection of the best variables will be the subject of future work.

#### 4. Conclusion

The UniSim process simulator was used to simulate and optimize a GTL plant. A rule of thumb for GTL is that for every 10,000 SCF (=282.6 Sm<sup>3</sup> =11.953 kmol) of natural gas, approximately 1 bbl (=159 liter) of fuel is produced (Patel, 2005). In our case study, we produce 17,315 bbl/day from 8195 kmol/hr natural gas, which is 5.23% higher than the rule of thumb. In the synthesis gas part, the optimal ratios of oxygen and water to methane at the nominal operating point were  $\frac{O_2}{CH_4}=0.708$ ,  $\frac{H_2O}{CH_4}=0.735$  and a good volume of the FT reactor was found to be 2200 m<sup>3</sup>.

There are 7 operational degrees of freedom (DOFs): Feed rates of oxygen and water, exit temperature of fired heater, flue gas recycle to ATR and FT, CO<sub>2</sub> removal rate and recycled CO<sub>2</sub> to ATR). By optimizing the operation for various disturbances, we found that 1 of the DOFs is always needed to satisfy an active constraint at the fired heater exit temperature. Furthermore, we found that 3 of the original DOFs can be kept constant at their optimal nominal values (flue gas recycle to FT, CO<sub>2</sub> removal rate, recycled CO<sub>2</sub> to ATR) when there are disturbances, so these are good self-optimizing variables. Further work is needed to find good controlled variables for the remaining 3 unconstrained DOFs ( $\frac{O_2}{\text{Natural Gas}}$ ,  $\frac{H_2O}{\text{Natural Gas}}$  and recycled flue gas to ATR).

#### References

- Aasberg-Petersen, K., J.-H. Bak Hansen, T. S. Christensen, I. Dybkjaer, P. Seier Christensen, C. Stud Nielsen, S. E. L. Winter Madsen and J. R. Rostrup-Nielsen, 2001, Technologies for large-scale gas conversion, *Applied Catalysis A: General* 221, 379-387.
- Aasberg-Petersen, K., T. S. Christensen, C. Stud Nielsen and I. Dybkjær, 2003, Recent developments in autothermal reforming and pre-reforming for synthesis gas production in GTL applications, *Fuel Processing Technology*, 83, 253-261.
- Ahón, V. R., Jr. E. F. Costa, J. E.P. Monteagudo, C.E. Fontes, Jr. E. C. Biscaia, P. L. C. Lage, 2005, A comprehensive mathematical model for the Fischer-Tropsch synthesis in well-mixed slurry reactors, *Chemical Engineering Science*, 60, 677-694.

- Bakkerud, P. K., 2009, Personal communication.
- Bakkerud, P. K., 2005, Update on synthesis gas production for GTL, *Catalysis Today*, 106, 30-33.
- Fox III, J. M. and S. S. Tam, 1995, Correlation of slurry reactor Fischer-Tropsch yield data, *Topics in Catalysis*, 2, 285-300.
- Patel, B., 2005, Gas Monetization: A Techno-Economic comparison of Gas-To-Liquid and LNG, 7th World Congress of Chemical Engineering, Glasgow.
- Sehabiague, L., R. Lemonie, A. Behkish, Y. J. Heintz, M. Sanoja, R. Oukaci, B. I. Morsi, 2008, Modeling and optimization of a large-scale slurry bubble column reactor for producing 10,000 bbl/day of Fischer-Tropsch liquid hydrocarbons, *Journal of the Chinese Institute of Chemical Engineers*, 39, 169-179.
- Skogestad, S., 2004, Control Structure Design for Complete Chemical Plants, *Computers and Chemical Engineering*, 28, 219-234.
- Yates, I. C. and C. N. Satterfield, 1991, Intrinsic Kinetics of the Fischer-Tropsch Synthesis on a Cobalt Catalyst, *Energy & Fuels*, 5, 168-173.



## **Appendix B (additional work)**

Plantwide Control of a Cumene Manufacture Process

Computer Aided Chemical Engineering, volume 29, 2011, pages 522-526, 21st European  
Symposium on Computer Aided Process Engineering



## Plantwide Control of a Cumene Manufacture Process

Vivek Gera<sup>a</sup>, Nitin Kaistha<sup>a</sup>, Mehdi Panahi<sup>b</sup>, Sigurd Skogestad<sup>b</sup>

<sup>a</sup>Chemical Engineering, Indian Institute of Technology Kanpur, 208016, Kanpur, India

<sup>b</sup>Chemical Engineering Department, NTNU, 7491, Trondheim, Norway

### Abstract

This work describes the application of the plantwide control design procedure of Skogestad (Skogestad, 2004) to the cumene production process. A steady state “top down” analysis is used to select the set of “self-optimizing” primary controlled variables which when kept constant lead to acceptable economic loss without the need to reoptimize the process when disturbances occur. Two modes of operation are considered: (I) given feed rate and (II) optimized throughput.

**Keywords:** cumene production, control structure design, self-optimizing control

### 1. Introduction

Cumene is an important industrial intermediate in the manufacture of phenolic and polycarbonate resins, nylon and epoxy and is conventionally produced by the Friedel Crafts alkylation of benzene with propylene. (Concentration unit: kmol/m<sup>3</sup>).

Main reaction:  $C_6H_6 + C_3H_6 \rightarrow C_9H_{12}$  (Cumene) ( $k=2.8E7$ ,  $E= 104174$  kJ/kmol)

Side reaction:  $C_9H_{12} + C_3H_6 \rightarrow C_{12}H_{18}$  (DIPB) ( $k=2.32E9$ ,  $E= 146742$  kJ/kmol)

Some research has already been done over the past few years which discusses the various aspects of operation, design and control of a cumene production plant.<sup>1, 2</sup> But none of them address the issue of control structure design in a systematic manner. In this work we try to address this by applying a part of Skogestad’s plantwide procedure of (Skogestad, 2004). The main steps of this procedure are as follows:

- Degree of freedom analysis.
- Definition of optimal operation (cost and constraints).
- Identification of important disturbances
- Identification of candidate controlled variables c.
- Evaluation of loss for alternative combinations of controlled variables
- Final evaluation and selection (including controllability analysis)

Two modes of operation are considered for the process: Mode 1: Given Throughput. Mode 2: Optimized/Maximum Throughput. (feed rate is also a degree of freedom).

### 2. Base Case Design

The base case design parameters and kinetics data and cost correlations were taken from Luyben (2010). Figure 1 provides a schematic of the conventional process. The fresh benzene and fresh C<sub>3</sub> (95% propylene and 5% n-propane) streams are mixed with the recycle benzene, vaporized in a vaporizer, preheated in a feed effluent heat exchanger (FEHE) using the hot reactor effluent, before being heated to the reaction temperature in a furnace. The heated stream is fed to a cooled packed bed reactor. The hot reactor effluent loses sensible heat in the FEHE and is further cooled using cooling water. The cooled stream is sent to a light out first distillation train. The inert n-propane and small amounts of unreacted propylene are recovered as vapour distillate from column 1. The bottom stream is further distilled in the recycle column to recover and recycle unreacted benzene as the distillate. The recycle column bottom stream is sent to the product column to recover 99.9% cumene as the distillate and the heavy DIPB as the bottoms.

### 2.1. Determination of column 1 pressure

The flash tank in the Luyben design has been replaced with a distillation column (column 1) to reduce the loss of benzene and hence increase the plant operating profit. A column operating pressure of 5 bar with a benzene loss of 0.12 kmol/h was found to be near optimal. Table 1 provides an economic comparison of the base case design with the original Luyben design (with a flash tank instead of column 1) for the same operating conditions. The yearly operating profit of the base-case design is noticeably higher than the Luyben design due to the reduction in the loss of precious benzene in the fuel gas stream. For completeness, economic / operating condition details of Mode I and Mode II optimum solutions, where the plant operating profit (defined later) is optimized, are also provided in Table 1.

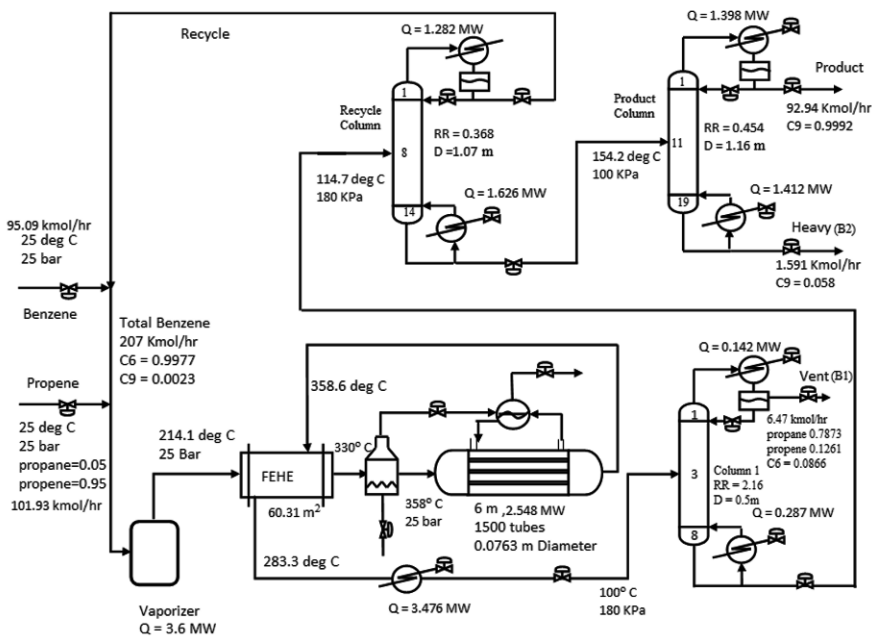


Figure 1: Base-case cumene process flowsheet

## 3. Economic optimization of the base case design

### 3.1. Definition of objective function ( $J$ ) and constraints

Total operational profit per year (365 days) was chosen as the objective function  $J$  which is to be maximized with

$$J = \text{Product revenue} - \text{reactant cost} + \text{DIPB credit} + \text{vent gas credit} + \text{reactor steam credit} - \text{preheater electricity cost} - \text{steam cost in reboilers and vaporizer}$$

Since the plant is already built, it has certain physical limitations associated with the unit operation equipment. Moreover it is always optimal to have the most valuable product at its constraint to avoid product give-away. The steady state degrees of freedom to maximize the Mode I / Mode II operating profit are noted in Table 2. Note that since  $J$  does not have a strong relationship with cooler outlet temperature it is fixed at 100 °C.

Table 1. Economic comparison of base-case design with original Luyben design

|                                     | <i>Unit</i>                   | <i>Luyben</i> | <i>Base case</i> | <i>Mode I</i> | <i>Mode II</i> |
|-------------------------------------|-------------------------------|---------------|------------------|---------------|----------------|
| Reactor inlet temp                  | °C                            | 358           | 358              | 361           | 346.99         |
| Total benzene flow                  | kmol/h                        | 207           | 207              | 245           | 269.7          |
| Hot Spot temp                       | °C                            | 430           | 421.60           | 417.50        | 411.3          |
| Benzene recycle                     | kmol/h                        | 207           | 207              | 245           | 269.70         |
| Vent                                | kmol/h                        | 9.98          | 6.47             | 6.02          | 19.04          |
| Heavy Bottom                        | kmol/h                        | 1.55          | 1.59             | 1.20          | 2.99           |
| Fresh Propene                       | kmol/h                        | 101.93        | 101.93           | 101.93        | 175.02         |
| Fresh Benzene                       | kmol/h                        | 98.78         | 95.09            | 95.00         | 153.87         |
| Product                             | kmol/h                        | 92.86         | 92.94            | 93.67         | 150.47         |
| Total Capital Cost                  | \$ 10 <sup>6</sup>            | 4.11          | 4.26             | 4.26          | 4.26           |
| Total Energy Cost                   | \$ 10 <sup>6</sup> /year      | 2.23          | 2.35             | 2.68          | 3.43           |
| Benzene cost                        | \$ 10 <sup>6</sup> /year      | 59.36         | 57.14            | 57.09         | 92.47          |
| Propylene cost                      | \$ 10 <sup>6</sup> /year      | 30.63         | 30.63            | 30.62         | 52.59          |
| Reactor steam credit                | \$ 10 <sup>6</sup> /year      | 0.40          | 0.54             | 0.53          | 0.86           |
| Vent (B1) credit                    | \$ 10 <sup>6</sup> /year      | 1.59          | 0.70             | 0.59          | 1.84           |
| Heavy (B2) credit                   | \$ 10 <sup>6</sup> /year      | 0.71          | 0.48             | 0.38          | 0.95           |
| Product revenue                     | \$ 10 <sup>6</sup> /year      | 107.74        | 107.87           | 108.72        | 174.64         |
| Total operational cost              | \$ 10 <sup>6</sup> /year      | 89.52         | 88.40            | 88.89         | 144.88         |
| <b>Total operational profit (J)</b> | <b>\$ 10<sup>6</sup>/year</b> | <b>18.23</b>  | <b>19.47</b>     | <b>19.83</b>  | <b>29.76</b>   |

Price Data: HP steam \$9.83/GJ, Steam generated \$6.67/GJ, Electricity cost \$16.8/GJ, Benzene price \$68.6/kmol, Propylene price \$34.3/kmol, Cumene price \$132.49/kmol.

Table 2. Steady state degrees of freedom

| <i>Process variables</i>   |  | <i>DOF</i>           |   |
|----------------------------|--|----------------------|---|
| Fresh propene flow rate    | 101.93 kmol/h <sup>#</sup>                 | 0/1*                 |   |
| Total benzene flow rate    | Variable                                   | 1                    |   |
| Furnace outlet temperature | Variable                                   | 1                    |   |
| Reactor cooler temperature | Fixed                                      | 0                    |   |
| Column 1                   | Condenser Temperature<br>x <sub>C3,B</sub> | 32.25 °C<br>Variable | 1 |
| Column 2                   | x <sub>C9,D</sub><br>x <sub>C6,B</sub>     | Variable<br>Variable | 2 |
| Column 3                   | x <sub>C9,D</sub><br>x <sub>C12,B</sub>    | 0.999<br>Variable    | 1 |

#: Fixed for Mode I. \*: Degree of freedom for Mode II

### 3.2. Optimization results

Ideally all dofs in Table 1 should be simultaneously optimized. However, to overcome convergence issues in UniSim, the separation section is optimized first followed by the rest of the plant (see e.g. Araujo et al, 2007). The optimization results obtained are summarized in Table 3.

For Mode I operation, none of the constraints are active while in Mode II operation (optimal throughput), the maximum furnace duty and product column boilup constraints are active. From an economical point of view, it is optimal to increase the Mode I feed rate without violating the constraints of the plant. As the propylene feed rate is

increased the profit increases due to higher production. The first constraint to become active is maximum furnace heating. However this is not the real bottleneck as feed rate can be further increased by lowering the reactor inlet temperature and/or recycle benzene flow and hence increasing the profit. As the throughput is further increased, the maximum product column boilup constraint becomes active for a fixed DIPB mol fraction in the product column bottoms. This mol fraction may be decreased to further increase the throughput and profit with the boilup constraint active. The DIPB mol fraction can however not be decreased too much as the profit decreases due to cumene product loss in the heavy fuel stream. The reported column 3  $x_{C12,B}$  value in Table 3 corresponds to this limit of maximum operating profit.

Table 3. Summary of Mode I and Mode II Optimization Results

| Process variables     |             | Mode I   |                      | Mode II           |                      |
|-----------------------|-------------|----------|----------------------|-------------------|----------------------|
|                       |             | Type     | Value                | Type              | Value                |
| Fresh propene         |             | Fixed    | 101.93 kmol/h        | Variable          | 175.02 kmol/h        |
| Total benzene         |             | Variable | 245 kmol/h           | Variable          | 269.7 kmol/h         |
| Rxx inlet temperature |             | Variable | 361 °C               | Max furnace duty* | 346.99 °C            |
| Cooler temperature    |             | Fixed    | 100 °C               | Fixed             | 100 °C               |
| Column 1              | Top T       | Fixed    | 32.25 °C             | Fixed             | 32.25 °C             |
|                       | $x_{C3,B}$  | Variable | 0.01                 | Variable          | 0.01                 |
| Column 2              | $x_{C9,D}$  | Variable | $5.5 \times 10^{-3}$ | Variable          | 0.0012               |
|                       | $x_{C12,B}$ | Variable | $2.7 \times 10^{-4}$ | Variable          | $3.5 \times 10^{-4}$ |
| Column 3              | $x_{C9,D}$  | Fixed    | 0.999                | Fixed             | 0.999                |
|                       | $x_{C12,B}$ | Variable | 0.9542               | Max boil up*      | 0.9628               |

\*: Variable is fixed by this constraint

#### 4. Self-optimizing Controlled Variables

Skogestad (2004) states that self-optimizing control is when one can achieve an acceptable economic loss with constant setpoints for appropriately chosen / designed controlled variables without the need to re-optimize for disturbances. In this work, four disturbances are considered as in Table 3.

Table 4. Set of disturbances considered

| SN. | Disturbance variable                    | Nominal Value | change      |
|-----|---|---------------|-------------|
| d1  | Propylene flow rate                     | 101.93 kmol/h | - 10 kmol/h |
| d2  | Column 1 condenser temperature          | 32.25 °C      | +3 °C       |
| d3  | Inert composition in the propylene feed | 5% propane    | +3 %        |
| d4  | Propylene flow rate                     | 101.93 kmol/h | +10 kmol/h  |

##### 4.1. Mode I Self Optimizing Controlled Variables

For each of the four disturbances, the plant is sequentially reoptimized for all 6 unconstrained dofs (see Table 2). We also reoptimize the process keeping the distillation column mole recoveries constant (i.e. using  $6 - 4 = 2$  degrees of freedom). The difference in the objective function for the two cases was observed to be very small for all the disturbances ( $< 0.07\%$ ). Hence we choose to use distillation column mole recoveries as controlled variables for two reasons: First, resulting loss values are very small. Second, it reduces the number of self-optimizing variables to be determined and simplifies the further analysis to a great extent as we are left with only 2 input variables instead of 6.

To choose the remaining two self-optimizing controlled variables, we use the “exact local method” (Halvorsen et al., 2003) which minimizes the worst case loss due to

suboptimal self-optimizing control policy. The branch and bound algorithm of Kariwala (2007) is used for the evaluation of the loss. Seven candidate controlled variables, namely, reactor inlet temperature, preheater duty, fresh benzene flow rate, total benzene flow rate, reactor feed benzene to propane ratio, reactor feed benzene mol fraction and vaporizer outlet temperature, are evaluated. The best set of two self optimizing variables for Mode I operation are thus found to be the reactor inlet temperature and the reactor feed benzene to propylene ratio.

#### 4.2 Mode II Self Optimizing Controlled Variables

The maximum furnace duty and maximum product column boil up are the two active constraints in Mode II. This leaves 5 (7 dof – 2 active constraints) unconstrained dof for which we need to find 5 self optimizing controlled variables. Similar to Mode I, the column purity specifications, namely, column 1  $x_{C3,B}$ , column 2  $x_{C9,D}$  and  $x_{C6,B}$  when kept at their optimized nominal values with no disturbance result in negligible loss for the set of disturbances considered (note that column 3  $x_{C12,B}$  is fixed by its maximum boilup constraint).

As in Mode I, the exact local method is used to select the best self optimizing variables for the remaining two unconstrained dof. The best set was found out to be fresh benzene flow rate and the reactor inlet propylene mol fraction. The economic loss for the next best set, which is total benzene flow and the reactor feed benzene to propylene is only slightly higher. Since the latter variable is a self-optimizing variable also in Mode I, we select this set as our choice of controlled variables in Mode II to simplify the transition from Mode I to Mode II. The transition would only require replacing the reactor inlet temperature controller with the total benzene flow controller.

### 5. Conclusion and future work

In this work, a cumene production plant has been systematically analyzed for economically optimal operation at given throughput (Mode I) and optimum throughput (Mode II). Results show that in Mode I operation, the optimized unconstrained column product purities are self optimizing along with the reactor inlet temperature and the reactor feed benzene to propylene ratio. In Mode II, the maximum furnace duty and product column boilup constraints are active. The self-optimizing variables are again the unconstrained column product purities along with the total benzene flow to the reactor and the reactor feed benzene to propylene ratio. Further work would focus on developing a plantwide control structure for the process and its dynamic validation.

### References

1. Luyben, W.L. (2010). Design and Control of the Cumene Process. *Ind. Eng. Chem. Res.* 49 (2), 719.
2. S. Skogestad (2000). Plantwide control: The search for the self-optimizing control structure. *J. Proc. Cont.*, 10, 487.
3. S. Skogestad (2004). Control structure design for complete chemical plants. *Comp. Chem. Engg.*, 28, 219–234.
4. I. J. Halvorsen, S. Skogestad, J. C. Morud and V. Alstad (2003). Optimal selection of controlled variables. *Ind. Eng. Chem. Res.*, 42, 3273.
5. V. Kariwala (2007). Optimal measurement combination for local self-optimizing control, *Ind. Eng. Chem. Res.*, 46, 3629.
6. A. Antonio, M. Govatsmark, S. Skogestad (2006). Application of plantwide control to the HDA process. I-steady state optimization and self-optimizing control. *Cont. Engg. Practice*, 15, 1222.



## Appendix C

### More information about CO<sub>2</sub> capture model used in this thesis (UniSim 2008)

The post-combustion CO<sub>2</sub> capturing model used in chapters 3, 4 and 5 has been simulated in UniSim simulator using Amine thermodynamic package. This thermodynamic package uses a non-equilibrium stage model and calculates a modified Murphree-type vapour efficiency. The stage efficiency is a function of the kinetic rate constants for the reactions, the physico-chemical properties of the amine solution, the pressure, temperature and the geometry of the column. Efficiency used is only for CO<sub>2</sub> component.

There are two thermodynamic models available for aqueous amine solutions, Kent-Eisenberg and Li-Mather models. For calculating the vapour phase model we can choose between ideal and non-ideal method. For the CO<sub>2</sub> capture simulation the Kent-Eisenberg model is used for aqueous phase and non-ideal method for vapour phase.

For further information about mass and energy balances, calculation of efficiency, chemical reactions etc. readers are referred to help of UniSim Design.

In our model, the diameter of the absorber is 2m with tray space of 0.5m (15 stages) and stripper diameter is 1.5m (20 stages) with the same tray space as absorber.

